Design, synthesis and molecular modeling studies of drug candidate compounds against prion diseases.

Thesis submitted for the degree of
Doctor Philosophiæ
in Statistical and Biological Physics

Candidate

Salvatore Bongarzone

Supervisors

Prof. Maria Laura Bolognesi
Prof. Paolo Carloni
Prof. Giuseppe Legname

Co-Supervisors

Prof. Andrea Cavalli
Prof. Marinella Roberti

September 2011

Index

1. Motivations and outline of the thesis

Prion diseases are a group of invariably fatal disorders, for which there is no cure. Despite their rare incidence in humans, prion diseases have captured very large attention from the scientific community due to the unconventional mechanism by which they are transmitted.[1] The central feature of prion diseases is the accumulation in the brain and some other tissues of the disease-associated PrP^{Sc}, which is derived from the host-encoded cellular PrP^{C}.[1] The conversion from a normal form (PrP^{C}) to an infectious isoform (scrapie, PrP^{Sc}) is triggered by the interaction between PrP^{C}-PrP^{Sc},[2] as well as protein-protein interaction (PPI).[3]

PrP^{C} belongs to the class of amyloid-forming proteins, which are associated with a variety of conformational diseases. Indeed, prion diseases share many pathologic features with other neurodegenerative disorders. They are all characterized by the presence in the nervous system of abnormal protein accumulation. These abnormal proteins form aggregates of amyloid fibrils that continuously increase in size. This event changes the metabolic processes of neurons, ultimately leading to neurodegeneration. Conformational neurodegenerative disorders include Alzheimer's disease (Aβ-amyloid neuritic plaques and neurofibrillary tangles), Parkinson's disease (α-synuclein, Lewy bodies), Huntington's disease (huntingtin protein aggregates) and Pick's disease (Pick bodies).[4-6]

As Prof. S. B. Prusiner recognizes already in his Nobel lecture in 1997, the "*Investigation of prion diseases suggest that new strategies for the prevention and treatment of these disorders may also find application in the more common degenerative disorders*".[a] Indeed, there is great interest in designing PrP^{Sc} blockers that may be also effective to prevent fibril formation in other neurodegenerative diseases.[1] However, in spite of decades of attempts at developing effective anti-prion drugs,[7-10] no drug has been identified for prion treatment. Several are the challenges one has to face when developing such drugs.

In this thesis, under the supervision of Prof. G. Legname, collaborator of Prof. S. B. Prusiner, I[b] have focused on two of them. The first challenge concerns molecular docking approaches of ligands known already to bind PrP^{C}. These studies are extremely difficult because of the lack of deep binding sites in PrP^{C}. Molecular docking methodologies are well suited to predicted activity profiles and identifying binding poses.[11] Unfortunately these approaches, whilst fast and useful for enzymes

[a] "The Nobel Prize in Physiology or Medicine 1997" http://nobelprize.org/nobel_prizes/medicine/laureates/1997/

[b] The research presented on this thesis was all performed as teamwork.

and receptors, are likely to fail here because of the lack of a well-defined binding cavity: only shallow binding sites are present in the structure of PrP^C (an issue addressed in **Chapters 2** and **3**). The second challenge (which constitutes the largest part of this thesis work) concerns the rational design of drug leads aimed at developing therapies for multifactorial diseases. Prion diseases, as other neurodegenerative diseases, are currently characterized as multifactorial disorders, where the pathogenic $PrP^C \rightarrow PrP^{Sc}$ conversion is interrelated with multiple molecular mechanisms involving reactive oxygen species (ROS) production, an imbalance of brain metal homeostasis, and increased oxidation of lipids, proteins, and DNA (see **Section 2.9**).[12] Therefore, the development of multifunctional antiprion compounds for prion diseases presents great challenges (this issue will be extensively addressed in **Chapters 4-7**)

This thesis is organized as follows.

Chapter 2 introduces prion diseases, PrP^C and its role in the cell. This Chapter will also introduce therapeutic strategies for prion therapy.

Chapters 3-4 present a novel computational protocol, called EMD (enhanced molecular docking) that combines standard docking methods with MD simulations and metadynamics based-free energy calculations in explicit solvent to address this issue.[13,14] The EMD protocol provides a step forward towards the development of a tool able to identify small organic molecules that stabilize PrP^C. I focused on **1** (*2-pyrrolidin-1-yl-N-[4-[4-(2-pyrrolidin-1-yl-acetylamino)-benzyl]-phenyl]-acetamide*, **Figure 1A**), which has been shown to bind by NMR to the structured part of the PrP, increasing its stability.[15] The computational study enable to identify alternative binding poses that satisfy all of the contacts emerging from NMR, in contrast to a previous model. Most importantly, these results provided an estimation of the experimental free energy of binding that is in very good agreement with the experimental one. Prompted by the relevance of this issue, it has been tried to establish a computational protocol that attempts to include conformational selection[16] and induced fit[17] processes, which play an important role for **1** binding to PrP^C, a protein lacking binding sites.

Chapter 5 focuses on the rational design to discovering small organic molecules that attack prion diseases on multiple fronts. Prion diseases, like other neurodegenerative diseases, are currently characterized as multifactorial processes that operate simultaneously and synergistically in the cell environment finally leading to cell death.[12] Indeed, the dominant drug discovery paradigm (one disease, one target, one molecule) ignores the polyetiological nature of many multifactorial diseases as well as prion diseases. Thus, this paradigm might be one possible factor behind the failure of many drugs to cure multifactorial diseases. In this respect, several lines of research have suggested that combination therapy (one disease, two or more targets, cocktail of drugs) or "multi-target-directed ligand" (MTDL) strategy (one disease, two or more targets, one drug) that simultaneously

target more than one process might be a more effective therapeutic option.[18] **Section 5.2** underscores advantages and disadvantages of the MTDL strategy.[19] To rational design MTDLs for prion diseases, I selected fragments with potential beneficial properties against PPI, unbalance of metal ions, and oxidative stress (OS). As PPI inhibitors, two hydrophobic heterocyclic motifs have been selected from literature. Quinoline and acridine are particularly frequent in compounds active against prion diseases.[20] In particular, considering the key role of a planar hydrophobic structure in perturbing PPIs in all conformational diseases, it is conceivable that these hydrophobic motifs have the potential to disrupt PPIs also in prion diseases. The term "prion-recognition motif" (PRM) will refer to a key fragment able to interact with prion proteins and to modulate PrP^C misfolding (This aspect will be dealt in **Section 5.5**).

The implication of OS in prion diseases suggested us the possibility to use antioxidant fragments to substitute and balance antioxidant deficiencies in the disease state. It has been argued that the presence of a PRM along with an antioxidant moiety might lead to discover more effective antiprion compounds. As a first effort to identify MTDLs with the simultaneous ability to prevent the conversion of PrP^C to PrP^{Sc} form and to reduce oxidative stress, I present the rational design, synthesis and structure-activity relationship of two classes of antiprion compounds. In **Chapter 6** and **7**, the structures of hit compounds representative the two classes are shown in **Figure 1B** (**39** and **64**). Compounds **39** and **64** owing to the presence of an antioxidant fragment, the benzoquinone ring or the lipoyl group respectively, (highlighted in red in **Figure 1B**), and a PRM (highlighted in green), are studied as inhibitors of PrP^{Sc} formation and antioxidants in scrapie-infected mouse hypothalamus cells (ScGT1). Indeed, these compounds simultaneously modulate at least two of the multiple targets involved in prion pathology.[21,22]

Chapter 8 discusses the rational design of an additional series of MTDLs potentially able to inhibit prion replication through multiple mechanisms.

The conclusions are summarized in **Chapter 9.**

The experimental section is discussed in **Chapter 10.**

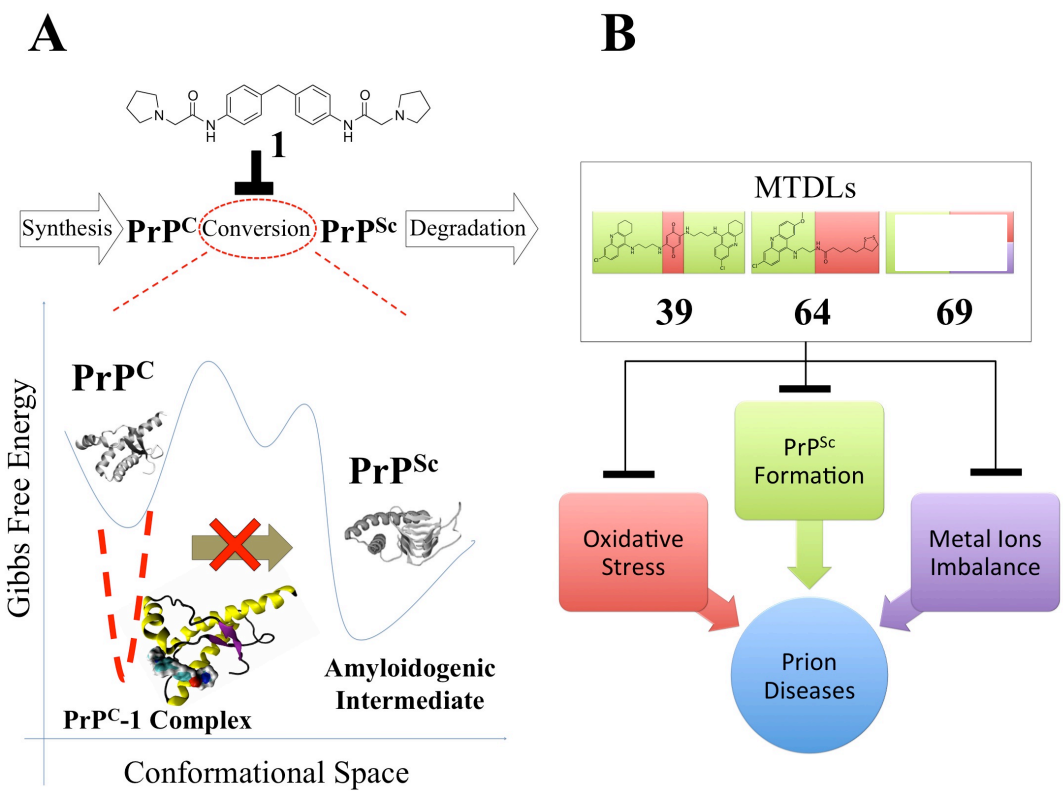

Figure 1. A) Antiprion compound **1** acts on the conversion step by stabilizing the PrP^{C} conformation and reducing the population of PrP^{Sc}. Illustration of the Gibbs free energy as a function of the conformational space to explain the inhibitory mechanism of **1**. **1** stabilizes the PrP^{C} conformation and reduces the population of PrP^{Sc}. The conformational space is multidimensional and only one arbitrary axis is shown here for the sake of clarity. B) Prion diseases pathogenesis involves a complex array of processes operating simultaneously and synergistically.[12] These include: i) protein aggregation;[2,24] ii) OS;[25-27] iii) reduced levels of potent free-radical scavenger;[28,29] iv) unbalance of metal ions;[30,31] and v) brain inflammation.[32]

References

(1) Prusiner, S. B. *Proc. Natl. Acad. Sci. U S A* **1998**, *95*, 13363.

(2) Aguzzi, A.; Calella, A. M. *Physiol. Rev.* **2009**, *89*, 1105.

(3) Prusiner, S. B. *Science* **1982**, *216*, 136-144.

(4) Kopito, R. R.; Ron, D. *Nature Cell Biol.* **2000**, *2*, E207-9.

(5) Brundin, P. Melki, R.; Kopito, R. *Nat Rev Mol Cell Biol.* **2010**, *11*, 301.

(6) Thompson, A. J.; Barrow, C. J. *Curr. Med. Chem.* **2002**, *9*, 1751-1762.

(7) Ludewigs, H. Zuber, C. Vana, K. Nikles, D. Zerr, I.; Weiss, S. *Expert Rev. Anti. Infect .Ther.* **2007**, *5*, 613-30.

(8) Krammer, C. Vorberg, I. Schätzl, H. M.; Gilch, S. *Infect. Disord. Drug Targets* **2009**, *9*, 3-14.

(9) Nunziante, M. Gilch, S.; Schätzl, H. M. *Chembiochem* **2003**, *4*, 1268-84.

(10) Sim, V. L.; Caughey, B. *Infect. Disord. Drug Targets* **2009**, *9*, 81-91.

(11) Kitchen, D. B. Decornez, H. Furr, J. R.; Bajorath, J. *Nat. Rev. Drug Discov.* **2004**, *3*, 935-49.

(12) Soto, C.; Satani, N. *Trends Mol. Med.* **2010**, *17*, 14-24.

(13) Kranjc, A. Bongarzone, S. Rossetti, G. Biarnés, X. Cavalli, A. Bolognesi, M. L. Roberti, M. Legname, G.; Carloni, P. *J. Chem. Theory Comput.* **2009**, *5*, 2565-2573.

(14) Biarnés, X. Bongarzone, S. Vargiu, A. V. Carloni, P.; Ruggerone, P. *J. Comput. Aided Mol. Des.* **2011**, *25*, 395-402.

(15) Kuwata, K. Nishida, N. Matsumoto, T. Kamatari, Y. O. Hosokawa-Muto, J. Kodama, K. Nakamura, H. K. Kimura, K. Kawasaki, M. Takakura, Y. Shirabe, S. Takata, J. Kataoka, Y.; Katamine, S. *Proc. Natl. Acad. Sci. U S A* **2007**, *104*, 11921-6.

(16) Boehr, D. D. Nussinov, R.; Wright, P. E. *Nat. Chem. Biol.* **2009**, *5*, 789-96.

(17) Koshland, D. E. *Proc. Natl. Acad. Sci. U S A* **1958**, *44*, 98-104.

(18) Doh-ura, K. *Rinsho shinkeigaku* **2009**, *49*, 946-8.

(19) Zhang, H.-Y. *Biochem. Biophys. Res. Commun.* **2006**, *351*, 578-81.

(20) Bongarzone, S.; Bolognesi, M. L. *Exp. Opin. Drug Discovery* **2011**, 1-18.

(21) Bongarzone, S. Tran, H. N. A. Cavalli, A. Roberti, M. Rosini, M. Carloni, P. Legname, G.; Bolognesi, M. L. *ChemMedChem* **2011**, *6*, 601-5.

(22) Bongarzone, S. Tran, H. N. A. Cavalli, A. Roberti, M. Carloni, P. Legname, G.; Bolognesi, M. L. *J. Med. Chem.* **2010**, 8197-8201.

(23) Gaeta, A.; Hider, R. C. *British J. Pharm.* **2005**, *146*, 1041-59.

(24) Legname, G. Baskakov, I. V. Nguyen, H.-O. B. Riesner, D. Cohen, F. E. DeArmond, S. J.; Prusiner, S. B. *Science* **2004**, *305*, 673-6.

(25) Milhavet, O. McMahon, H. E. Rachidi, W. Nishida, N. Katamine, S. Mangé, A. Arlotto, M. Casanova, D. Riondel, J. Favier, A.; Lehmann, S. *Proc. Natl. Acad. Sci. U S A* **2000**, *97*, 13937-42.

(26) Pamplona, R. Naudí, A. Gavín, R. Pastrana, M. a; Sajnani, G. Ilieva, E. V. Río, J. A. Del; Portero-Otín, M. Ferrer, I.; Requena, J. R. *Free Radic. Biol. Med.* **2008**, *45*, 1159-66.

(27) Kim, J. I. Choi, S. I. Kim, N. H. Jin, J. K. Choi, E. K. Carp, R. I.; Kim, Y. S. *Ann. N. Y. Acad. Sci* **2001**, *928*, 182-6.

(28) Singh, N. Singh, A. Das, D.; Mohan, M. L. *Antioxid. Redox Signal.* **2010**, *12*, 1271-94.

(29) Arlt, S. Kontush, A. Zerr, I. Buhmann, C. Jacobi, C. Schröter, A. Poser, S.; Beisiegel, U. *Neurobiol. Disease* **2002**, *10*, 150-6.

(30) Rana, A. Gnaneswari, D. Bansal, S.; Kundu, B. *Chem. Biol. Interac.* **2009**, *181*, 282-91.

(31) Lehmann, S. *Curr. Opin. Chem. Biol.* **2002**, *6*, 187–192.

(32) Perry, V. H. Cunningham, C.; Boche, D. *Curr. Opin. Neurology* **2002**, *15*, 349-54.

2. Introduction to Prion Diseases

Prion diseases or transmissible spongiform encephalopathies (TSEs) are a group of neurological disorders, for which there is neither early diagnosis nor a cure.[1,2] They include bovine spongiform encephalopathy (BSE) of cattle, scrapie of sheep, chronic wasting disease (CWD) of deer, moose and elk, Creutzfeldt-Jakob (CJD) and Gerstmann-Sträussler-Scheinker (GSS) diseases of humans.[3] The human pathology has three distinct aetiologies: they might be autosomal dominantly inherited conditions; acquired from exposure to prions; or they might arise sporadically.[4,5]

In the'90s, more than 280,000 cattle suffering from BSE (**Figure 2**)[c] provoked a worldwide food crisis with huge economic consequences for the European Union and other countries.[6]

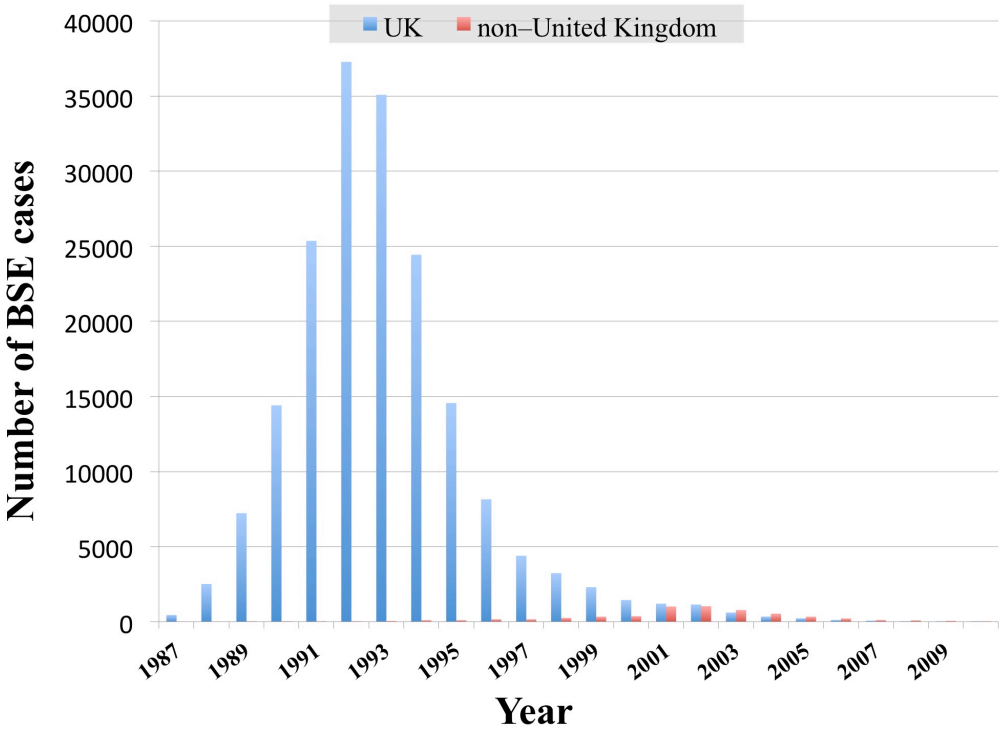

Figure 2. Incidence of BSE. Reported BSE cases in the United Kingdom (UK) and in countries and states excluding the UK. Non–United Kingdom BSE events include cases from countries of the European Union and outside the European Union (Canada, Israel, Liechtenstein, Japan, Switzerland, and the United States).

[c] http://www.oie.int/en/animal-health-in-the-world/bse-specific-data/number-of-reported-cases-worldwide-excluding-the-united-kingdom and http://www.oie.int/en/animal-health-in-the-world/bse-specific-data/number-of-cases-in-the-united-kingdom

In addition, transmission of BSE to humans is believed to have caused ≥ 200 cases of variant CJD (vCJD)[d]. In particular, vCJD has occurred in several areas of the world (see **Figure 3**).

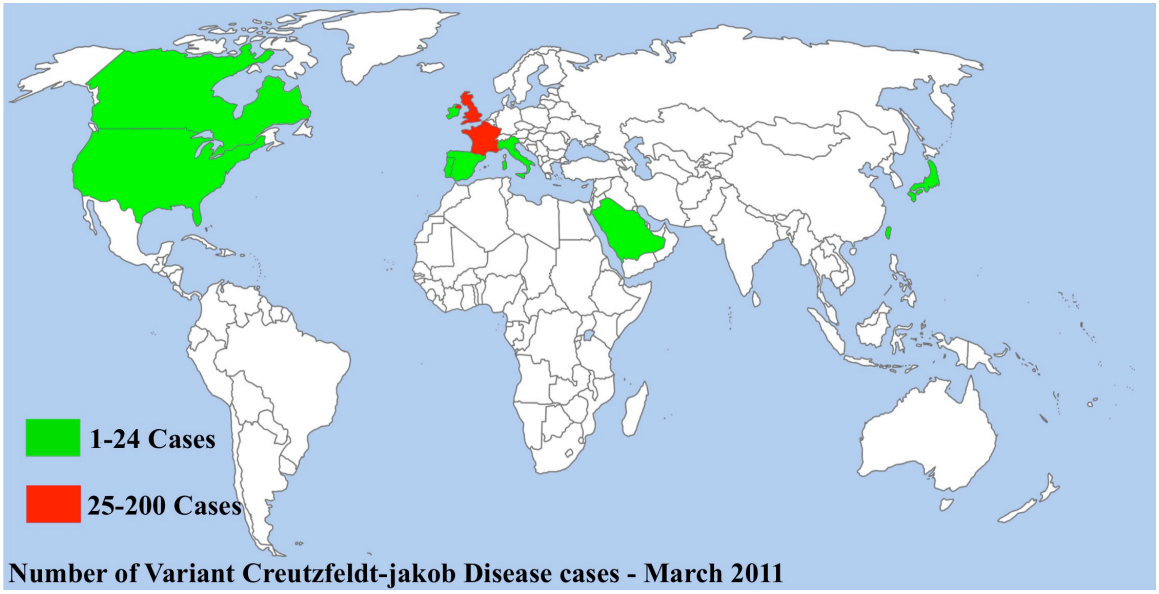

Figure 3. Geographic distribution of variant of Creutzfeldt-Jakob disease. vCJD occurs mainly in United Kingdom and France. The map was built from cases reported in the vCJD Web site.[d] Update to March 2011

Prion diseases are characterized by widespread neurodegeneration; therefore, affected individuals or animals exhibit clinical symptoms of both cognitive and motor dysfunction. The typical microscopic features of prion diseases are vacuolation of the grey matter of the central nervous system (CNS), prominent neuronal loss, exuberant reactive astrogliosis and a variable degree of cerebral accumulation of PrP^{Sc} aggregates.[1,2]

2.1. The prion-only hypothesis

Despite their rare incidence, prion diseases have captured broad consideration from the scientific community due to the unorthodox mechanism by which prion diseases are transmitted. According to the "protein-only hypothesis", in the CNS of the infected host, PrP^{C} is converted into an abnormal insoluble amyloidogenic isoform, that is PrP^{Sc} or prion.[2] The latter acts as a template for PrP^{C} leading to nascent PrP^{Sc} molecules. The process of conversion is associated with

[d] http://www.cjd.ed.ac.uk/vcjdworld.htm

conformational changes of secondary structure from α-helices to β-sheets. The term "prion" (a small **pro**teinaceous **in**fectious particle that is resistant to inactivation by most procedures that modify nucleic acids) was proposed by Prof. S. B. Prusiner to distinguish the infectious pathogen that causes prion diseases from viruses and viroids.[7] The infectious principle consists purely of protein and is capable of replicating and transmitting infections without the need for informational nucleic acids.[7] Numerous experiments have provided evidence that PrP^C is a key player in prion replication as well as in prion-induced neurodegeneration.[8] PrP^C expression is categorically required for neurodegeneration in host neurons, because the presence of PrP^{Sc} alone does not cause disease.[9] Indeed mice lacking the prion gene are resistant to the infection.[10,11]

2.2. Structural chemistry of PrP^C

PrP^C is a normal cell-surface glycoprotein linked to the plasma membrane by a glycosylphosphatidylinositol (GPI) membrane anchor. In humans, PrP^C is a 253 amino acids (aa) protein (see **Figure 4A**), which has a molecular weight of 35-36 kDa. The preprotein PrP^C is produced as a precursor protein containing two signals peptides. The 22 amino acids (signal peptide) at the N-terminus targets the protein to the endoplasmic reticulum, while the 23 amino acid sequence at the C-terminus is essential for the addition of the GPI moiety. Peptide 1–22 is cleaved as signal peptide during trafficking, and peptide 230–253 is replaced by the glycosyl-phosphatidylinositol-anchor (see **Figure 4A**).[7] Following the cleavage of the signal peptides, most of mammalian PrP^C is exported to the cell surface as an N-glycosylated protein.

As indicated in **Figure 4B**, PrP^C containing an amino flexible, random coil sequence that spans approximately half of its amino-acid residues, and a carboxy C-terminal globular domain (GD) of about 100 aa, the major structural features of which are remarkably preserved among both mammalian and non-mammalian species. N-terminal PrP^C contains two hexarepeats and five octarepeats. The octapeptide repeats can coordinate Cu^{2+} ions in cooperative fashion with high affinity, and display weaker binding properties towards other divalent cations, such as Zn^{2+}, Fe^{2+}, Mn^{2+} and Ni^{2+}.[12] The tridimensional structure of the GD of PrP^C was determined by nuclear magnetic resonance.[13-17] This is arranged in three α-helices corresponding to residues 144–154, 173–194, and 200–228, interspersed with an antiparallel β-pleated sheet formed by β-strands at residues 128–131 and 161–164. A single disulfide bond is found between cysteine residues 179 and 214 (in human numbering).[16,18]

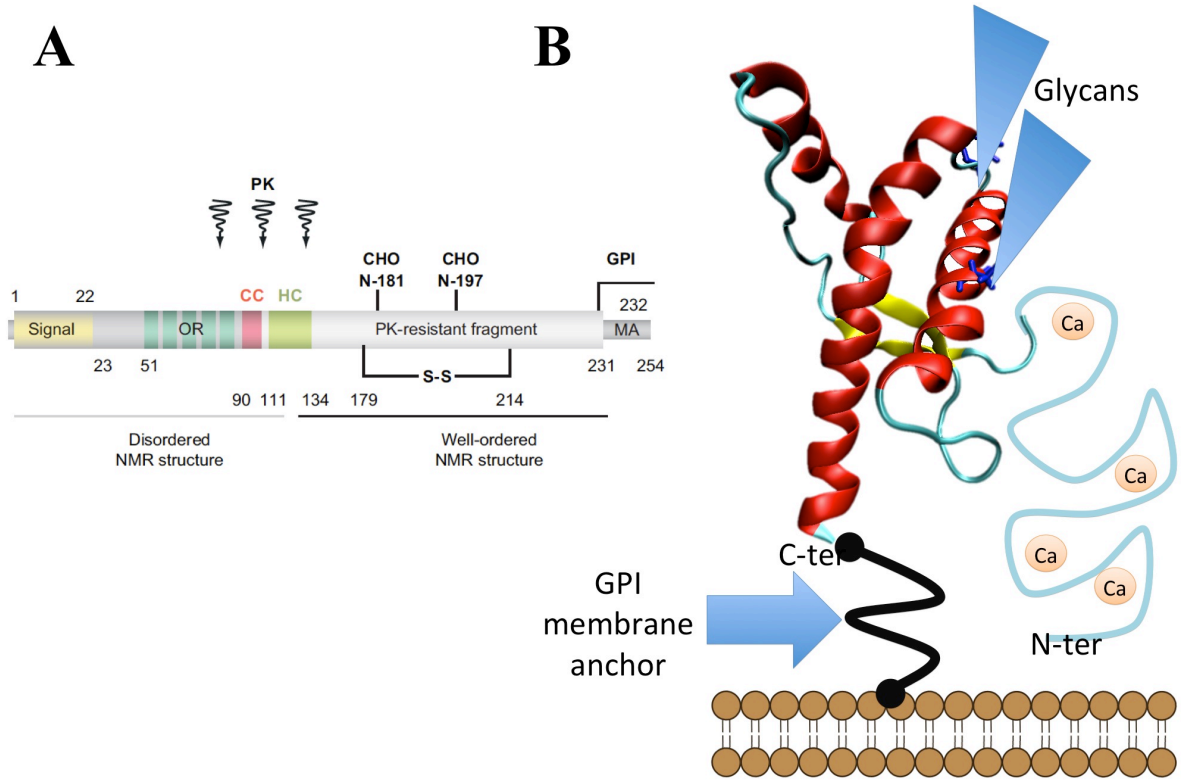

Figure 4. A) Schematic representation of the primary structure of PrP^{C} and its post-translational modifications. S-S, single disulfide bridge; MA, membrane anchor region; the proteinase K (PK) resistant core of PrP^{Sc} is depicted in grey; the approximate cutting site within PrP^{Sc} is indicated by the arrow. The size of the PK resistant fragment is variable, being cut at various positions between amino acids 78-102. B) Schematic representation of the PrP^{C} showing its GPI membrane anchor, the two N-linked glycans and the octapeptide repeats that bind metal ions.

Full-length PrP^{C} is found in non-, mono-, or diglycosylated forms, corresponding to the variable occupancy of residues Asn-181 and Asn-197 in human PrP^{C} and Asn-180 and Asn-196 in mice.[19,20]

2.3. Physiological processes involving PrP^{C}

Although PrP^{C} is highly expressed in the CNS, its biological role is not well established.[21] Several processes are influenced by PrP^{C}. Neurite outgrowth, including growth of axons and dendrites, are reduced in neurons lacking PrP^{C}.[22] Other processes include neuronal survival, neurite outgrowth, synapse formation, maintenance, and function, and maintenance of myelinated fibers (reviewed in 21, see **Figure 5**). The prion protein has been considered to function as an antioxidant, a metal transporter, a cell adhesion molecule, and a signal transducer.[23-25] **Table 1** summarizes all the cellular processes in which PrP^{C} is demonstrated to be involved.[21] A possible role of PrP^{C} as a

cellular receptor for the amyloid β-oligomers implicated in Alzheimer's disease has been suggested,[26] however, this remains controversial.[27,28]

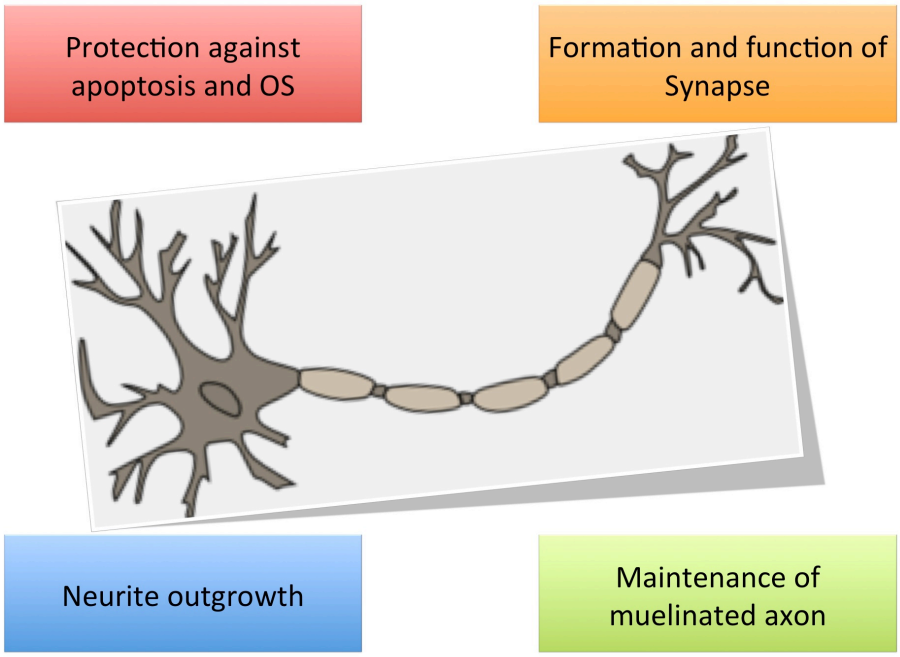

Figure 5. Physiological functions proposed for PrP^C (Adapted from ref. 21).

Table 1. Cellular distribution and activities of PrP^C in cell types in which known or putative functions have been described (Adapted from ref. 1).

Cell type	Process	Function
Neuron	Neuritogenesis	Adhesion, signalling
	Synaptogenesis, polarization	Signalling
	Survival, trophic effects	Anti-apoptotic
		Pro-apoptotic
	Copper binding	Copper endocytosis
		Copper homeostasis
		SOD activity
	Redox homeostasis	Signalling
Neural stem cells	Neurogenesis	Unknown
	Differentiation	Unknown
Hematopoietic stem cells	Long-term renewal	Anti-apoptotic? Homing?
T cells	Activation	Signalling?
	Development	Antioxidant
Leukocytes	Differentiation	Unknown
	Phagocytosis	Unknown
	Inflammatory response	Homing

2.4. Structural conversion from PrP^C to PrP^{Sc}

There are two models to explain $PrP^C \rightarrow PrP^{Sc}$ conformational conversion.

The "template-directed refolding" hypothesis predicates an instructionist role for PrP^{Sc} on PrP^C (**Figure 6A**). According to this model, a high energy barrier is preventing the conversion from PrP^C to PrP^{Sc}, therefore the need of an exogenously introduced PrP^{Sc} molecule is necessary for the replication to start: PrP^{Sc} interacts with and converts an endogenous molecule of PrP^C into a newly formed, β-sheet rich PrP^{Sc} isoform. The newly formed PrP^{Sc} molecule, in turn, can transform other endogenous PrP^C molecules. This hypothesis is supported by several experiments. Transgenic mouse studies have provided genetic[29] and biochemical[30] evidence that the conversion of PrP^C to PrP^{Sc} occurs through the formation of a PrP^C/PrP^{Sc} complex. However, such a complex has never been isolated to purity. Nevertheless, the existence of such partially structured monomeric folding

intermediate of the prion protein is also suggested by hydrogen-deuterium exchange[31] and high-pressure spectroscopy experiments.[32]

Alternatively, the "seeded nucleation model" proposes that PrP^{Sc} exists in equilibrium with PrP^{C}. PrP^{C} and PrP^{Sc} are in a reversible thermodynamic equilibrium, which strongly favours the PrP^{C} conformation. Only when several molecules of PrP^{Sc} are aggregated (into oligomeric or fibril-like seeds), the replication can start. In this case, the seed recruits other monomeric PrP^{Sc} molecules and stabilizes them. The fragmentation of the aggregates increases the number of seeds that can actively recruit new PrP^{Sc} molecules, thus accelerating the replication process, the prion accumulation, and finally giving rise to the disease. In a nondisease state, such equilibrium would be shifted toward the PrP^{C} conformation, such that only small amounts of PrP^{Sc} would coexist with PrP^{C}. But in this case, PrP^{Sc} could not represent the infectious agent, since it would be ubiquitous. According to this hypothesis, the infectious agent would consist of a highly ordered aggregate of PrP^{Sc} molecules. The aggregated state would be an intrinsic property of infectivity. Monomeric PrP^{Sc} would be innocuous, but it might be prone to incorporation into nascent PrP^{Sc} aggregates (**Figure 6B**).

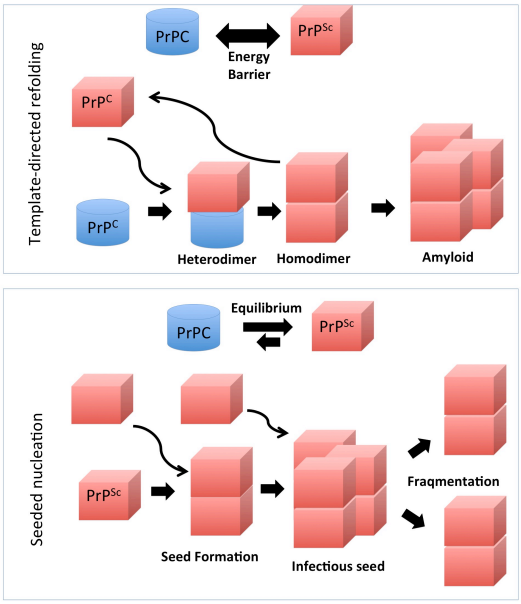

Figure 6. Theoretical models for the formation of PrP^{Sc} amyloid from PrP^{C}

These two models cannot be considered mutually exclusive, and indeed the different aetiology of prion diseases (genetic, infective or sporadic) can be fitted in both the models:[33-35]

- In *inherited* disease, genetic mutation of the *PRNP* gene may destabilize the tertiary structure of PrP^{C} promoting the spontaneous conversion to PrP^{Sc}, or these mutations can lower the energy barrier from PrP^{C} to PrP^{Sc}, thus facilitating and accelerating PrP^{Sc} aggregation.
- In *infective* disease, the ingestion of an already preformed PrP^{Sc} aggregate can directly convert endogenous PrP^{C} molecules, or act as an already preformed PrP^{Sc}-aggregate and recruit PrP^{Sc} molecules.
- In *sporadic* form, biochemical modifications (whose characteristics are at present unknown) of PrP^{C}, or other environmental aspects, can perturb PrP^{C} tertiary structure and then favour the conversion into PrP^{Sc}. However, if and what biochemical and environmental mechanisms are at the basis of sporadic form is yet to be clarified.

2.5. PrP^{Sc} models

Extensive characterization of PrP^{Sc} was undertaken in an attempt to understand its structural features. A key problem with much of the literature on PrP^{Sc} fold is that there are considerable disagreements.[36] As shown in **Figure 7**, several different structural models of PrP^{Sc} have been promulgated based on a range of theoretical and experimental data. The three most prominent are:

• A β-helix based on fiber diffraction and electron microscopy studies of brain-derived PrP^{Sc}.[37,38] The first of these models, guided by digital reconstitution of two-dimensional, p3 symmetry crystals sometimes observed in PrP^{Sc} isolates, postulates a β-helical structure.[37] By threading a portion of the prion protein sequence through a known β-helical fold, it was proposed that residues ~90-175 form left-handed β-helices, which associate into trimers, with two preserved α-helices (see **Figure 7A**).

• A parallel and in-register β-sheet model proposed from spin labelling and electron paramagnetic resonance studies of recombinant misfolded prion protein.[39] Structural data suggest that prion protein conversion to amyloid fibrils involves major refolding of the entire α-helical domain. Indeed, two recent studies, using hydrogen-deuterium exchange[40] and site-directed spin labelling,[39] indicate that the β-sheet core of the human prion protein amyloid maps to the C-terminal part of PrP encompassing residues ~160/ 170-220. Distance information obtained from spin labelling studies demonstrated that residues within this core region form single-molecule layers that stack on top of one another with parallel in-register alignment of β-strands (see **Figure 7B**).

• An extension of the native β-sheet has been proposed from immunologic studies[41] and molecular dynamics simulations at low pH.[42] This model depicts a trimeric oligomer, which is postulated to stack in a spiral-like manner to form higher-order protofibrillar aggregates. Here, the amyloid β-core consists of a three-β-strand sheet (residues 116-119, 129-132, and 160-164, respectively), and

an isolated strand (residues 135-140), with all three α-helices retaining their native monomeric conformation (see **Figure 7C**)

The lack of agreement on even basic features of the PrP^{Sc} fold may derive in part from an inherent heterogeneity in misfolding. Although there is one native structure for PrP^{C}, there may be multiple misfolded structures, each arising from a local energetic minimum in the conformation space of PrP^{Sc}. Environmental conditions, including the presence of PrP^{Sc} seeds of a particular subtype, and variation in the PrP primary sequence may steer PrP^{C} molecules into one of a range of misfolded geometries.

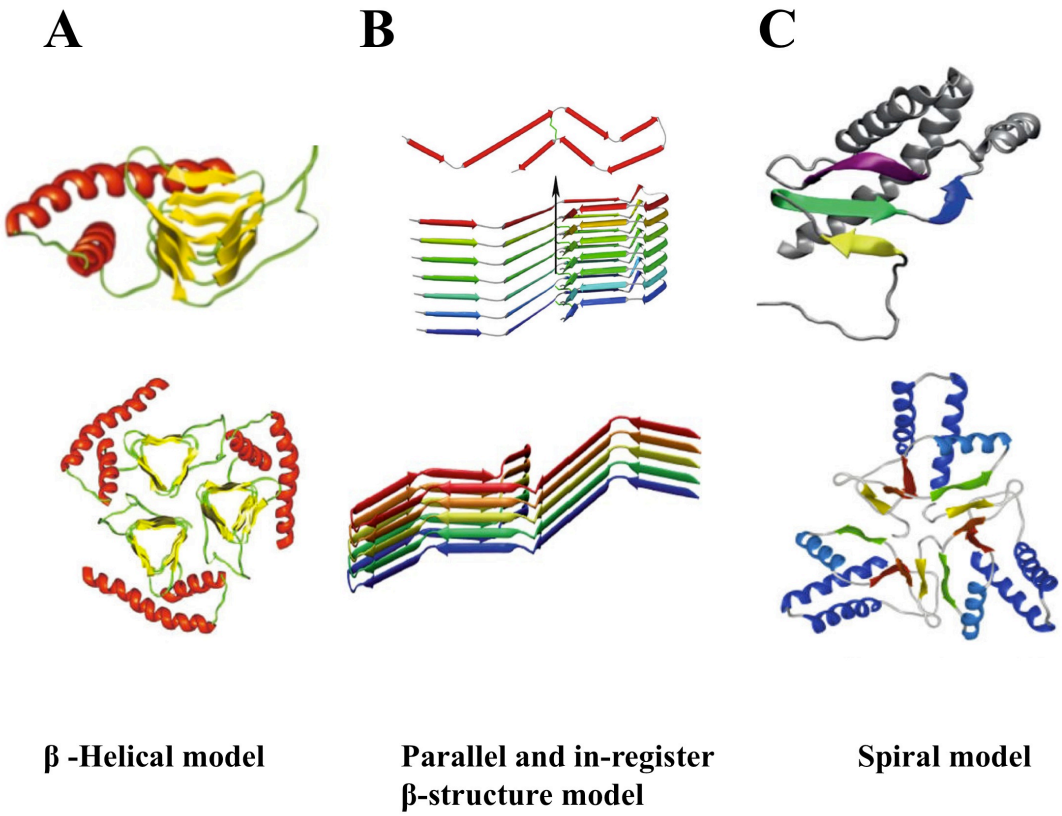

Figure 7. Structural models of PrP^{Sc} and/or PrP amyloid fibrils. A) β-Helical model, where residues ~90-175 are shown to form left-handed β-helices that associate into trimers, leaving the most C-terminal helices of monomeric PrP^{C} intact.[37] B) Parallel and in-register β-structure model determined experimentally for recombinant PrP amyloid fibrils.[40] In this model, residues, 160-220, form the PrP amyloid core with tight interdigitation of side chains. Individual monomers stack to form single-molecule layers so that the same residues are perfectly aligned. C) Spiral model depicting the amyloid core as being comprised of a three stranded β-sheet and an isolated β-strand, with complete retention of all three native α-helices.[42]

Since each study described above employed a different methodology for generating PrP^{Sc}, it is possible that each one accessed a different stable misfolded conformer, some or all of which may be relevant in disease. This is supported by the well-known existence of strains in prion disease with distinct neuropathological features.[43] In this sense the search for the PrP^{Sc} structure, while not futile, may yield a plurality of valid possibilities rather than a single definitive answer.[36]

However, the divergent models provided by structural studies may ultimately reflect the conformational variability of PrP aggregates associated with TSE disorders where, in addition to the existence of multiple prion strains, there are indications that neurotoxic and infectious PrP are distinct conformational species. Clearly, despite recent advances, major discoveries in structural biology of mammalian prions are still to be made.[44] Understanding molecular mechanism of protein misfolding and aggregation is useful to aim to inhibit or reverse the conformational changes as a therapy to protein conformational disease.

2.6. Prion neuroinvasion in humans

Neuroinvasion typically begins upon ingestion of the PrP^{Sc} agent. Strong evidence suggests that the feeding of BSE-contaminated meat and bone meal to livestock was responsible for the outbreak of BSE in England, and subsequent consumption of diseased cattle by humans is believed to be responsible for the emergence of vCJD.[2,45] After oral infection PrP^{Sc} can be found in Peyer's patches in the gut and is followed by prion propagation to splenic lymphoid tissue and/or in gut-associated lymphoid tissue (GALT; including tonsil), resulting in prion transport by splenic innervation to the brainstem and spinal cord.[44,46]

The route of infection is defined by three phases (see **Figure 8**):

- The first phase is, after ingestion, the invasion of the gut-associated lymphoid tissues (GALT). Onodera et al. discovered that neonatal Fc receptor (nFcR), which contributes to the uptake of maternal antibodies into the intestine, plays a role in PrP^{Sc} incorporation into the intestine.[47] Another study demonstrated that the iron binding protein ferritin forms a complex with a fragment PrP^{Sc} to enhance the transport of PrP^{Sc} in an intestinal endothelial cell model, suggesting a role for ferritin in transport of infected prion protein across the intestine.[48]
- After incubation in lymphoid tissue such as the GALT and spleen, the PrP^{Sc} spreads to the CNS via the enteric nervous system. This invasion occurs in the retrograde direction along efferent fibers of both sympathetic and parasympathetic nerves
- The final phase is the infection of the spinal cord and brain leading to characteristic spongiform degeneration and astroglial activation.

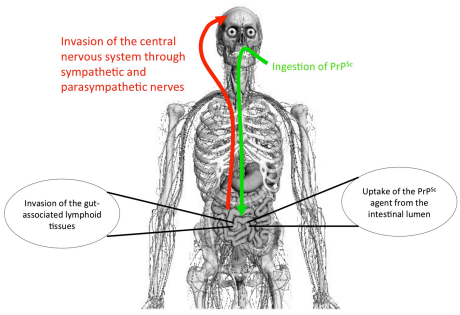

Figure 8. Schematic representation of the potential mechanism of neuroinvasion in transmissible spongiform encephalopathies. (i) Initial uptake of the PrP^{Sc} agent from the intestinal lumen has been proposed to occur through a number of alternative mechanisms. (ii) After amplification of the TSE agent in lymphoid tissue such as the GALT and spleen, invasion of the central nervous system is believed to proceed through sympathetic and parasympathetic nerves.

2.7. Cellular Mechanisms of Prion Toxicity

Once PrP^{Sc} fibrils are formed, the cellular pathological mechanisms by which prion exert their neurotoxic effects are still under debate.[49] Three mechanisms have been proposed as possible mechanisms of neurotoxicity.[5] These are:

- "loss-of-function" mechanism

It remains possible that prion neurodegeneration is related, at least in part, to "loss of function" of PrP^{C}. But the "loss-of-function" mechanism appears to be incompatible with the observation that $PRNP^{0/0}$ mice are relatively normal and do not display features of prion disease (see **Figure 9**).[50] In potential agreement with this hypothesis, Brown and co-workers have shown that lack of PrP expression results in neuronal sensitivity to oxidative stress; however, this did not lead to neurodegeneration.[51]

- "gain of function" mechanism

Based on this hypothesis, a toxic, possibly infectious, product is produced during the process of conversion of PrP^{C} to PrP^{Sc}. The protein aggregates, accumulated in the nervous system, are presumed to possess a novel neurotoxic activity that is independent of the normal, physiological function of the parent protein (**Figure 9**). For example, PrP^{Sc} aggregates may block axonal transport, interfere with synaptic transmission, or physically damage cellular membranes.[8,21] In contrast, other studies show that accumulation of PrP^{Sc} within PrP^{C}-expressing tissue grafted into the brains of $PRNP^{0/0}$ mice does not damage the neighbouring PrP^{C}-null tissue[10] and the accumulation of PrP^{Sc} in glial cells around PrP^{C}-null neurons does not induce cell death in the knockout neurons, arguing against a direct toxic effect of PrP^{Sc} *per se.*

- "subversion-of-function" mechanism

Another possibility is that PrP^{Sc} subverts or modifies the normal function of PrP^{C} (the "subversion of function"), rather than causing a complete loss of PrP^{C} function (**Figure 9**). For example, the PrP^{C} activity might be altered after binding to PrP^{Sc} (or to another pathogenic intermediate), such that a neurotoxic rather than a neuroprotective stimulus is delivered.

However, the physiological function(s) of PrP^{C} is (are) still unknown, and a lot of controversies surrounding the several proposed functions of PrP^{C} are still under debate.

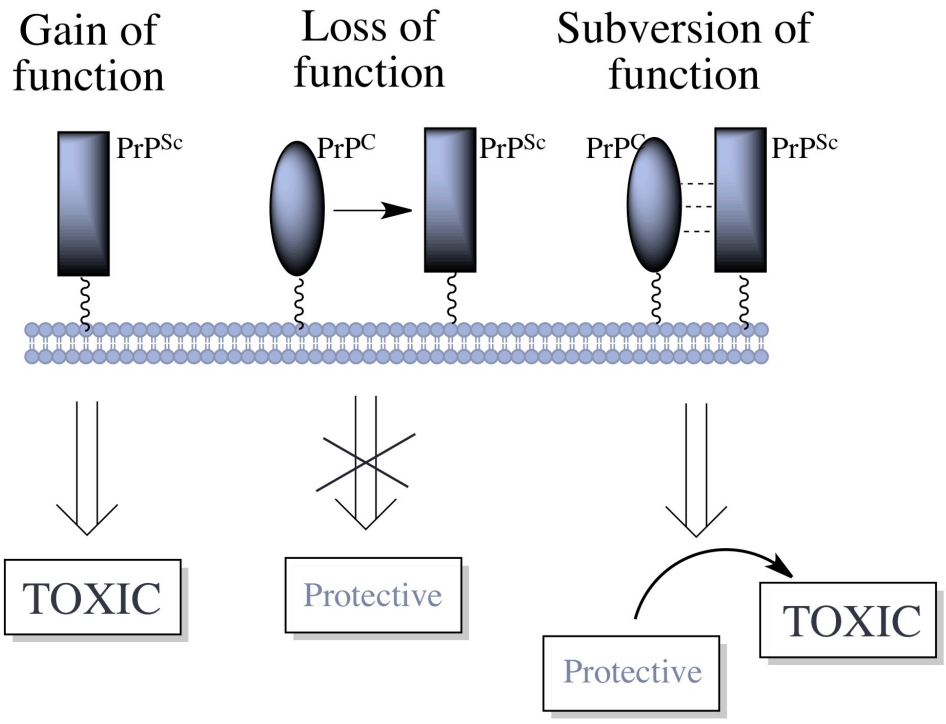

Figure 9. The "gain of function" mechanism: PrP^{Sc} possesses a novel neurotoxic activity that is independent of the normal function of PrP^{C}. The "Loss of function" mechanism: PrP^{C} possesses a normal, physiological activity, in this case neuroprotection, that is lost upon conversion to PrP^{Sc}. The "Subversion-of-function" mechanism: the normal neuroprotective activity of PrP^{C} is subverted by binding to PrP^{Sc} (Adapted from ref. 52)

2.8. Therapeutic approaches to prion diseases

Based on knowledge of prion cell biology, several strategies for intervention can be envisioned that target different stages of prion biogenesis and PrP^{Sc} formation and aggregation. Main strategies for intervention are shown in **Figure 10**.[53] These can be accomplished by:

- eliminating PrP^{C}
- stabilizing PrP^{C}
  - preventing PrP^{C} unfolding
  - interfering with binding of PrP^{C} to PrP^{Sc}
- enhancing PrP^{Sc} clearance.

Several studies indicate that the removal of PrP^{C} is important for subsequent conversion into PrP^{Sc}. Therefore, targeting PrP^{C} synthesis or cell surface localization or enhancing endocytosis of PrP^{C} might be viable anti-prion strategies.

PrP^{C} and PrP^{Sc} are localized in specific regions of the cellular membrane, called lipid rafts, rich in cholesterol and sphingolipids. Lipid rafts have been proposed as potential targets for PrP^{Sc} formation.[54] Therefore, potential compounds, which change membrane cholesterol levels altering PrP^{C} and PrP^{Sc} distribution, might block prion conversion. The statins, lovastatin and squalestatin, are inhibitors of two enzymes of the cholesterol synthetic pathway. Treatment of the cells with lovastatin[55] or squalestatin[56] prevents the accumulation of PrP^{Sc} in infected cell lines. The antifungal drug Amphotericin B and its analogue, MS-8209, reduce PrP^{Sc} formation in cell culture by intercalation into and disruption of the cell membrane. Amphotericin B has also been shown to prolong incubation time of prion diseases in hamster.[57]

Among the compounds tested for inhibition of PrP^{Sc} accumulation in cultured cells, suramin was found effective.[58] Suramin treatment prevents the cell surface localization of PrP^{C} by binding to PrP^{C} and inducing its intracellular aggregation in the Golgi compartment.[58] The PrP^{Sc} aggregates are PK sensitive, and can be easily degraded by the cells and do not accumulate.[58] Polyanionic compounds like pentosan polysulfate (PPS) or dextran sulfate (DS) enhance endocytosis of PrP^{C}, thereby leading to its depletion at the cell surface.[59]

A major focus of drug discovery efforts has been the PrP conversion reaction. Many compounds have been shown to prevent the conversion by directly binding PrP^{C} and blocking the conversion

from PrP^{C} to PrP^{Sc}. An increasing number of studies have found that binders of PrP^{C} are potent antiprion compounds in scrapie-infected cell lines.[60-67]

PrP^{Sc} was the most obvious target for anti-prion therapeutics because it can easily be quantified by Western-blotting of proteinase K-resistant PrP^{Sc}. Currently cell-based assays are the most used method for screening anti-PrP^{Sc} compounds, although it is difficult to define the compound's mode of action in a "black box" cell assay where only the reduction of PrP^{Sc} levels is monitored. Thus, a compound shown to reduce PrP^{Sc} in cells may act by slowing formation or accelerating the breakdown of PrP^{Sc} and this may be through on- or off-target effects. The assumption that neurodegeneration derives from direct toxicity of PrP^{Sc} has been increasingly challenged, not least by the recognition of sub-clinical prion infection, the state in which animals can have high levels of infectivity without clinical disease. Targeting PrP^{Sc} may appear to be the most logical approach, but such targeting may be not enough to block the disease progression.[68] Phuan *et al.* have shown by using a chemical proteomics approach, that bis-acridine compounds, potent antiprion compounds,[69] interact selectively with PrP^{Sc}.[70]

Another strategy is devoted to enhance the cellular clearance of PrP^{Sc} (**Figure 10**). Treatment with the polycationic lipopolyamine DOSPA decreased the PrP^{Sc} levels in the cells by enhancing PrP^{Sc} clearance and blocking de novo formation of PrP^{Sc}.[71]

Further discussion of this issue can be found in ref. 35,46,68,72,73

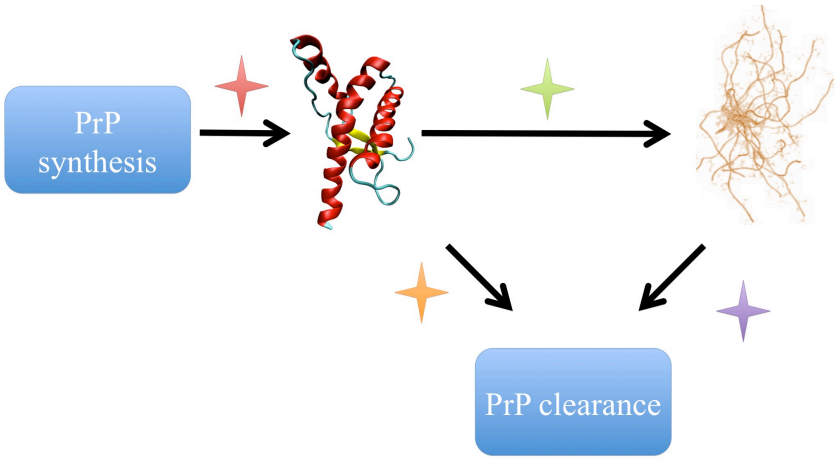

Figure 10. Potential therapeutic targets to block prion propagation.

2.9. Prion diseases: a multifactorial disorder

Nowadays the protein-only theory has become widely accepted and therefore current therapeutic strategies are primarily aimed at preventing conversion of $PrP^{C} \rightarrow PrP^{Sc}$. Targeting PrP^{C} has the potential to remove the substrate for the pathogenesis and is applicable regardless of the disease aetiology. While this hypothesis stands for in vitro conversion of PrP^{C} to PrP^{Sc}, the mechanism underlying in vivo conversion, although not fully elucidated yet, seems to be more complex, possibly involving other pathways.[74] During the last decade, it has been gradually accepted that prion disease pathogenesis involves a complex array of processes operating simultaneously and synergistically.[74]

These include:

(i) protein aggregation;[8,75]

(ii) oxidative stress (OS) accompanied by lipid and protein oxidation;[76-80]

(iii) reduced levels of potent free-radical scavenger, such as polyunsaturated fatty acids, α-tocopherol, and glutathione;[76-80]

(iv) unbalance of metal ions;[80,81]

(v) brain inflammation with activation of astrocytes and microglia.[82]

2.9.1. Oxidative stress (OS)

There is growing evidence that OS, induced by ROS or free radicals, plays key role in the pathogenesis of neurodegenerative disorders including prion diseases.[83] Cell culture experiments reveal that cerebellar cells lacking PrP^{C} are more sensitive to OS and undergo cell death more readily than wild-type cells.[78,84,85] Choi *et al.* have reported that the levels of malondialdehyde (MDA) and heme oxygenase-1, which are oxidative stress markers, and the generating rate of free radicals, especially superoxide anion (O^{2-}), were significantly increased in the brains of scrapie-infected mice (**Figure 11**).[83,85-87] Increased lipid peroxidation and reduced activities of cytochrome c oxidase and ATPase were observed in mitochondria from scrapie-infected animals.[88] In the mitochondria of infected mice, level of oxidized form of glutathione and calcium content were markedly increased, whereas mitochondrial membrane potential and energy metabolites (ATP/ADP ratio) were decreased.[89] Milhavet *et al.* demonstrated that prion-infected hypothalamic neuronal GT1 cells displayed a higher sensitivity to induced oxidative stress over non-infected cells.[78] In

addition, the infected cells presented an increased lipid peroxidation and signs of apoptosis associated with a dramatic reduction in the activities of the glutathione-dependent and superoxide dismutase antioxidant systems.[78] There are many evidences that PrP^C itself has a oxidative stress-protective activity.[90,91] Oxidative stress can therefore be the consequence of an increased production of reactive species or a decrease in the capacity of antioxidant defences to remove them, or both.[79] Some studies have confirmed the role of PrP^C in the OS by pointing out deregulations of nitric oxide metabolism. Ovadia *et al.* reported a decrease in neuronal nitric oxide synthase (NOS) activity associated with an abnormal folding of the enzyme in infected neuroblastoma cell cultures and in brain extracts of infected mice.[92] In a latter study, the same group confirmed these results in the brain of PRNP0/0 mice and suggested that PrP^C could play a role in the cellular targeting of the neuronal NOS.[93]

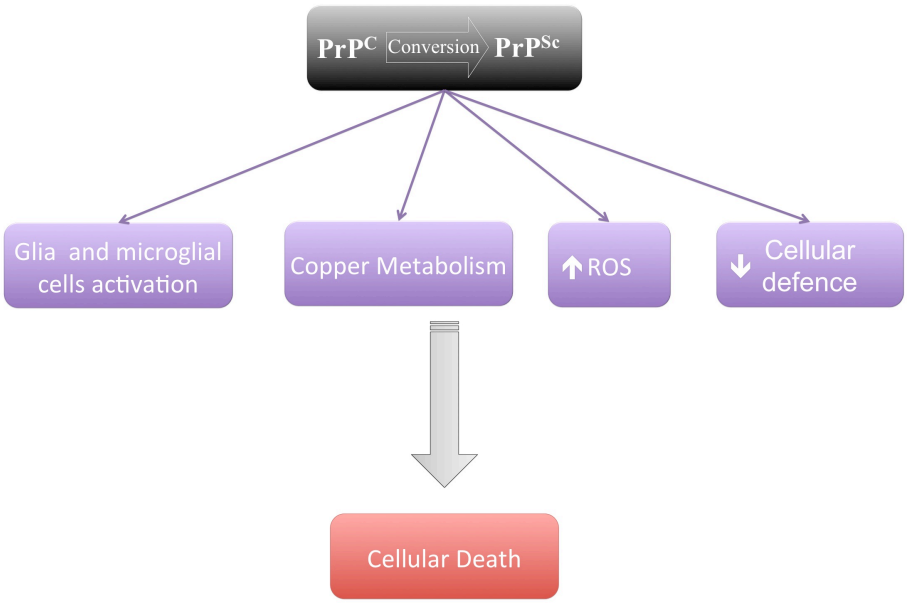

Figure 11. Conversion of PrP^C into PrP^{Sc} increases the sensitivity of neuronal cells to oxidative stress through one or several of the following mechanisms: i) Cu metabolism could be modified influencing the redox status or the oxidative enzyme systems of the cell; ii) the production of ROS could be directly modified through, for example, the SOD-like activity of PrP^C; and iii) the conversion could act on protein regulation and/or transcription factors involved in response to oxidative stress. Moreover, prion infection activates glia and microglial cells triggering the death of already impaired neurons.

2.9.2. Metal ions and prion diseases

PrP^C may function as a metal binding protein because divalent cations such as Cu^{2+}, Zn^{2+} and Mn^{2+} can bind to octapeptide repeat sequences in the N-terminus.[12,81] Since the binding of these metals to the octapeptide has been proposed to influence both structural and functional properties of prion

proteins, alterations in transition metal levels might alter the course of the disease.[81,94-96] In the following, we are going to depict the critical function of metal ions in the physiopathology of prion diseases.[94]

2.9.2.1. Copper and PrP^C

PrP^C binds five Cu^{2+} ions under physiological conditions. Four copper-binding sites are within the octapeptide repeat sequence Pro-His-Gly-Gly-Gly-Trp-Gly-Gln, between residues 61 and 91 of PrP^C (human numbering). This region binds copper ions with femto- and nanomolar affinity, and other metal ions like Ni^{2+}, Zn^{2+}, and Mn^{2+} with affinities lower by at least three orders of magnitude. The fifth copper-binding domain is between residues 91 and 111 and is coordinated by histidine residues at positions 96 and 111 of the PrP^C sequence.[97] Also, the high conservation of the metal binding regions among various mammalian species indicates a relation between copper and the prion protein.[98]

The functional role of PrP^C in copper uptake from the extracellular milieu has been studied in cultured cells and mouse models.[81] In mouse neuroblastoma cells, extracellular copper ions stimulate the endocytosis of PrP^C, supporting the idea that PrP^C may bind and deliver extracellular copper ions to endocytic compartments. Deletion of the octapeptide repeat region or mutation of His residues within this region abolishes copper uptake by PrP^C, emphasizing the role of this region in copper binding.[80]

Recently, studies have been undertaken to verify the concentrations of metals in mice affected by prion disease. Interestingly, changes of copper levels were observed in samples of brain, liver and blood. In particular, a reduction of Cu^{2+} was found in the brain, while significant increases were observed in the liver.[91,99] This evidence suggests a role of the prion protein as a possible copper transporter in the CNS. Additional studies have shown that over-expression of PrP^C resulted in higher binding of copper in the membrane fraction, which further supports the possible notion that PrP^C is a copper transporter.[98]

Not only does the PrP^C seem to act as a copper transporter, but studies have also shown PrP^C has superoxide dismutase (SOD)-like activity, enabling its effective functioning as an antioxidant in CNS.[100] Studies with recombinant prion protein showed proper protein folding in the presence of copper, endowing PrP^C with antioxidant capacities. Further, two atoms of copper bound to PrP^C were sufficient for SOD-like activity.[12] However, although the SOD-like function of PrP^C was demonstrated in vitro,[101] other studies have disproved the possibility that prion protein functions as a SOD-like protein in vivo.[102]

Together, these studies suggest a role for PrP^C in cellular copper uptake and transport,[103] maintenance of physiologically safe copper concentrations at the synapse, upregulation of PrP^C expression in response to copper,[80,95] although authentication of these interactions in functional assays is incomplete.

2.9.2.2. Manganese and PrP^C

An interesting feature of PrP^C is that it does not only bind copper specifically, but also manganese. A study undertaken on a mouse scrapie model has demonstrated changes in the levels of copper and manganese in the brain of scrapie-infected mice prior to the onset of clinical symptoms.[100,104] Brazier *et al.* have used isothermal titration calorimetry to identify the manganese binding sites in $mPrP^C$. This study indicated that the main manganese binding site is associated with His-95 in the so-called "fifth site" normally associated with copper binding.[105]

2.9.2.3. Iron and PrP^C

The interaction of PrP^C with iron deserves a special note, because iron is required for optimal neuronal growth, and, like copper, is considered a toxin because of its ability to exist in two oxidation states, ferric (Fe^{3+}) and ferrous (Fe^{2+}).[80] Free iron can catalyze the conversion of hydrogen peroxide to reactive hydroxyl radicals by the Fenton reaction, resulting in oxidative damage. Furthermore, iron-dependent lipid peroxidation generates potentially toxic peroxyl/alkoxyl radicals, and iron is known to convert neutral catechols to neurotoxic intermediates, leading to neurotoxicity. Because imbalance of cellular iron homeostasis can result in the generation of ROS, the transport of iron in and out of the cells is tightly regulated. Within cells, iron is present in ferritin, which serves the general function of intracellular iron sequestration, detoxification, and storage. Free iron does not exist in physiological systems, and is always found bound to various iron transporting proteins and iron bound enzymes. More recently, Fernaeus *et al.* have demonstrated that iron regulation is disturbed in scrapie infected mouse neuroblastoma cells.[106,107] More recently Singh et al. have suggested a functional role for PrP^C in cellular iron uptake and transport.[108-110]

References

(1) Caughey, B.; Baron, G. S. *Nature* **2006**, *443*, 803-10.

(2) Prusiner, S. B. *Proc. Natl. Acad. Sci. U S A* **1998**, *95*, 13363.

(3) Prusiner, S. B.; DeArmond, S. J. *Ann. Rev. Neurosci* **1994**, *17*, 311-39.

(4) Aguzzi, A. *J. Neurochemistry* **2006**, *97*, 1726-39.

(5) Collinge, J. *Annual review of neuroscience* **2001**, *24*, 519-50.

(6) Aguzzi, A. Sigurdson, C.; Heikenwalder, M. *Ann. Rev. Pathology* **2007**.

(7) Prusiner, S. B. *Science* **1982**, *216*, 136-144.

(8) Aguzzi, A.; Calella, A. M. *Physiol. Rev.* **2009**, *89*, 1105.

(9) Büeler, H. Aguzzi, A. Sailer, A. Greiner, R. a; Autenried, P. Aguet, M.; Weissmann, C. *Cell* **1993**, *73*, 1339-47.

(10) Brandner, S. Isenmann, S. Raeber, A. Fischer, M. Sailer, A. Kobayashi, Y. Marino, S. Weissmann, C.; Aguzzi, A. *Nature* **1996**, *379*, 339-343.

(11) Brandner, S. Raeber, A. Sailer, A. Blättler, T. Fischer, M. Weissmann, C.; Aguzzi, A. *Proc. Natl. Acad. Sci. U S A* **1996**, *93*, 13148-51.

(12) Stöckel, J. Safar, J. Wallace, A. C. Cohen, F. E.; Prusiner, S. B. *Biochemistry* **1998**, *37*, 7185-93.

(13) Calzolai, L.; Zahn, R. *J. Biol. Chem.* **2003**, *278*, 35592-6.

(14) Calzolai, L. Lysek, D. A. Guntert, P. Schroetter, C. von; Riek, R. Zahn, R.; Wuthrich, K. *Proc. Natl. Acad. Sci. U S A* **2000**, *97*, 8340-8345.

(15) Riek, R. Hornemann, S. Wider, G. Billeter, M. Glockshuber, R.; Wuthrich, K. *Nature* **1996**, *382*, 180-182.

(16) Lopez Garcia, F. *Proc. Natl. Acad. Sci. U S A* **2000**, *97*, 8334-8339.

(17) Zahn, R. *Proc. Natl. Acad. Sci. U S A* **2000**, *97*, 145-150.

(18) Lysek, D. A. Schorn, C. Nivon, L. G. Esteve-Moya, V. Christen, B. Calzolai, L. Schroetter, C. von; Fiorito, F. Herrmann, T. Güntert, P.; Wüthrich, K. *Proc. Natl. Acad. Sci. U S A* **2005**, *102*, 640-5.

(19) Rudd, P. M. Endo, T. Colominas, C. Groth, D. Wheeler, S. F. Harvey, D. J. Wormald, M. R. Serban, H. Prusiner, S. B. Kobata, A.; *et al. Proc. Natl. Acad. Sci. U S A* **1999**, *96*, 13044.

(20) Lawson, V. A. Collins, S. J. Masters, C. L.; Hill, A. F. *J. Neurochemistry* **2005**, *93*, 793-801.

(21) Aguzzi, A. Baumann, F.; Bremer, J. *Ann. Rev. Neuroscience* **2008**, *31*, 439-77.

(22) Bremer, J. Baumann, F. Tiberi, C. Wessig, C. Fischer, H. Schwarz, P. Steele, A. D. Toyka, K. V. Nave, K.; Weis, J.; Aguzzi, A. *Nature Neuroscience* **2010**, *13*, 310-8.

(23) Martins, V. R.; Brentani, R. R. *J. Neurochemistry* **2002**, *41*, 353-355.

(24) Martins, V. R. Mercadante, a F. Cabral, a L. Freitas, a R.; Castro, R. M. *Brazilian J. Med. Biol. Res.* **2001**, *34*, 585-95.

(25) Wechselberger, C. *Exp. Cell Res.* **2002**, *281*, 1-8.

(26) Laurén, J. Gimbel, D. a; Nygaard, H. B. Gilbert, J. W.; Strittmatter, S. M. *Nature* **2009**, *457*, 1128-32.

(27) Calella, A. M. Farinelli, M. Nuvolone, M. Mirante, O. Moos, R. Falsig, J. Mansuy, I. M.; Aguzzi, A. *EMBO Mol. Med.* **2010**, *2*, 306-314.

(28) Balducci, C. Beeg, M. Stravalaci, M. Bastone, A. Sclip, A. Biasini, E. Tapella, L. Colombo, L. Manzoni, C. Borsello, T. Chiesa, R. Gobbi, M. Salmona, M.; Forloni, G. *Proc. Natl. Acad. Sci. U S A* **2010**, *107*, 2295-300.

(29) Prusiner, S. B. Scott, M. Foster, D. Pan, K. M. Groth, D. Mirenda, C. Torchia, M. Yang, S. L. Serban, D.; Carlson, G. A. *Cell* **1990**, *63*, 673-86.

(30) Meier, P. Genoud, N. Prinz, M. Maissen, M. Rulicke, T. Zurbriggen, A. Raeber, A. J.; Aguzzi, A. *Cell* **2003**, *113*, 49-60.

(31) Kuwata, K. Li, H. Yamada, H. Legname, G. Prusiner, S. B. Akasaka, K.; James, T. L. *Biochemistry* **2002**, *41*, 12277-83.

(32) Nicholson, E. M. Mo, H. Prusiner, S. B. Cohen, F. E.; Marqusee, S. *J. Mol. Biol.* **2002**, *316*, 807-15.

(33) Prusiner, S. B. *Science* **1991**, *252*, 1515-1522.

(34) Prusiner, S. B. *Trends Biochem. Sci.* **1996**, *21*, 482-7.

(35) Nunziante, M. Gilch, S.; Schätzl, H. M. *Chembiochem* **2003**, *4*, 1268-84.

(36) Guest, W. C. Plotkin, S. S.; Cashman, N. R. *J. Toxicol. Environ. Health A* **2011**, *74*, 154-60.

(37) Govaerts, C. Wille, H. Prusiner, S. B.; Cohen, F. E. *Proc. Natl. Acad. Sci. U S A* **2004**, *101*, 8342-7.

(38) Wille, H. Michelitsch, M. D. Guenebaut, V. Supattapone, S. Serban, A. Cohen, F. E. Agard, D. A.; Prusiner, S. B. *Proc. Natl. Acad. Sci. U S A* **2002**, *99*, 3563-8.

(39) Cobb, N. J. Sönnichsen, F. D. McHaourab, H.; Surewicz, W. K. *Proc. Natl. Acad. Sci. U S A* **2007**, *104*, 18946-51.

(40) Lu, X. Wintrode, P. L.; Surewicz, W. K. *Proc. Natl. Acad. Sci. U S A* **2007**, *104*, 1510-5.

(41) Cohen, F. E. *J. Mol. Biol.* **1999**, *293*, 313–320.

(42) DeMarco, M. L.; Daggett, V. *Biochemistry* **2007**, *46*, 3045-54.

(43) Hill, A. F. Joiner, S. Linehan, J. Desbruslais, M. Lantos, P. L.; Collinge, J. *Proc. Natl. Acad. Sci. U S A* **2000**, *97*, 10248-53.

(44) Cobb, N. J.; Surewicz, W. K. *Biochemistry* **2009**, *48*, 2574-85.

(45) Aguzzi, A.; Polymenidou, M. *Cell* **2004**, *116*, 313–327.

(46) Cashman, N. R.; Caughey, B. *Nature Rev. Drug Discov.* **2004**, *3*, 874-84.

(47) Uraki, R. Sakudo, A. Michibata, K. Ano, Y. Kono, J. Yukawa, M.; Onodera, T. *Plos One* **2011**, *6*, e17928.

(48) Mishra, R. S. Basu, S. Gu, Y. Luo, X. Zou, W.-Q. Mishra, R. Li, R. Chen, S. G. Gambetti, P. Fujioka, H.; Singh, N. *J. Neurosci.* **2004**, *24*, 11280-90.

(49) Hetz, C. Maundrell, K.; Soto, C. *Trends Mol. Medicine* **2003**, *9*, 237-43.

(50) Büeler, H. Fischer, M. Lang, Y. Bluethmann, H. Lipp, H. P. DeArmond, S. J. Prusiner, S. B. Aguet, M.; Weissmann, C. *Nature* **1992**, *356*, 577-82.

(51) Brown, D. R. Nicholas, R. S.; Canevari, L. *J. Neurosci. Res.* **2002**, *67*, 211-224.

(52) Harris, D. A.; True, H. L. *Neuron* **2006**, *50*, 353-357.

(53) Mallucci, G. Dickinson, A. Linehan, J. Klöhn, P.-C. Brandner, S.; Collinge, J. *Science* **2003**, *302*, 871-4.

(54) Taraboulos, A. Raeber, A. J. Borchelt, D. R. Serban, D.; Prusiner, S. B. *J. Mol. Biol.* **1992**, *3*, 851-63.

(55) Taraboulos, A. Scott, M. Semenov, A. Avrahami, D. Laszlo, L. Prusiner, S. B.; Avraham, D. *J. Cell Biol.* **1995**, *129*, 121.

(56) Bate, C. Salmona, M. Diomede, L.; Williams, A. *J. Bio. Chem.* **2004**, *279*, 14983-90.

(57) Xi, Y. G. Ingrosso, L. Ladogana, A. Masullo, C.; Pocchiari, M. *Nature* **1992**, *356*, 598-601.

(58) Gilch, S. Winklhofer, K. F. Groschup, M. H. Nunziante, M. Lucassen, R. Spielhaupter, C. Muranyi, W. Riesner, D. Tatzelt, J.; Schätzl, H. M. *EMBO J.* **2001**, *20*, 3957-66.

(59) Gabizon, R. Meiner, Z. Halimi, M.; Ben-Sasson, S. A. *J. Cell. Phys.* **1993**, *157*, 319-325.

(60) Touil, F. Pratt, S. Mutter, R.; Chen, B. *J. Pharm. Biomed Anal.* **2006**, *40*, 822-32.

(61) Reddy, T. R. K. Mutter, R. Heal, W. Guo, K. Gillet, V. J. Pratt, S.; Chen, B. *J. Med. Chem.* **2006**, *49*, 607-15.

(62) Guo, K. Mutter, R. Heal, W. Reddy, T. R. K. Cope, H. Pratt, S. Thompson, M. J.; Chen, B. *Eur. J. Med. Chem.* **2008**, *43*, 93-106.

(63) Cope, H. Mutter, R. Heal, W. Pascoe, C. Brown, P. Pratt, S.; Chen, B. *Eur. J. Med. Chem.* **2006**, *41*, 1124-43.

(64) Heal, W. Thompson, M. J. Mutter, R. Cope, H. Louth, J. C.; Chen, B. *J. Med. Chem.* **2007**, *50*, 1347-53.

(65) Kuwata, K. Nishida, N. Matsumoto, T. Kamatari, Y. O. Hosokawa-Muto, J. Kodama, K. Nakamura, H. K. Kimura, K. Kawasaki, M. Takakura, Y. Shirabe, S. Takata, J. Kataoka, Y.; Katamine, S. *Proc. Natl. Acad. Sci. U S A* **2007**, *104*, 11921-6.

(66) Nicoll, A. J. Trevitt, C. R. Tattum, M. H. Risse, E. Quarterman, E. Ibarra, A. A. Wright, C. Jackson, G. S. Sessions, R. B. Farrow, M. Waltho, J. P. Clarke, A. R.; Collinge, J. *Proc. Natl. Acad. Sci. U S A* **2010**, 1-6.

(67) Vogtherr, M. Grimme, S. Elshorst, B. Jacobs, D. M. Fiebig, K. Griesinger, C.; Zahn, R. *J. Med. Chem.* **2003**, *46*, 3563-4.

(68) Trevitt, C. R.; Collinge, J. *Brain* **2006**, *129*, 2241-65.

(69) May, B. C. H. Fafarman, A. T. Hong, S. B. Rogers, M. Deady, L. W. Prusiner, S. B.; Cohen, F. E. *Proc. Natl. Acad. Sci. U S A* **2003**, *100*, 3416-21.

(70) Phuan, P.-W. Zorn, J. a; Safar, J. Giles, K. Prusiner, S. B. Cohen, F. E.; May, B. C. H. *J. Gen. Vir.* **2007**, *88*, 1392-401.

(71) Winklhofer, K. F.; Tatzelt, J. *J. Biol. Chem.* **2000**, *381*, 463-9.

(72) Soto, C.; Satani, N. *Trends Mol. Med.* **2010**, *17*, 14-24.

(73) Legname, G. Baskakov, I. V. Nguyen, H.-O. B. Riesner, D. Cohen, F. E. DeArmond, S. J.; Prusiner, S. B. *Science* **2004**, *305*, 673-6.

(74) Arlt, S. Kontush, A. Zerr, I. Buhmann, C. Jacobi, C. Schröter, A. Poser, S.; Beisiegel, U. *Neurobiology of Disease* **2002**, *10*, 150-6.

(75) Klamt, F. Dal-Pizzol, F. Conte da Frota, M. L. Walz, R. Andrades, M. E. Silva, E. G. da; Brentani, R. R. Izquierdo, I.; Fonseca Moreira, J. C. *Free Radic. Biol. Med.* **2001**, *30*, 1137-44.

(76) Milhavet, O. McMahon, H. E. Rachidi, W. Nishida, N. Katamine, S. Mangé, A. Arlotto, M. Casanova, D. Riondel, J. Favier, A.; Lehmann, S. *Proc. Natl. Acad. Sci. U S A* **2000**, *97*, 13937-42.

(77) Pamplona, R. Naudí, A. Gavín, R. Pastrana, M. a; Sajnani, G. Ilieva, E. V. Río, J. A. Del; Portero-Otín, M. Ferrer, I.; Requena, J. R. *Free Radic. Biol. Med.* **2008**, *45*, 1159-66.

(78) Singh, N. Singh, A. Das, D.; Mohan, M. L. *Antioxid. Redox Signal.* **2010**, *12*, 1271-94.

(79) Lehmann, S. *Curr. Opin. Chem. Biol.* **2002**, *6*, 187–192.

(80) Perry, V. H. Cunningham, C.; Boche, D. *Curr. Opin. Neurology* **2002**, *15*, 349-54.

(81) Kim, J. I. Choi, S. I. Kim, N. H. Jin, J. K. Choi, E. K. Carp, R. I.; Kim, Y. S. *Ann. N. Y. Acad. Sci* **2001**, *928*, 182-6.

(82) Milhavet, O.; Lehmann, S. *Brain Res.* **2002**, *38*, 328-39.

(83) Choi, S. I. Ju, W. K. Choi, E. K. Kim, J. Lea, H. Z. Carp, R. I. Wisniewski, H. M.; Kim, Y. S. *Acta Neuropathologica* **1998**, *96*, 279-86.

(84) Choi, Y. G. Kim, J. I. Lee, H. P. Jin, J. K. Choi, E. K. Carp, R. I.; Kim, Y. S. *Neurosci. Letters* **2000**, *289*, 173-6.

(85) Lee, D. W. Sohn, H. O. Lim, H. B. Lee, Y. G. Kim, Y. S. Carp, R. I.; Wisniewski, H. M. *Free Radic. Res.* **1999**, *30*, 499-507.

(86) Choi, S. I. Ju, W. K. Choi, E. K. Kim, J. Lea, H. Z. Carp, R. I. Wisniewski, H. M.; Kim, Y. S. *Acta Neuropathologica* **1998**, *96*, 279-86.

(87) Hur, K. Kim, J.-I. Choi, S.-I. Choi, E.-K. Carp, R. I.; Kim, Y.-S. *Mech. Ageing Dev.* **2002**, *123*, 1637-47.

(88) Rambold, A. S. Müller, V. Ron, U. Ben-Tal, N. Winklhofer, K. F.; Tatzelt, J. *EMBO J.* **2008**, *27*, 1974-84.

(89) Wong, B. S. Pan, T. Liu, T. Li, R. Petersen, R. B. Jones, I. M. Gambetti, P. Brown, D. R.; Sy, M. S. *Biochem Biophys Res Commun* **2000**, *275*, 249-52.

(90) Ovadia, H. Rosenmann, H. Shezen, E. Halimi, M. Ofran, I.; Gabizon, R. *J. Biol. Chem.* **1996**, *271*, 16856-61.

(91) Keshet, G. I. Ovadia, H. Taraboulos, A.; Gabizon, R. *J. Neurochemistry* **1999**, *72*, 1224-31.

(92) Gaeta, A.; Hider, R. C. *British J. Pharm.* **2005**, *146*, 1041-59.

(93) Singh, N. Das, D. Singh, A.; Mohan, M. L. *Curr. Iss. Mol. Biol.* **2010**, *12*, 99-107.

(94) Rana, A. Gnaneswari, D. Bansal, S.; Kundu, B. *Chem. Biol. Interac.* **2009**, *181*, 282-91.

(95) Brown, D. R. Guantieri, V. Grasso, G. Impellizzeri, G. Pappalardo, G.; Rizzarelli, E. *J. Inorg. Biochem.* **2004**, *98*, 133-143.

(96) Choi, C. J. Kanthasamy, A. Anantharam, V.; Kanthasamy, A. G. *Neurotoxicology* **2006**, *27*, 777-87.

(97) Thackray, A. M. Knight, R. Haswell, S. J. Bujdoso, R.; Brown, D. R. *Biochem. J.* **2002**, *362*, 253-8.

(98) Brown, D. R. Qin, K. Herms, J. W. Madlung, A. Manson, J. Strome, R. Fraser, P. E. Kruck, T. Bohlen, A. von; Schulz-Schaeffer, W. Giese, A. Westaway, D.; Kretzschmar, H. *Nature* **1997**, *390*, 684-7.

(99) Brown, D. R. Wong, B. S. Hafiz, F. Clive, C. Haswell, S. J.; Jones, I. M. *Biochem. J.* **1999**, *344 Pt 1*, 1-5.

(100) Hutter, G. Heppner, F. L.; Aguzzi, A. *Biological Chem.* **2003**, *384*, 1279-85.

(101) Millhauser, G. L. *Ann. Rev. Phys. Chem.* **2007**, *58*, 299-320.

(102) Brown, D. R. Schulz-Schaeffer, W. J. Schmidt, B.; Kretzschmar, H. a *Exper. Neurology* **1997**, *146*, 104-12.

(103) Brazier, M. W. Davies, P. Player, E. Marken, F. Viles, J. H.; Brown, D. R. *J. Biol. Chem.* **2008**, *283*, 12831-9.

(104) Fernaeus, S.; Land, T. *Neurosci. Letters* **2005**, *382*, 217-20.

(105) Fernaeus, S. Hälldin, J. Bedecs, K.; Land, T. *Brain Res.* **2005**, *133*, 266-73.

(106) Singh, A. Mohan, M. L. Isaac, A. O. Luo, X. Petrak, J. Vyoral, D.; Singh, N. *PloS One* **2009**, *4*, e4468.

(107) Singh, A. Kong, Q. Luo, X. Petersen, R. B. Meyerson, H.; Singh, N. *PloS One* **2009**, *4*, e6115.

(108) Singh, A. Isaac, A. O. Luo, X. Mohan, M. L. Cohen, M. L. Chen, F. Kong, Q. Bartz, J.; Singh, N. *PLoS Pathogens* **2009**, *5*, e1000336.

3. Computational studies of ligand/target complexes when the targets lack a deep binding cavity

Standard molecular docking protocols (MDPs, **Figure 12**) allow predicting the three dimensional structure of macromolecular complexes as well as their binding affinity at a low computational cost.[1-3] These protocols require information about the structure of the target (Protein, DNA, RNA) and the ligand (small organic molecule) as well as the presumable interfacing region between them.[1] They are based on a step-wise process. First, a proper *search algorithm* (see **Section 4.2**) generates various configurations of the ligand within the binding site of the target. In the second step, each configuration is evaluated and ranked according to an *energy function* (see **Section 4.3**). These energy functions are usually based on effective potentials that are empirically trained to reproduce experimental binding affinities of validated training data sets of target-ligand complexes. This simplicity makes standard MDPs computationally cheap. It allows them to be used as a tool for virtual drug screening. In fact, these methods are routinely used in early stages of drug discovery to pre-screen large datasets of compounds. Thus, a remarkable decrease in the number of compounds to be synthesized and tested experimentally in the subsequent stages is achieved. In spite of these successes, there are still many important cases for which MDPs are challenged. These include the prediction of the poses of transition metal and/or alkylating drugs, of ligands causing large structural changes, and of ligands not binding to specific pockets. More important, solvation effects are not taken into account in these approaches.[4,5] Free energy simulations may be then used to investigate the molecular association process and to predict binding affinity. Here we propose an enhanced molecular docking protocol (EMD in **Figure 12**) that extends MDPs with free energy simulations in explicit solvent to predict the structure and energetics of ligands binding to protein surfaces. Different classes of computational methods can be used.[6,7] These include among the others: Thermodynamic Integration,[10] MM/PBSA and MM/GBSA,[11] Adaptive Bias Force Steering,[12] Linear Interaction Energy,[50] Steered Dynamics,[14,15] Metadynamics,[8,53] Umbrella Sampling.[54] We use the metadynamics[8,9] along with MDP to predict ligand binding poses onto protein surfaces for which a specific binding pocket is not defined. Such method treats explicitly the conformational flexibility of the receptor and also takes into account water solvation of the system.

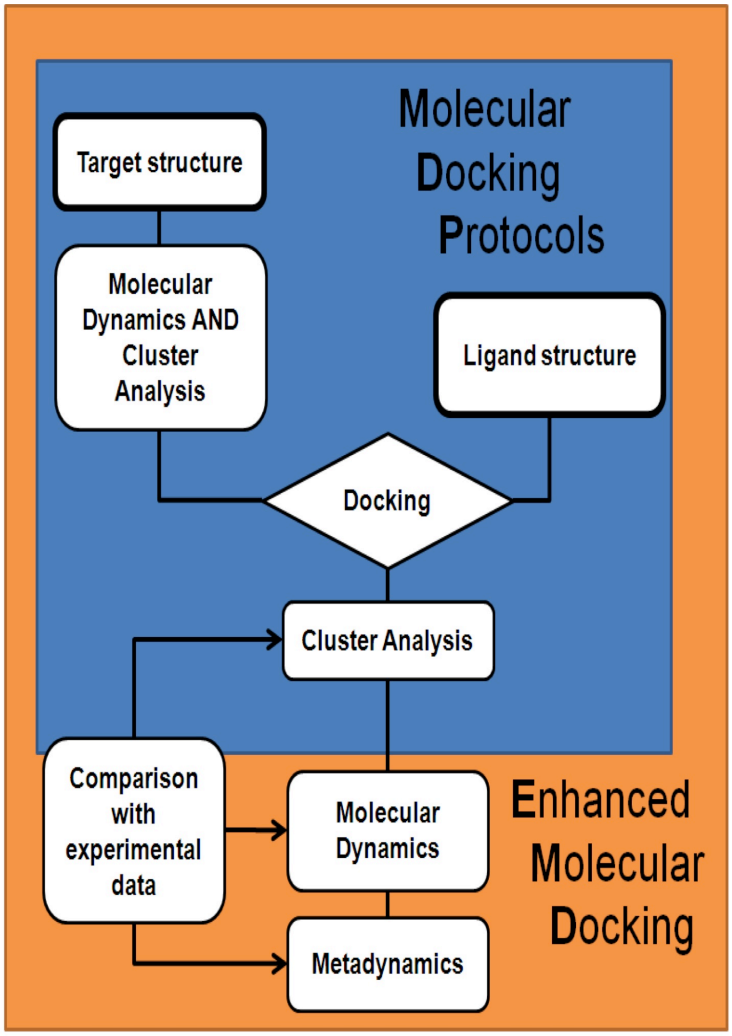

Figure 12. Molecular Docking Protocols (MDPs) are used to guess putative ligand binding regions on target surfaces, based on structural information on the two separated moieties. Structural information on the target may come from NMR or X-ray studies and, in some cases, also from molecular simulation. Ligand may be docked on a putative binding site. Cluster analysis is used to group MD conformers and/or ligand/target adducts into representative structures. In the Enhanced Molecular Docking (EMD) approach, MD simulations may be used to relax the structures and to investigate the role of hydration. Enhanced sampling simulation techniques in explicit solvent (here metadynamics) allow to explore the ligand binding space and to predict free energy of binding.

Four colleagues of Statistical and Biological Physics Sector (International School for Advanced Studies, SISSA/ISAS) carried out this work.
I, together with Dr. A. Kranjc, studied the structure of the ligand, performed molecular docking calculations and cluster analysis.
Dr. G. Rossetti performed molecular dynamic simulations and cluster analysis.
Dr. X. Biarnes performed metadynamics.
We together compared the computational results with experimental data.

3.1. Compound 1

We focus on a small organic molecule able to bind to $hPrP^{C}$, which can interfere with its conversion to the pathogenic form PrP^{Sc}. The ligand **1** is a symmetric molecule composed by two pyrrolidine rings connected by acetamides to a diphenylmethane core.

1 (**Figure 13**) has been shown to significantly inhibit the PrP^{Sc} production in the neuronal mouse cells chronically infected with the Fukuoka-1 strain at 10 μM.[18] The effect of the compound was dose-dependent, and by repeating the experiment Kuwata *et al.* established that the effective concentration for 50% reduction of PrP^{Sc} in scrapie-infected GT cells $EC_{50} \approx 1.35$ μM.[18] Treatment of infected mice with **1** showed slightly but significantly extension of the survival time.[18]

To identify the putative sites for interaction of **1** with PrP, Kuwata *et al.* have analyzed the chemical shift perturbation of ^{1}H-^{15}N heteronuclear single quantum coherence NMR spectra of a uniformly ^{15}N-labeled PrP. A comparison of the spectra revealed that several cross peaks (corresponding to N159, V189, T192, K194, and E196) shifted significantly upon the addition of **1**. Binding of **1** to PrP^{C} was confirmed by the surface plasmon resonance (SPR), and its dissociation constant was estimated to be 3.9 ± 0.2 μM.[18]

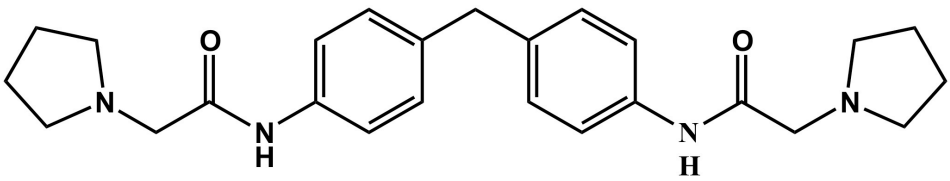

Figure 13. Chemical structure of **1**

3.2. Compound 1 and mPrP^{C}

The reported chemical shifts perturbations of mPrP^{C} induced by **1** binding affect most significantly amino acid residues on one side of the protein surface (Asn159 at α1- β2 loop, Lys194 at α2, Glu196, Thr199 at α2-α3 loop and Val210 at α3). In addition, Val189 and Thr192, located on the other side of the PrP surface, are also perturbed (**Figure 14** and **Table 2**). This suggests that multiple binding sites may be present. Despite this, an ad hoc model of the **1**-mPrP^{C} adduct, constructed by docking and energy minimization exhibited a single binding mode of **1** connecting Asn159 and Glu196, nevertheless such single binding mode could not explain the contacts with Val189, Thr192.[18]

Table 2. NMR chemical shift changes (δ) upon **1** binding to the mPrP^{C}

δ >0.9 ppm	0.5ppm< δ <0.9 ppm
Asn159	Glu196
Lys194	Arg156
Val189	Val210
Thr192	Thr199

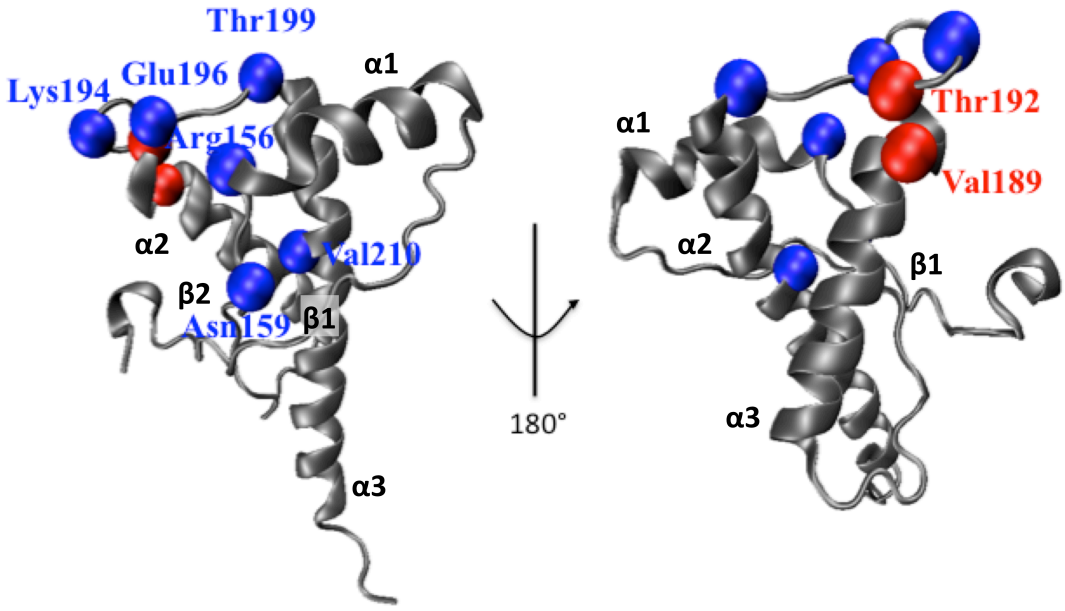

Figure 14. Residues involved in the interactions with **1**.

Subsequent quantum-mechanical studies, based on this model, pointed out that these two residues, along with Gln160 and Lys194, are important for the binding. However, such single binding mode was not consistent with the presence of the contacts between the ligand and Val189, Thr192 and Thr199.[19] Given the lack of deep binding pockets along the protein structure of PrP^C, it is reasonable to assume that **1** will not bind specifically to a single site. This hypothesis was also encouraged from NMR data, which enables several residues located on distant regions of PrP^C surface interacting with **1** to be identified.[18]

Here we have applied our EMD protocol to provide: i) structural model of the adduct **1**-PrP^C; ii) affinity constant to be compared to experimental data. The EMD protocol emerges therefore as a useful approach to investigate ligands sticking on protein surfaces.

3.3. Compound 1 and $hPrP^C$

Compounds **1** was studied by Kuwata *et al.* with murine cell lines expressing $mPrP^C$.[18] We are interested to ligands binding $hPrP^C$ because we focused our drug discovery project to the human cases. The sequence similarity is as high as 98%, and the root-mean-square difference (RMSD) of the backbone between the molecular dynamics (MD) structures of $hPrP^C$ (PDB code: 1HJM) is the same (0.26 (0.02 nm) as that between the NMR structures of $hPrP^C$ and $mPrP^C$ (PDB code: 1AG2) (0.27 nm). Therefore, significant changes of the structure on passing from the $mPrP^C$ to the $hPrP^C$ are not expected. For this reason, we applied our EMD protocol to study the interaction between ligand **1** and $hPrP^C$.

3.4. Computational methods

Structure of the ligand and Identification of Protonation States

Titration curves calculated by the ChemAxon software[e] suggested that in aqueous solution at pH=7.4, molecule **1** is present in two protonation states (neutral, $\mathbf{1}^{0}$ and monoprotonated, $\mathbf{1}^{+}$) while at pH=4.5 it exists in the diprotonated form ($\mathbf{1}^{2+}$) (**Figure 15**). This method was used because it has been proved to be reliable: in a pK_a calculation for 1000 molecules, less than 0.5 % turned out to differ by more than 0.5 pH unit from the experimental value. Before docking, all the three protomers underwent geometry optimization at the B3LYP/6-31G** level of theory by means of the Gaussian03 software (g03).[20]

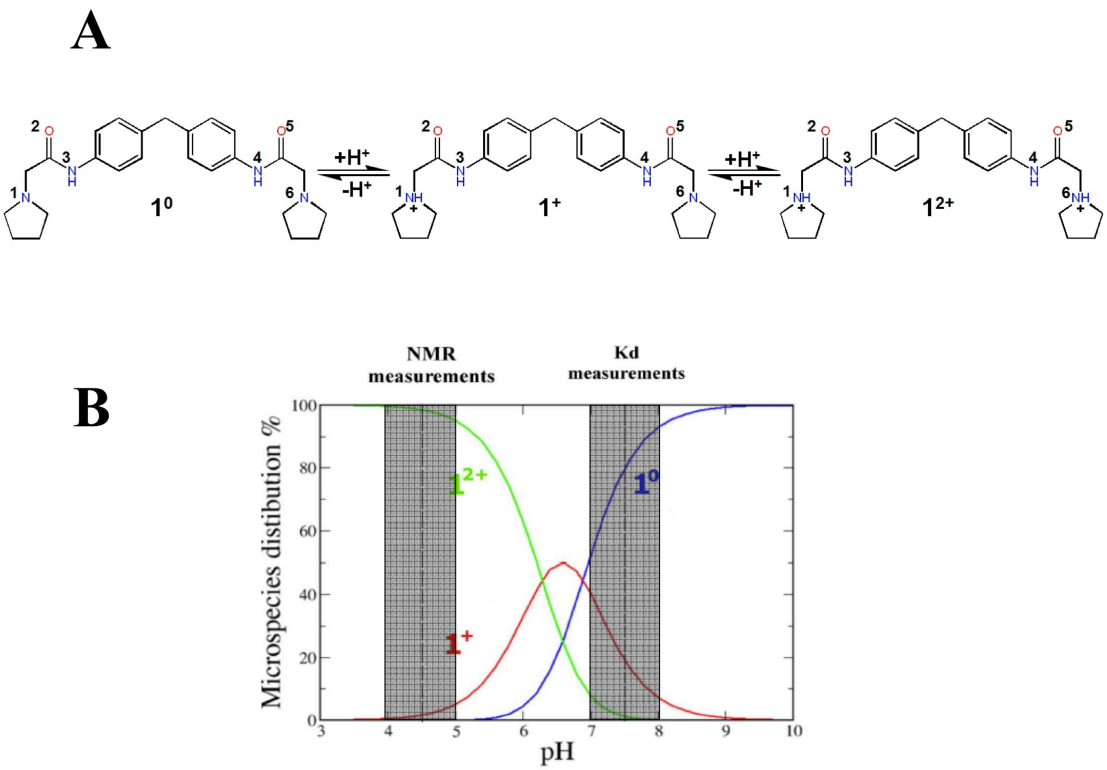

Figure 15. A) Acid-Base equilibrium of **1**. B) Titration curve of **1** calculated by the ChemAxon software (www.chemaxon.com). At the pH of the K_d measurements, **1** is present in neutral ($\mathbf{1}^{0}$) and monoprotonated ($\mathbf{1}^{+}$) states. At the pH of the NMR measurements, it exists also in diprotonated ($\mathbf{1}^{2+}$) form. These two pH ranges are highlighted in the figure.

[e] www.chemaxon.org

Target structure – Molecular Dynamics – Cluster Analysis

The NMR structure of $hPrP^C$ C-terminal GD resolved at pH 7 (residues 125-228, PDB ID: 1HJM) is used in this study. Protonation states were assigned by the web server H++[f] assuming pH 7.4.

The protein was inserted into a cubic box of water molecules, ensuring that the solvent shell would extend for at least 0.8 nm around the system. Three sodium counterions were added to neutralize the system. The AMBER99 force field[21] was used for the protein. Sodium ions were modeled with the AMBER-adapted [13]Åqvist potential. The TIP3P model was used to describe the water molecules.[22] The system was minimized by imposing harmonic position restraints of 1000 $kJ \cdot mol^{-1} \cdot nm^{-2}$ on the solute atoms, allowing the equilibration of the solvent without distorting the solute structure. After an energy minimization of the entire system without harmonic restraints, the temperature was gradually increased from 0 K to 298 K in 12 steps. In each step, the temperature was increased by 25 K in 100 ps of MD.

Constant temperature-pressure (T=298 K, P=1 bar) 20-ns dynamics were then performed through the Nosé-Hoover[23,24] thermostat and Andersen-Parrinello-Rahman[25] barostat coupling schemes. Periodic boundary conditions were applied. The final simulation box equilibrated at around 6.69 x 6.69 x 6.69 nm. Long-range electrostatic interactions were treated with the particle mesh Ewald (PME) [26,27] method, using a grid with a spacing of 0.12 nm combined with a fourth-order B-spline interpolation to compute the potential and forces in between grid points. The cutoff radius for the Lenard-Jones interactions as well as for the real part of PME calculations was set to 0.9 nm. The pair list was updated every 2 steps, and the LINCS algorithm[28] was used to constrain all bond lengths involving hydrogen atoms which allows for a time step of 2 fs. The MD trajectory of the protein alone was clustered with the Gromos method[29] and as result 20 different conformations were obtained, which were used along with the NMR structure for docking of compound **1**.

Docking procedure – Cluster Analysis

The optimized structures of compound **1** ($\mathbf{1^0}$, $\mathbf{1^+}$ and $\mathbf{1^{2+}}$) were docked to the NMR structure of $hPrP^C$ and to its 20 different conformations obtained by the cluster analysis of the MD trajectory.

The GOLD 3.1[30,31] and Autodock 3.0.5[32,33] programs were used for docking. In GOLD, the docking region was defined as a sphere of 3.5 nm radius around His187, so that the whole protein was screened. The ChemScore (CS)[34] and GoldScore (GS)[35] scoring functions were used for ranking. For each protomer and scoring function, 100 docking runs were performed.

In Autodock, a Lamarckian genetic search algorithm was used to identify low-energy binding sites and orientations of compound **1** protomers. Binding modes were ranked by the scoring function implemented in

[f] http://biophysics.cs.vt.edu/

Autodock. A grid map of 12.6 nm x 12.6 nm x 12.6 nm dimensions was centered to the center of mass of the protein, with the point grid spacing set to 0.0475 nm. Gasteiger atom charges were assigned to the protein atoms using AutoDockTools. Water molecules were excluded from the protein before docking. 100 randomly seeded docking runs were performed for each protomer.

The binding poses were identified by AClAP 1.0 clustering procedure.[36]

In the **Chapter 4**, I will discuss Docking method and Cluster Analysis in more details.

Hydration and thermal stability of 1-hPrPC adducts

10-ns MD simulations of the adducts ($hPrP^C$-$\mathbf{1^0}$, $hPrP^C$-$\mathbf{1^+}$ and $hPrP^C$-$\mathbf{1^{2+}}$) allowed for a proper hydration of the system and for identification of collective motions that may be essential for PrP^C-ligand interactions. The protomers were bound to the binding site I (BS I**).** The simulation protocol was the same as for the free protein. For the three ligands, the gaff force field was used.[37] The atomic restrained electrostatic potential (RESP) charges[38,39] were calculated by using the resp module of AMBER after geometry optimization and electrostatic potential calculations of each protomer at the B3LYP/6-31G** level of theory by means of the g03 software.[20]

Dissociation free energy calculations

The dissociation free energies of $\mathbf{1^0}$, $\mathbf{1^+}$ and $\mathbf{1^{2+}}$ were calculated using metadynamics[8,40-43] in its bias-exchange variant[40-43] as a function of collective variables (CVs), which should be relevant for describing the dissociation process. CVs used in this work are: (i) the distance between the center of mass of the ligand and the center of mass of the protein binding site; (ii) the number of polar contacts between the ligand and one portion of the protein BS I; (iii) the number of polar contacts between the ligand and the other portion of the protein BS I; (iv) the number of water bridge contacts between the ligand and the protein BS I; (v) the RMSD difference of the system with respect to an equilibrated MD structure taken from the previous Section; (vi) the RMSD fluctuation of the residues defining the protein BS I. The choice of these CVs was based on previous ligand-target interaction metadynamics studies as well as by observations based on the former MD simulations.[40-43]

The calculations do not require in principle the previous knowledge of the protein-ligand adduct structure. However, for computational efficiency we exploit the fact that all the target regions detected from NMR are in the close proximity of BS I. Therefore, here we explored only this region.

Six independent metadynamics simulations were run in parallel. Each replica was biased by different one-dimensional time-dependent potentials, which were built as a function of each of the collective variables defined above. Exchanges among replicas were attempted every 10 ps using a metropolis acceptance criterion.[44]

Similar set-up was shown to improve the sampling of the configurational space and the convergence of the results.[40-43]

At the end of the different replica simulations, the explored phase space, in terms of the six collective variables used in this study, was clustered using the gromos method.[29]The clustering radius for each collective variable was set to 0.1 nm, 0.2, 0.4, 2.5, 0.05 nm, 0.02 nm, respectively. The free energy corresponding to each cluster was then reconstructed from the populations of clusters observed during the simulations. The free energy value was corrected by the corresponding bias potentials acting on that cluster as in a usual weighted histogram analysis.

Details on metadynamics can be found in references: 8,9,40,44-46.

Two reference states of the ligand-protein system, bound and unbound, needed to be defined to provide the corresponding dissociation free energy value. The bound state was considered as the lowest free energy cluster. The unbound state was considered to be a cluster showing no contacts with the BS I (lowest values of CVs *ii* and *iii*) and at the same time with a higher RMSD with respect to the initial docked structure (highest value of CV *v*). Given the size of the simulation box the ligand is not fully detached from the protein in its unbound state. Therefore, the residual dissociation energy of the unbound state was roughly estimated in implicit solvent using an adaptive Poisson Boltzmann solver.[40-43] It was estimated as the difference in solvation energy of the complex minus the solvation energy of each component plus the intermolecular Coulomb interaction. The standard free energy of dissociation was obtained by applying the following relationship: $\Delta G^0 = \Delta G - RT \times ln[L]$, where ΔG is the total dissociation free energy as a result of our simulation, R is the molar constant, and [L] is the concentration of the ligand in our simulation box (i.e. 5.5 mM, corresponding to 1 molecule in 6.69^3 nm^3). The standard free energy is related to the dissociation equilibrium constant (K_d) by $\Delta G = -RT \times \ln(K_d)$.

3.5. Results and Discussion

In this study, we focus on the binding of compound **1** (**Figure 13**) to the surface of $hPrP^C$. Two different conditions are considered: at neutral pH, where experimental affinity has been measured and at acidic pH, where NMR chemical shift perturbations have been obtained to identify the key residues involved in binding.

We use the computational protocol summarized in **Figure 12**:

(i) Identification of ligand protonation state at different pH.
(ii) Use of MDPs to provide a first guess of putative binding poses.
(iii) Use of MD simulations to relax the adduct structures in aqueous solution (step 1 in EMD).
(iv) Use of metadynamics to predict:
- the energetics of binding of **1** to $hPrP^C$
- the binding poses of the compound to $hPrP^C$

3.5.1. Protonation state of 1

The tertiary nitrogen atoms in the pyrrolidine rings of **1** can exist in different protonation states: deprotonated, monoprotonated or diprotonated (**Figure 15**). At pH=7.4 where the K_d has been measured, approximate pKa calculations (www.chemaxon.org) suggest that, in water, **1** exists in both the neutral form ($\mathbf{1^0}$) and the monoprotonated form ($\mathbf{1^+}$) (**Figure 15**). In the latter, one of the two pyrrolidine nitrogen atoms is protonated.

At pH=4.5 where the NMR experiments were performed, the pK_a calculations indicate a mainly diprotonated state ($\mathbf{1^{2+}}$, with both pyrrolidine nitrogen atoms protonated), as well as a small amount of $\mathbf{1^+}$. The calculated concentration of $\mathbf{1^0}$ in bulk water is very low (**Figure 15**). However, ligand-protein binding does not occur in pure water and the electrostatic field of the protein should be taken into account. Indeed, simple electrostatic potential calculations show an increase of the positive charge density in the putative binding region of the protein defined by the NMR contacts (**Figure 16**). This suggests that the protein environment there will favour the accumulation of neutral $\mathbf{1^0}$. Therefore, binding poses involving the neutral form should be considered even at acidic pH. Based on these analyses, we performed calculations on all of the three protomers.

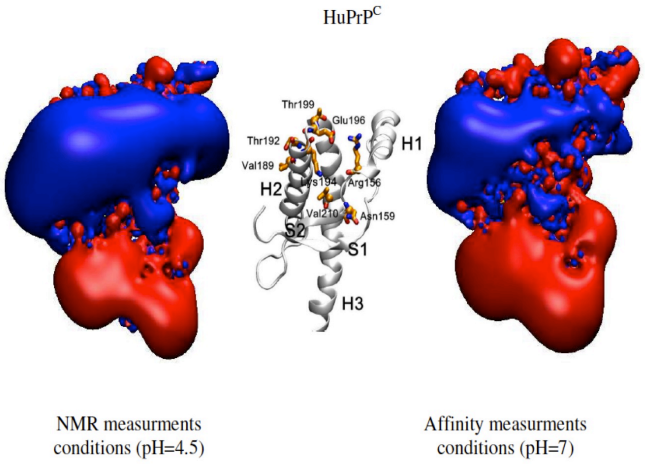

Figure 16. Figure Electrostatic potential generated by hPrP^C at different experimental conditions. Left: NMR measurements conditions (pH=4); Right: Affinity measurements conditions (pH=7). Red volume represents the regions at -1.2 eV; Blue volume represents the regions at +1.2 eV. Center: Residues involved in **1** binding to the prion protein (in licorice), as emerging from chemical shift changes.

3.5.2. Use of MDPs to provide a first guess of putative binding regions

The three protomers were docked to the hPrP^C NMR structure and 20 conformers obtained from the 20-ns MD simulations of the protein in aqueous solution. Three putative BSs I, II and III were identified (**Figure 17**). BS I is defined by the α2 helix and the loop connecting β2 and helix α1. BS II consists of the α2-α3 helices. BS III is defined by the α3 helix, the N-terminal of α2 helix, and the loop between α1 helix and β1 sheet. Only BS I contains the residues that show chemical shift changes upon binding of compound **1** and it is closer to all the other residues involved in the binding. It was therefore the only one selected for the subsequent free energy studies.

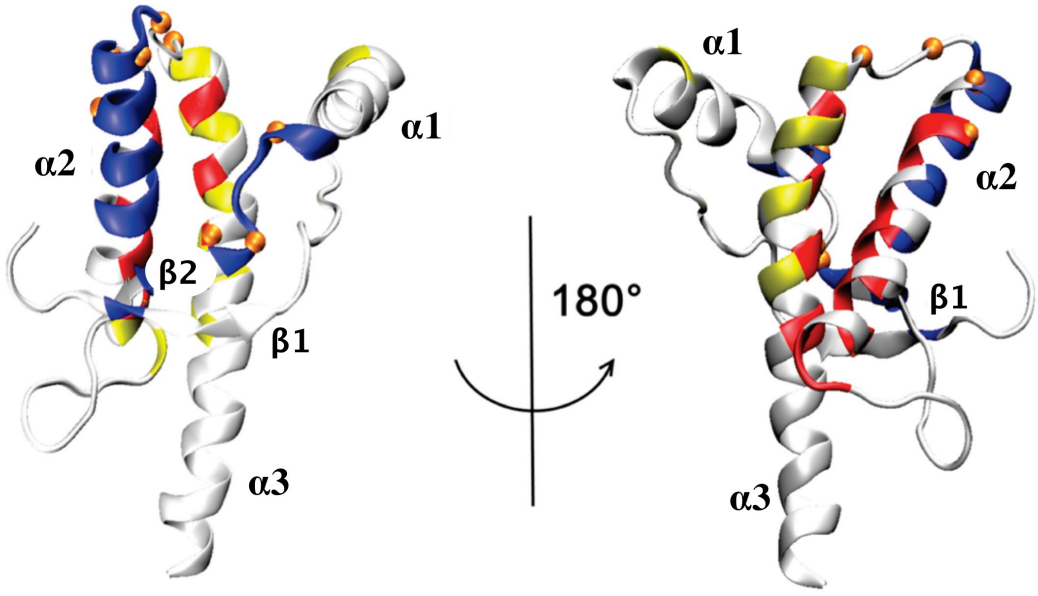

Figure 17. Three different binding regions (I, II, and III shown in blue, red, and yellow, respectively), as obtained after MDP procedures. Orange spheres represent compound **1** binding aminoacids defined by the NMR chemical shift study. The figure shows $hPrP^{C}$.

3.5.3. Use of MD simulations to relax the structure in aqueous solution

The adducts for each of the three protomers docked at BS I underwent 10 ns of MD calculations in aqueous solution. The ligands maintained completely ($\mathbf{1}^{+}$ and $\mathbf{1}^{2+}$) or partially ($\mathbf{1}^{0}$) the pose identified in the docking. Most importantly, the structural determinants of the three protomers turned out to be consistent with most of the ligand-protein contacts identified by NMR (see **Table 2**). However, the ligand-protein contacts with Val189, Thr192, Thr199 and Val210 could not be predicted by MDP. A simpler docking approach, combined with energy minimization of protomer $\mathbf{1}^{0}$ obtained similar results to our findings (*Figure 3 in Kuwata et al. 2007*).[9,47-49]

3.5.4. Free energy calculations were then used to explore the ligand binding space in explicit solvent

These simulations allowed to identify alternative binding poses for each protomer of the ligand and to predict the dissociation free energy. The free energy simulations were performed as a function of 6 collective variables that took into account rearrangements of the ligand and protein, hydrogen bond contacts and water bridges. These variables have been already used to characterize ligand-target molecular recognition processes using the metadynamics approach.[18]

3.5.4.1. hPrP^{C}-1^{0} complex.

In the lowest free energy cluster identified by the metadynamics calculations, **1^{0}** is located in the wide cleft formed by helices α1, α2 and α3 (**1^{0}**.B1 in **Figure 18**), similarly to the model proposed by Kuwata *et al.* for mPrP^{C}.[18] In the global minimum, **1^{0}** is located in the wide cleft formed by helices α1, α2 and α3 (**1^{0}**.B1 in **Figure 18**), similarly to the model proposed by Kuwata *et al.* for mPrP^{C}.[18] The contacts **1^{0}** forms with the hPrP^{C} are consistent with the reported chemical shift changes on Glu196, upon **1** binding (**Table 2**), as well as with a recent quantum chemical study. They are also consistent with chemical shift changes on Arg156, Thr199, and Val210 upon **1** binding (**Table 2**). The phenyl groups of **1^{0}** form a π-cation interaction with Arg156 and a water-mediated H-bond is present between Thr199 and the pyrrolidine nitrogen (N1; **Figure 18**). The pyrrolidine ring forms hydrophobic interactions with Val210 (as well as with Pro158, Thr183). The hPrP^{C}-**1^{0}** complex is further stabilized with a direct H-bond between Thr190 and the carbonyl group of **1^{0}** (O2; **Figure 18**).

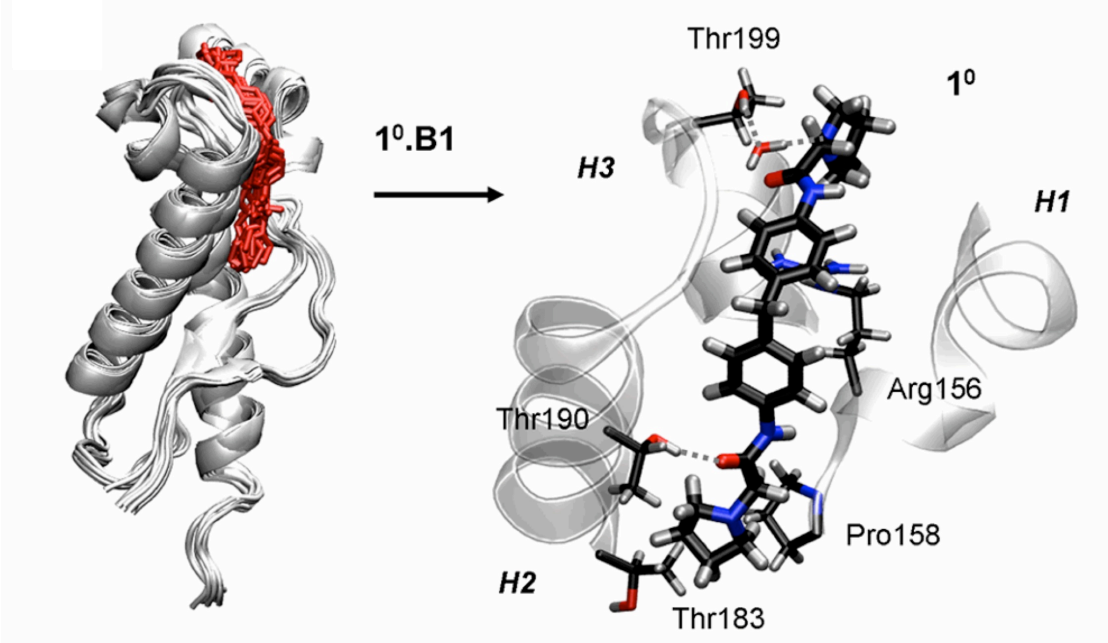

Figure 18. Three dimensional structures of hPrP^{C} in complex with **1^{0}**. These structures correspond to the bound-states free energy minima (1^{0}.B1), as calculated with the metadynamics method.

The unbound state of hPrP^{C}-**1^{0}** system corresponds to a conformation in which the ligand has no contact with the protein. The conformation of Lys194 changes upon ligand dissociation (**Figure 19**). This is consistent with the significant chemical shift change reported for this residue.

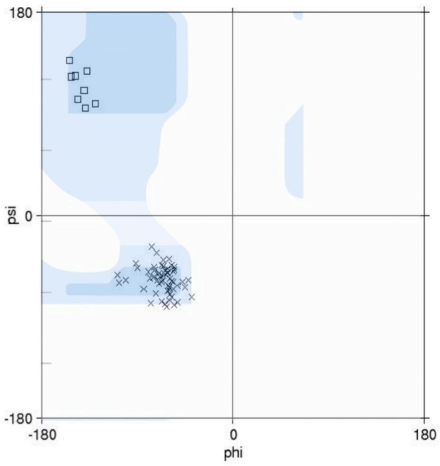

Lys 194

Figure 19. Ramachandran plot of residue Lys194 for the $\mathbf{1^0}$ adduct: Crosses indicate the conformation of the residue when the ligand is bound, and empty squares when the ligand is not bound.

Smaller conformational changes were also observed for other residues in the α2-α3 loop (res. 195-199). These rearrangements were not observed with the MD calculations, possibly because they are induced during the ligand binding process simulated here.

The unbound state of $hPrP^C$-$\mathbf{1^0}$ is 5.5 kcal/mol ± 0.9 higher in energy with respect to the global minimum. The ligand is not completely detached from the protein, although $\mathbf{1^0}$ is already separated by 5 layers of water molecules between the two moieties. The remaining free energy for complete dissociation was estimated to be –0.7 kcal/mol by means of the Poisson-Boltzmann equation. Thus, we estimated the dissociation free energy to be 4.7 kcal/mol in our simulation conditions. Considering also the concentration of the species in the simulation box, the standard dissociation free energy is estimated to be 7.8 kcal/mol. This is in very good agreement with the experimental value of 7.5 kcal/mol (corresponding to $K_d = 3.9 \pm 0.2$ μM) reported by Kuwata *et al*.[18]

3.5.4.2. $hPrP^C$-1^+ complex

Four different stable binding poses of $\mathbf{1^+}$ were identified on $hPrP^C$ surface (**Figure 20**). In the global minimum, $\mathbf{1^+}$ lays along the loop connecting helices α2 and α3 ($\mathbf{1^+}$.B1 in **Figure 20**). It forms a remarkable hydrophobic interaction with Thr199, consistent with the chemical shift changes reported for this residue.[18] The amidic nitrogen atoms of $\mathbf{1^+}$ (N3 and N4; In **Figure 20**) are H-bonded to Thr201 and Asn197, respectively. This induces a subtle conformational change of the Glu196 and Asn197 backbone upon ligand binding which may be the cause of the chemical shift displacement reported experimentally for Glu196. Additionally, the neutral pyrrolidine ring of $\mathbf{1^+}$ is accommodated by the hydrophobic cleft formed by Ile184, Thr188, Phe198, Val203 and Met206,

which further stabilizes the complex. No water-mediated interactions were observed between $\mathbf{1}^{+}$ and $hPrP^{C}$.

With the corrections described above, the dissociation free $hPrP^{C}$-$\mathbf{1}^{+}$ complex ($\mathbf{1}^{\mathbf{1+}}$**.B1** in **Figure 20**) and the corresponding unbound state, with the corrections described above, turns out to be 8.6 kcal/mol. This is similar to that predicted for $\mathbf{1}^{\mathbf{0}}$ and in good agreement with experimental data.

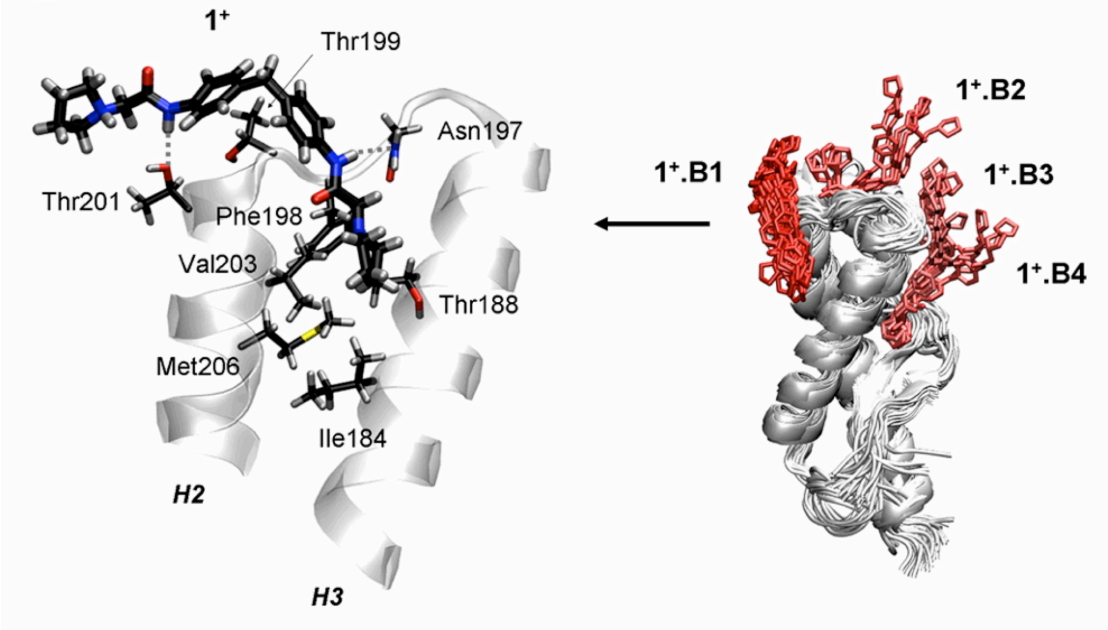

Figure 20. Three dimensional structures of $hPrP^{C}$ in complex with $\mathbf{1}^{+}$. These structures correspond to the bound-state free energy minima (1^{+}.B1-B4), as calculated with the metadynamics method.

3.5.4.3. hPrP^{C}-1^{2+} complex

Five different stable binding poses of **1**$^{2+}$ were identified on hPrP^{C} surface (**Figure 21**). In the most stable conformation, **1**$^{2+}$ binds yet in another position of hPrP^{C}, laying along helix α2 (**1**$^{2+}$.B1 in **Figure 21**). Half part of **1**$^{2+}$ is in close contact with hPrP^{C} surface in the cleft formed by Val189, Thr192 and Thr193. Indeed, these positions were reported to interact directly with the ligand according to NMR experiments (**Table 2**). Two layers of water molecules are present between the protein surface and the rest of the molecule, presumably due to the presence of Lys185. In the other accessible poses, **1**$^{2+}$ covers different regions of the protein surface (**Figure 21**). The interaction with Lys194 is conserved in the majority of the poses. This result is consistent with the chemical-shift changes of this residue upon ligand binding. The dissociation free energy of **1**$^{2+}$ was not calculated, as this protomer is not present at the conditions in which the K_d was measured.

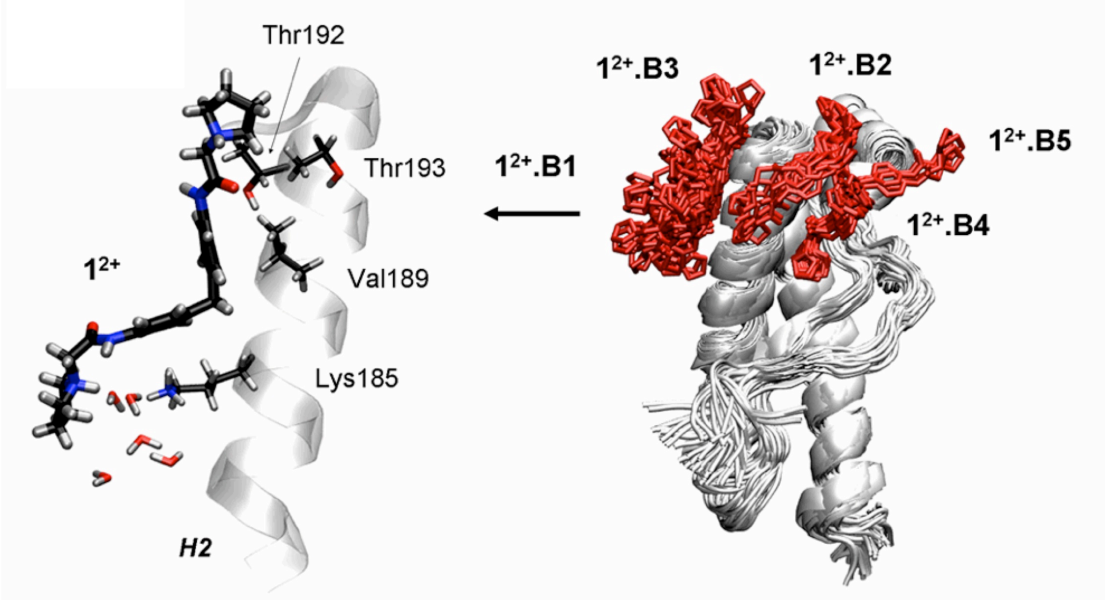

Figure 21. Three dimensional structures of hPrP^{C} in complex with **1**$^{2+}$. These structures correspond to the bound-state free energy minima (1^{2+}.B1-B5), as calculated with the metadynamics method.

3.6. Conclusion

Our proposed EMD protocol was applied to identify the hPrP^{C} sites where **1**, in its different protonation states (0, +1, +2, see **Figure 15**), preferably binds. This protocol combines standard MDP with metadynamics, see **Figure 12**. As in any MDP, MD simulations were used initially to relax the protein structure in aqueous solution. Secondly, representative PrP^{C} structures were selected by statistical analysis of the MD simulation. Standard docking calculations were then used to dock the ligand **1** on these protein structures, providing a first guess of putative binding regions. MDP was not sufficient to explain all distant contacts reported by NMR.[18] Successively, metadynamics was used to simulate the **1** binding process from solution to PrP^{C} surface. These simulations allowed us to identify alternative binding poses of **1** onto hPrP^{C} surface and also to predict the binding affinity. These predictions were comparable to experimental data obtained via NMR chemical shift perturbations and affinity measurements. We observed a multiple binding site pattern of **1** complementing that proposed by Kuwata *et al.*[18] Taken together, these provide a structural basis to explain all experimental NMR-contacts (see **Figure 22**).

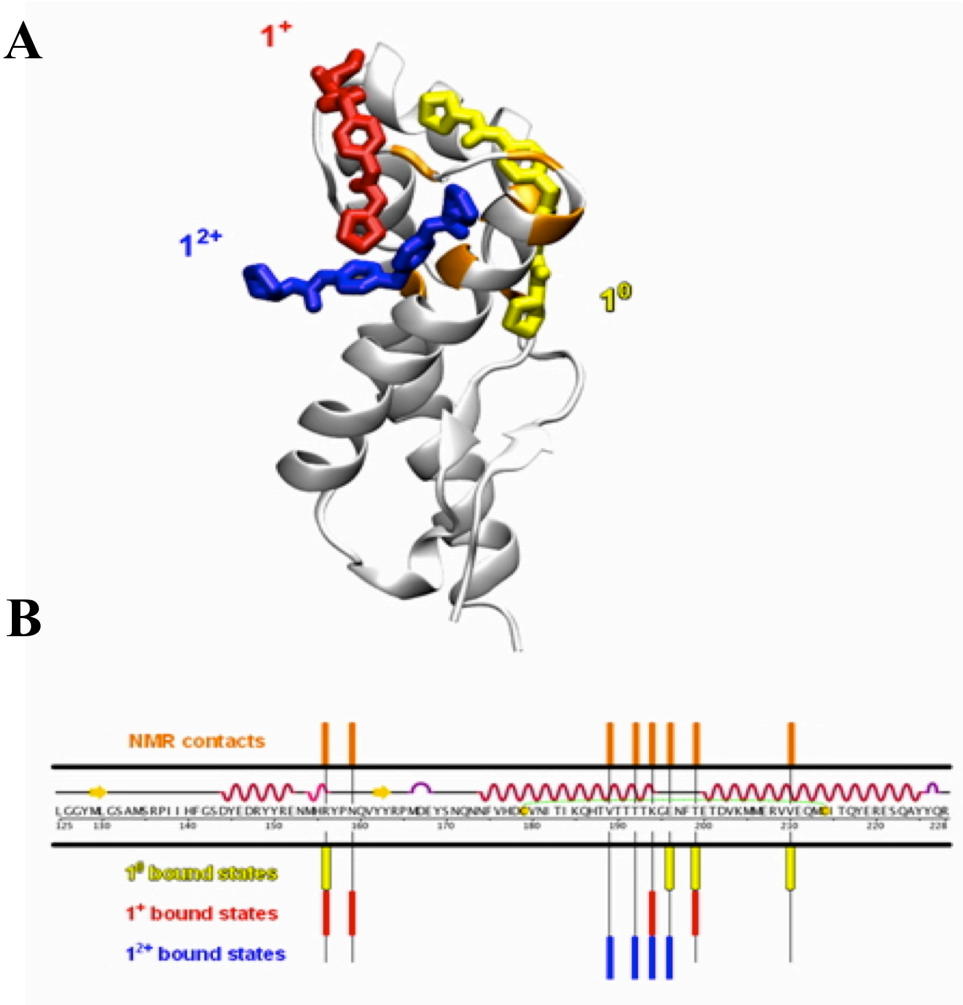

Figure 22. (A) Superimposition of $\mathbf{1}^{0}$ (yellow), $\mathbf{1}^{+}$ (red) and $\mathbf{1}^{2+}$ (blue) binding poses. (B) The residues of mPrP^{C} experimentally found to be involved in binding are highlighted in orange bars.

This result was not predictable a priori and could only be obtained when MDPs are extended with enhanced sampling simulations. This example represents a step forward to identify the binding of small organic molecules that to cavity-less proteins, in which water-mediated interactions become important and the ligand can bind at the same time in multiple sites of the protein surface. We conclude that our approach is a useful tool to predict poses and affinity of ligands binding to proteins with fibrillation properties.

References

(1) Kitchen, D. B. Decornez, H. Furr, J. R.; Bajorath, J. *Nat. Rev. Drug Discov.* **2004**, *3*, 935-49.

(2) Huang, S.-Y.; Zou, X. *Int. J. Mol. Sci.* **2010**, *11*, 3016-34.

(3) Yuriev, E. Agostino, M.; Ramsland, P. a *J. Mol. Recognition* **2010**, 149-164.

(4) Michel, J. Tirado-Rives, J.; Jorgensen, W. L. *J. Am. Chem. Soc.* **2009**, *131*, 15403-11.

(5) Santos, R. Hritz, J.; Oostenbrink, C. *J. Chem. Inf. Model* **2010**, *50*, 146-54.

(6) Gilson, M. K.; Zhou, H. X. *Annu. Rev. Biophys. Biomol. Struct.* **2007**, *36*, 21-42.

(7) Deng, Y.; Roux, B. *J. Phys. Chem. B* **2009**, *113*, 2234-46.

(8) Laio, A.; Parrinello, M. *Proc. Natl. Acad. Sci. U S A* **2002**, *99*, 12562-6.

(9) Gervasio, F. L. Laio, A.; Parrinello, M. *J. Am. Chem. Soc.* **2005**, *127*, 2600-7.

(10) Straatsma, T. P.; McCammon, J. A. *J. Chem. Phys.* **1991**, *95*, 1175.

(11) Gouda, H. Kuntz, I. D. Case, D. A.; Kollman, P. A. *Biopolymers* **2003**, *68*, 16-34.

(12) Darve, E. Rodríguez-Gómez, D.; Pohorille, A. *J. Chem. Phys.* **2008**, *128*, 144120.

(13) Åqvist, J. Medina, C.; Samuelsson, J.-E. *Protein Eng.* **1994**, *7*, 385-391.

(14) Isralewitz, B. Baudry, J. Gullingsrud, J. Kosztin, D.; Schulten, K. *J. Mol. Graph. Model.* **2001**, *19*, 13-25.

(15) Colizzi, F. Perozzo, R. Scapozza, L. Recanatini, M.; Cavalli, A. *JACS* **2010**, *132*, 7361-71.

(16) Bussi, G. Laio, A.; Parrinello, M. *Phys. Rev. Lett.* **2006**, *96*, 10-13.

(17) Torrie, G.; Valleau, J. *J. Comput. Phys.* **1977**, *23*, 187-199.

(18) Kuwata, K. Nishida, N. Matsumoto, T. Kamatari, Y. O. Hosokawa-Muto, J. Kodama, K. Nakamura, H. K. Kimura, K. Kawasaki, M. Takakura, Y. Shirabe, S. Takata, J. Kataoka, Y.; Katamine, S. *Proc. Natl. Acad. Sci. U S A* **2007**, *104*, 11921-6.

(19) Yamamoto, N.; Kuwata, K. *J. Phys. Chem. B* **2009**, *113*, 12853-12856.

(20) W., F. G. Gaussian 03, Revision B.01 **2004**.

(21) Case, D. A. Cheatham, T. E. Darden, T. Gohlke, H. Luo, R. Merz, K. M. Onufriev, A. Simmerling, C. Wang, B.; Woods, R. J. *J. Comput. Chem.* **2005**, *26*, 1668-88.

(22) Jorgensen, W. L. Chandrasekhar, J. Madura, J. D. Impey, R. W.; Klein, M. L. *J. Chem. Phys.* **1983**, *79*, 926-935.

(23) Hoover, W. G. *Phys. Rev. A* **1985**, *31*, 1695-1697.

(24) Nosé, S.; Klein, M. L. *Mol. Phys.* **1983**, *50*, 176-1055.

(25) Parrinello, M.; Rahman, A. *J. Appl. Phys.* **1981**, *52*, 7182-7190.

(26) Darden, T. York, D.; Pedersen, L. *J. Chem. Phys.* **1993**, *98*, 10089-10092.

(27) Essmann, U. Perera, L. Berkowitz, M. L. Darden, T. Lee, H.; Pedersen, L. G. *J. Chem. Phys.* **1995**, *103*, 8577-8593.

(28) Hess, B. Bekker, H. Berendsen, H. J. C.; Fraaije, J. G. E. M. *J. Comput. Chem.* **1997**, *18*, 1463-1472.

(29) Daura, X. Gademann, K. Jaun, B. Seebach, D. Gunsteren, W. F. van; Mark, A. E. *Angew. Chem. Int. Ed.* **1999**, *38*, 236-240.

(30) Jones, G. Willett, P. Glen, R. C. Leach, a R.; Taylor, R. *J. Mol. Biol.* **1997**, *267*, 727-48.

(31) Verdonk, M. L. Cole, J. C. Hartshorn, M. J. Murray, C. W.; Taylor, R. D. *Proteins* **2003**, *52*, 609-23.

(32) Osterberg, F. Morris, G. M. Sanner, M. F. Olson, A. J.; Goodsell, D. S. *Proteins* **2002**, *46*, 34–40.

(33) Morris, G. M. Goodsell, D. S. Halliday, R. S. Huey, R. Hart, W. E. Belew, R. K.; Olson, A. J. *J. Comp. Chem.* **1998**, *19*, 1639-1662.

(34) Nissink, J. W. M. Murray, C. Hartshorn, M. Verdonk, M. L. Cole, J. C.; Taylor, R. *Proteins* **2002**, *49*, 457-71.

(35) Jones, G. Willett, P. Glen, R. C. Leach, A. R.; Taylor, R. *J. Mol. Biol.* **1997**, *267*, 727-748.

(36) Bottegoni, G. Rocchia, W. Recanatini, M.; Cavalli, A. *Bioinformatics* **2006**, *22*, e58-65.

(37) Wang, J. Wolf, R. M. Caldwell, J. W. Kollman, P. A.; Case, D. A. *J. Comp. Chem.* **2005**, *26*, 114-114.

(38) Cornell, W. Cieplak, P. Bayly, C. I.; Kollmann, P. A. *J. Am. Chem. Soc.* **1993**, *115*, 9620–9631.

(39) Bayly, C. I. Cieplak, P. Cornell, W.; Kollman, P. A. *J. Phys. Chem.* **1993**, *97*, 10269-10280.

(40) Leone, V. Marinelli, F. Carloni, P.; Parrinello, M. *Curr. Opin. Struct. Biol.* **2010**, *20*, 148-154.

(41) Pietrucci, F. Marinelli, F. Carloni, P.; Laio, A. *Journal of the American Chemical Society* **2009**, *131*, 11811-11818.

(42) Piana, S.; Laio, A. *Phys. Rev. Lett.* **2008**, *101*, 1-4.

(43) Todorova, N. Marinelli, F. Piana, S.; Yarovsky, I. *J. Phys. Chem. B* **2009**, *113*, 3556-3564.

(44) Piana, S.; Laio, A. *J. Phys. Chem. B* **2007**, *111*, 4553-9.

(45) Bussi, G. Gervasio, F. L. Laio, A.; Parrinello, M. *Journal of the American Chemical Society* **2006**, *128*, 13435-41.

(46) Vargiu, A. V. Ruggerone, P. Magistrato, A.; Carloni, P. *The journal of physical chemistry. B* **2006**, *110*, 24687-24695.

(47) Branduardi, D. Gervasio, F. L. Cavalli, A. Recanatini, M.; Parrinello, M. *J. Am. Chem. Soc.* **2005**, *127*, 9147-9155.

(48) Fiorin, G. Pastore, A. Carloni, P.; Parrinello, M. *Biophysical J.* **2006**, *91*, 2768-2777.

(49) Vargiu, A. V. Ruggerone, P. Magistrato, A.; Carloni, P. *Nucleic acids research* **2008**, *36*, 5910-5921.

4. Computational methods: molecular docking and cluster analysis

Computational molecular docking is a research technique for predicting whether one molecule will bind to a target, usually protein. Ligand is a small molecule – compared to a protein, which is a macromolecule. When binding to a protein, the ligand changes the conformation of the larger molecule, thereby affecting the protein operation. In protein-ligand docking the goal is to predict the position and orientation of a ligand when it is bound to a protein receptor or enzyme. The initial situation is such where the structure of the inspected protein and the ligand are known. Because of the excess of possible conformations due to huge number of degrees of freedom in large systems such as macromolecules, all possible conformations cannot be compared. The problem must be somehow limited. Simplifying the model can reduce the need for computational power. Of course, the active site, where the protein-ligand interactions occur, must be modeled as precisely as possible but the further regions of the macromolecule can be modeled less precisely because of their interaction with the active region being much weaker.

Molecular docking is a computational tool and represents a crucial component of many drug discovery projects, from *hit* identification to *lead* optimization and beyond, such as structure-based design and virtual screening techniques.[1] It is widely used to predict binding modes and select putative ligands for a biological target.[2] The docking methodology was pioneered during the early 1980s and remains a current and highly active area of research, thanks also to its short time and low computational cost.[3]

In particular, it is a multi-step process in which each step introduces one or more additional degrees of complexity. Initially, the process begins with the application of algorithms that sample the several degrees of conformational freedom of small molecules "posing" them in the binding site. The algorithms are complemented by scoring functions that are designed to describe the biological activity through the evaluation of interactions between the ligand and the potential target as well as the entropic cost of the ligand conformation.

Some of these scoring functions adopted for molecular docking try to estimate the free energy of binding of the ligand-target complex.[4] Unfortunately, this estimation is not always reliable because of the high error associated to it. However, the molecular docking represents a useful technique in the computer-aided drug design and discovery context towards delicate issues such as the

identification of molecular features that are responsible for specific biological recognition and/or the prediction of chemical modifications to improve potency of ligands.

Both these programs adopt genetic algorithms[5] to generate the single poses of ligands into the binding site of protein target, which are evaluated by their appropriate scoring functions.

Molecular docking is a computational procedure that predicts binding mode of a ligand in its target protein. This is achieved by minimizing a scoring function, which describes the interactions between ligand and target with respect to the atomic positions of the two moieties. In the following paragraph I will explain these issues.

In this work, GOLD 3.0.1[6] and AutoDock 4.0[7,8] programs were used to predict ligand-protein interactions.

4.1. Algorithms in molecular docking

Several algorithms are used in molecular docking programs to obtain the pose of ligand in the binding site of protein.[6,9] In general, the docking problem is the search for the minimum of a function that depends on a large number of degrees of freedom, namely the position and the geometrical arrangement of ligand (its conformation) and of its target.

The algorithms adopted in molecular docking can be divided in three types of searches: systematic, stochastic and deterministic; some algorithms combine more than one of these approaches.

Systematic algorithms explore a grid of values for each degree of freedom considered, in a combinatorial way. As the number of degrees of freedom increases, the number of evaluations needed increases rapidly and termination criteria are inserted to prevent the algorithm from sampling space that is known to lead to the wrong solution. Stochastic search algorithms make random changes on the degrees of freedom of the system. To improve convergence, multiple independent runs are performed. In deterministic searches, the initial state determines the move that can be made to generate the next state, which generally has the same or a lower energy than the initial state.

4.2. Genetic Algorithms (GAs)

The Genetic Algorithms (GAs) belong the class of stochastic algorithms and are based on the language of natural genetics and evolutionary biology. GAs are computer programs that mimic the process of evolution by manipulating a collection of *n* data structures called chromosomes. Indeed, using genetic operations they search for possible conformations of ligands.[5,9]

The quality of results depends on the starting genes, the number of evolutionary events and the scoring function adopted to select the most favourable conformers. Firstly, the GA generates an initial population as set of chromosomes (conformations of ligands randomly chosen and determined into the binding pocket). The chromosomes are defined by one or more strings of genes (variables), that can assume binary, integer or real values corresponding to: i) ligand translation (x, y, z coordinates of the center of mass); ii) ligand orientation (rotation angles); iii) ligand conformation (torsion angle for each rotatable bond). The population undergoes to a fitness evaluation of ligand-protein complex: each chromosome is associated to a score based on a function that approximately estimates the binding free energy/fitness. Starting from an initial population of chromosomes (parents), randomly generated and subsequently evaluated on the basis of specific scoring function, the GA repeatedly applies the three genetic operators, such as *reproduction*,

crossover and *mutation*, to obtain a new population of chromosomes (children) that replace the least-fit members of the population.

- *reproduction* represents the selection process of the fittest members scored of a population that will survive in the next generation;
- *crossover* combines chromosomes by performing a one or two-point crossing on the parent strings resulting in the children ones (as higher the number of crossover points is, more information is exchanged between the parent strings);
- *mutation* randomly modifies one o more gene(s) to give the offspring chromosomes.

Thus, in contrast with the only *reproduction* operator, crossover and mutation allow the exploration of the conformational space through the introduction of children chromosomes to be submitted to a new cycle of genetic operations. The whole cycle is repeated until some generations are defined and/or until some conditions (i.e. RMSD, ΔG) are satisfied.

GOLD uses an island-based genetic algorithm search strategy and includes rotational flexibility for selected receptor hydrogen along with full ligand flexibility. AutoDock [7,8] uses a genetic algorithm as a global optimizer combined with energy minimization as a local search method. The ligand is flexible, while the receptor is rigid.

4.2.1. Genetic algorithm in GOLD

GOLD employs a so-called island-based genetic algorithm. This means that not only one large population of chromosomes (described in the previous section) is manipulated, but also several sub-populations (i.e. islands) are considered and individual chromosomes can migrate among them. This feature improves the efficiency of search. In addition, information concerning H-bonds between the ligand and the protein target is also encoded in the chromosome. The H-bonds are matched with a least squares fitting protocol to maximize the number of inter-molecular ones. A population of potential solutions (in this case, possible docking poses of ligand) is set up at random. Each member of the population is encoded as a chromosome which contains information on: i) the mapping of ligand H-bounded atoms onto complementary protein ones; ii) mapping of hydrophobic points on the ligand onto protein ones; conformation around flexible ligand bonds and protein OH-groups. Each chromosome is assigned a fitness score based on its predicted binding affinity and the chromosomes within the population are ranked according to fitness. The population of chromosomes is iteratively optimized.[10]

4.2.2. Genetic algorithm in Autodock

The AutoDock adopts a GA in which it is implemented a local search method, initially proposed by Solis and Wets,[11] that allows to minimize the scoring function of selected individuals. The optimized atomic coordinates (phenotype) are stored back in the chromosome (genotype). Then, the new chromosome enters into a new iteration of genetic operators employed by GA. Given this transfer of information from phenotype to genotype this algorithm is called Lamarckian genetic algorithm (LGA).[7]

4.3. Scoring Functions

The evaluation and ranking of predicted ligand conformations is a crucial aspect of molecular docking. Thus, the design of reliable scoring functions is of fundamental importance. Scoring functions implemented in docking programs make various assumptions and simplifications in the evaluation of modeled complexes and do not fully account for a number of physical phenomena that determine molecular recognition for example, entropic effects. Essentially, three types or classes of scoring functions are currently applied: force-field-based, empirical and knowledge-based scoring functions.

Molecular mechanics force fields usually quantify the sum of two energies, the receptor–ligand interaction energy and internal ligand energy (such as steric strain induced by binding). Most force-field scoring functions only consider a single protein conformation, which makes it possible to omit the calculation of internal protein energy, which greatly simplifies scoring. Various force-field scoring functions are based on different force field parameter sets.

The empirical scoring functions are fit to reproduce experimental data, such as binding energies and/or conformations, as a sum of several parameterized functions. The design of these scoring functions is based on the idea that binding energies can be approximated by a sum of individual uncorrelated terms. The coefficients of the various terms are obtained from regression analysis using experimentally determined binding energies and, potentially, X-ray structural information.

There are also the scoring functions knowledge-based, which are designed to reproduce experimental structures rather than binding energies. In knowledge-based functions, ligand–protein complexes are modeled using relatively simple atomic interaction-pair potentials. A number of atom-type interactions are defined depending on their molecular environment. In common with empirical methods, knowledge-based scoring functions attempt to implicitly capture binding effects that are difficult to model explicitly.

Here, we revise the scoring functions implemented in the programs used in the thesis: GoldScore and ChemScore for GOLD, and the empirical scoring function from AutoDock

4.3.1. GoldScore (GS) in GOLD

GS is a force-field-based scoring function and, in particular, it is defined the weighted sum of the following components (scores: *S*; see the equation reported below): the energies from H-bonds (S_{hb_ext}) and van der Waals interactions (S_{vdw_ext}) of complex protein/ligand, and the ones from internal van der Waals (S_{vdw_int}) and torsional strain (S_{tors_int}) of ligand.[6,12]

$$GS = S_{hb\_ext} + S_{vdw\_ext} + S_{tors\_int} + S_{vdw\_int}$$

Optionally, a fifth component describing the intra-molecular hydrogen bond (S_{hb_ext}) energy of ligand may be added. GS is defined as a fitness function, where every single component is coupled to some give coefficients. These were empirically determined on the basis of adjustments performed to best reproduce a series of known crystallographic ligand/protein complexes.

The H-bond term considers the difference between the interactions of protein and ligand in the complex and free in water, thus accounting for desolvation effect: initially the donor (*d*) and the acceptor (*a*) are considered in solution and, then, on coming together (*da*) water (*w*) is stripped off. Therefore, the H-bond energy E_{ij} between a donor *i* and an acceptor *j* between the ligand and the protein is composed by the following terms:

$$E_{ij} = (E_{da} + E_{ww}) - (E_{dw} + E_{aw})$$

The interaction energies for each donor and acceptor types are pre-calculated with quantum mechanics and molecular mechanics approaches for a set of model fragments. For all the poses of ligand generated, the possible combinations of donors *i* and acceptors *j* between the ligand and the protein's atoms surrounding it are evaluated and a weight w_{ij} between 0 and 1 is assigned to each bond on the basis of both the distance between donor and acceptor and the angle formed by donor, H atom and acceptor:

$$w_{ij} = w_{distance(ij)} + w_{angle(iHj)}$$

$$w_{distance(ij)} = \begin{cases} 1, & d_{LP} \le 0.25\ \text{Å} \\ \left(-\frac{10}{33} d_{LP} + \frac{35}{33}\right)^2, & 0.25 < d_{LP} \le d_{\max}\text{Å} \\ 0, & d_{LP} > d_{\max}\text{Å} \end{cases}$$

$$w_{angle(iHj)} = \begin{cases} 1, & \vartheta > 160° \\ \left(-\frac{1}{150}\vartheta + \frac{1}{15}\right)^2, & 10° < \vartheta \le 160° \\ 0, & \vartheta \le 10° \end{cases}$$

The distance d_{LP} is between the donor and the acceptor's lone pair. In default implementation of GOLD, d_{max} varies linearly from 4.0 Å at the first iterations to 1.5 Å after 75000 iterations to let only close-contacts H-bond contribute to GS fitness value of the final solutions. Similarly, is the angle between the donor, the H atom and the acceptor lone pair. The H-bond energy term in the scoring function is then given by the sum of all individual H-bond energies, multiplied by their weights:

$$E_{hb} = \sum_{ij} w_{ij}\, E_{ij}$$

The internal energy contribution is considered in GS function only when it is positive to avoid a lower minimization of the internal energy of ligand than of the one of reference conformation. It is the sum of the steric and torsional energies ligand: the steric energy is described by a sum over all the atoms $i \neq j$, separated by a distance d_{ij}, in the ligand of a 6-12 potential term:

$$E_{ij} = \frac{C}{d_{ij}^{12}} - \frac{D}{d_{ij}^{6}}$$

whereas the torsional one, associated with four consecutively bonded atoms I, j, k, l, is given by:

$$E_{ijkl} = \frac{1}{2} V_{ijkl} \left[1 + \frac{n_{ijkl}}{|n_{ijkl}|} \cos\left(|n_{ijkl}|\, \omega_{ijkl}\right)\right]$$

where ω_{ijkl} is the torsional angle, n_{ijkl} the periodicity and V_{ijkl} the barrier of rotation.

The term E_{vdw} describes the close-contact interaction energy and it is calculated as the sum over all pairs of atoms *i* and *j*, respectively from ligand and protein, which are distanced between them less than 1.5 times the sum of their van der Waals radii. A 4-8 potential is used to describe this interaction:

$$E_{ij} = \frac{A}{d_{ij}^8} - \frac{B}{d_{ij}^4}$$

where d_{ij} is the distance between two atoms. If $E_{ij} > sE_{ij,min}$, a linear cut-off is applied to switch off this interaction, $E_{ij,min}$ being the minimum of E_{ij} and *s* being a scaling factor whose value increases logarithmically during the run in order to encourage the close contacts. *A* and *B* were chosen with the aim at reproducing the minimum of the standard 12-6 potential of the form. The 4-8 potential is preferred because it is softer and allows the algorithm to easily form close-contacts with the protein.

4.3.2. ChemScore in GOLD

ChemScore was derived empirically from a set of 82 protein-ligand complexes for which measured binding affinities were available.[13,14] Unlike GoldScore, ChemScore was trained by regression against measured affinity data. ChemScore estimates the total free energy change that occurs on ligand binding as a sum of different components:

$$\text{ChemScore} = c_0 + c_{hbond}\, S_{hbond} + c_{metal}\, S_{metal} + c_{lipo}\, S_{lipo} + c_{rot}\, H_{rot} + P_{\text{clash}} + c_{\text{internal}}\, P_{\text{internal}} + (c_{\text{covalent}} P_{\text{covalent}} + P_{\text{constraint}})$$

where c_{hbond}, c_{metal}, and c_{lipo} are scores for hydrogen bonding, acceptor-metal, and lipophilic interactions, respectively. H_{rot} is a score representing the loss of conformational entropy of the ligand upon binding to the protein. The "*c*" terms are coefficients derived from a multiple linear regression analysis on a training set of 82 protein–ligand complexes from the PDB

$\boldsymbol{S_{hbond}}$ The summation function for hydrogen bond strengths is

$$S_{hbond} = \sum_{DA} B(\Delta r_{DA}, \Delta r_1, \Delta r_2)\, B(\Delta\alpha_{DA}, \Delta\alpha_{DA}, \Delta\alpha_{DA})$$

with $\Delta r_{DA} = |r_{DA} - r_0|$ and, $\Delta\alpha_{DA} = |\alpha_{DA} - \alpha_0|$, where r_{DA} is the H···A distance, and $\alpha_{DA}$the D-H···A angle for a given donor–acceptor pair. r_0 and α_0 are the ideal hydrogen-bond distance and angle, respectively. $\Delta r_1, \Delta r_2, \Delta\alpha_{DA}, \Delta\alpha_{DA}$ are constants that control the deviation from the ideal hydrogen-bond distance and angle.

The hydrogen-bond term is computed as a sum over all possible acceptor-donor pairs such that one atom belongs to the protein and the other to the ligand. Each term in the summation is the product of three Gaussian-smoothed block functions. The purpose of the block functions is to reduce the contribution of a hydrogen bond according to how much its geometry deviates from *(a)* ideal H···A distance (where 'H' is the hydrogen atom linked to the donor atom ('D'), '···' the hydrogen bond, and 'A' the acceptor atom), *(b)* ideal D-H…A angle (where D-H is a covalent bond between donor and hydrogen atom), and *(c)* ideal directionality with respect to the acceptor atom. The maximum contribution of a given acceptor-donor pair to the summation is 1; this will occur if the pair forms a hydrogen bond of "ideal" geometry.

The S_{hbond}, S_{metal}, and S_{lipo} terms all make use of a block function, B, of the following shape (see Panel A and B):

A

$$B(x, x_{ideal}, x_{\max}) = \begin{cases} 1 \text{ if } x \le x_{ideal} \\ 1.0 - \dfrac{x - x_{ideal}}{x_{max} - x_{ideal}} \text{ if } x_{ideal} \le x \le x_{max} \\ 0 \text{ if } x > x_{max} \end{cases}$$

B

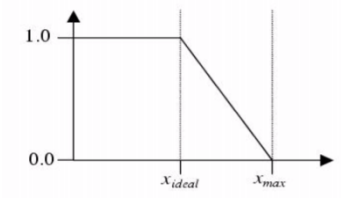

C

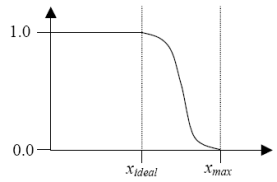

In ChemScore the block function is convoluted with a Gaussian function (see panel C).

S_{metal} The metal-binding term in ChemScore is computed as a sum over all possible metal-ion acceptor pairs, where the acceptor is an atom in the ligand that is capable of binding to a metal. It only has a distance dependency.

S_{lipo} The lipophilic term is defined in a similar way.

$$S_{lipo} = \sum_{Ll} B(\Delta r_{Ll}, \Delta r_L, \Delta r_l)$$

The summation here is over all pairs of lipophilic atoms in protein and ligand. r_{Ll} is the distance between protein and ligand atom for a given pair of lipophilic atoms. $r_L$and r_l are constants controlling the range of lipophilic interactions. Lipophilic atoms are defined as non-accepting sulphurs, non-polar carbon atoms and non-ionic chlorine, bromine and iodine atoms.

The final ChemScore fitness function contains terms such as clash penalty term (H_{rot}) and internal torsion term.

$\boldsymbol{H_{rot}}$ estimates the flexibility penalty for molecules with frozen rotatable bonds:

$$H_{rot} = 1 + \left(1 - \frac{1}{N_{rot}}\right) \sum_{r} \frac{1}{2} \left(P_{nl}(r) + P'_{nl}(r)\right)$$

$\boldsymbol{N_{rot}}$ being the number of frozen rotatable bonds, and $P_{nl}(r)$ and $P'_{nl}(r)$ the percentages of polar atoms on either side of the rotatable bond.

Clashes between protein and ligand atoms and ligand internal torsional strain are accommodated by penalty terms ($\mathbf{P_{clash}}$) in order to prevent poor geometries in docking. The clash penalty terms differ on the nature of the contact, whether it is a hydrogen-bonding contact, a metal-binding contact or neither of these. Covalent and constraint scores may also be included.

4.3.3. Scoring function in Autodock

In AutoDock[7] the implemented scoring function is defined as an empirical binding free energy function:

$$\Delta G = \Delta G_{vdW} \sum_{i,j} \left(\frac{A_{ij}}{r_{ij}^{12}} - \frac{B_{ij}}{r_{ij}^{6}}\right) + \Delta G_{hbond} \sum_{i,j} E(\phi) \left(\frac{C_{ij}}{r_{ij}^{12}} - \frac{D_{ij}}{r_{ij}^{10}}\right) + \Delta G_{elec} \sum_{i,j} \left(\frac{q_i\, q_j}{\varepsilon\,(r_{ij})\, r_{ij}}\right)$$
$$+ \Delta G_{tor}\, N_{tor} + \Delta G_{sol} \sum_{i,j} \left(S_i\, V_j + S_j V_i\right) e^{\left(-\frac{r_{ij}^2}{2\sigma^2}\right)}$$

The summations are performed over all pairs of ligand atoms, *i*, and protein atoms, *j*, in addition to all pairs of atoms in the ligand separated by three or more bonds. r_{ij} is the distance between the atoms, φ is the H-bond angle, and q_i is the electrostatic charge of atom *i*. All five ΔG terms on the right hand side are coefficients empirically determined using linear regression analysis from a set of thirty protein-ligand complexes with known binding constants. The first three terms are in vacuo interaction terms: Lennard/Jones 12-6 dispersion-repulsion term; a directional 12-10 hydrogen bonding term; screened Coulomb electrostatic potential. ΔG_{tor} is a measure of the unfavorable entropy of ligand binding due to the restriction of conformational degrees of freedom, and N_{tor} is the number of sp^3 bonds in the ligand. The last term approximately accounts for the desolvation free energy upon ligand binding. For each atom in the ligand, fragmental volumes of surrounding

protein atoms (V*j*) are weighted by an exponential function and then summed, evaluating the percentage of volume around the ligand atom that is occupied by protein atoms. This percentage is then weighted by the atomic salvation parameter of the ligand atom (S_i) to give the desolvation energy.

4.4. Cluster Analysis

AClAP implements a hierarchical agglomerative clustering algorithm.[15,16] Hierarchical'' means that clusters at a higher level are union of clusters at lower levels, while ''agglomerative'' means that clusters never break apart during the formation process. The global hierarchy can be represented by means of a dendrogram, a tree showing different clustering levels, spanning from 1 to *n*. RMSD is taken as a measure of conformation-to-conformation distance. Therefore, the clustering algorithm starts with *n* unitary clusters; at each step, the two closest clusters are merged, until only one cluster containing all the poses is reached.[17] The way the inter-cluster distance is evaluated by the average linkage method. Once the hierarchical tree is built, KGS penalty function is used to define the best clustering level and to prune it. At the end for each cluster, the representative conformation is calculated.[15,16]

References

(1) Kitchen, D. B. Decornez, H. Furr, J. R.; Bajorath, J. *Nat. Rev. Drug Discov.* **2004**, *3*, 935-49.

(2) Yuriev, E. Agostino, M.; Ramsland, P. a *J. Mol. Recognition* **2010**, 149-164.

(3) Onodera, K. Satou, K.; Hirota, H. *J. Chem. Inf. model.* **2007**, *47*, 1609-18.

(4) Pérez, C.; Ortiz, a R. *J. Med. Chem.* **2001**, *44*, 3768-85.

(5) Jones, G. Willett, P. Glen, R. C. Leach, A. R.; Taylor, R. *J. Mol. Biol.* **1997**, *267*, 727-748.

(6) Jones, G. Willett, P. Glen, R. C. Leach, a R.; Taylor, R. *J. Mol. Biol.* **1997**, *267*, 727-48.

(7) Morris, G. M. Goodsell, D. S. Halliday, R. S. Huey, R. Hart, W. E. Belew, R. K.; Olson, A. J. *J. Comp. Chem.* **1998**, *19*, 1639-1662.

(8) Morris, G. M. Huey, R. Lindstrom, W. Sanner, M. F. Belew, R. K. Goodsell, D. S.; Olson, A. J. *J. Comput. Chem.* **2009**, *30*, 2785-91.

(9) Taylor, R. D. Jewsbury, P. J.; Essex, J. W. *J. Comput. Aided Mol. Des.* **2002**, *16*, 151-66.

(10) Schulz-Gash, T.; Stahl, M. *Drug Discov. Today* **2004**, *1*, 231-239.

(11) Solis, F. J.; Wets, R. J.-B. *Math. Operat. Res* **1981**, *6*, 19-30.

(12) Jones, G. Willett, P.; Glen, R. C. *J. Mol. Biol.* **1995**, *245*, 43-53.

(13) Verdonk, M. L. Cole, J. C. Hartshorn, M. J. Murray, C. W.; Taylor, R. D. *Proteins* **2003**, *52*, 609-23.

(14) Eldridge, M. D. Murray, C. W. Auton, T. R. Paolini, G. V.; Mee, R. P. *J. Comput. Aided Mol. Des.* **1997**, *11*, 425–445.

(15) Bottegoni, G. Rocchia, W. Recanatini, M.; Cavalli, A. *Bioinformatics* **2006**, *22*, e58-65.

(16) Bottegoni, G. Cavalli, A.; Recanatini, M. *J. Chem. Inf. Model* **2006**, *46*, 852-62.

(17) Kelley, L. A. Gardner, S. P.; Sutcliffe, M. J. *Protein Eng. Des. Sel.* **1997**, *10*, 737-741.

5. Design, synthesis and evaluation of three classes of anti-prion compounds to attack prion diseases on multiple fronts

The multi target directed ligand (MTDL) theory is becoming an interesting approach in the drug discovery field, being particularly used to combat multifactorial diseases. For the last ten years, many research groups have been involved in designing and synthesizing MTDLs against cancer, depression, schizophrenia and neurodegenerative disorders. With the aim of exploiting for the first time this approach in prion diseases, we developed two series of MTDLs able to act as antioxidants and simultaneously slow down PrP^{Sc} aggregation (**Chapters 6** and **7**). Additionally, a compound with dual antiprion and metal chelator activity has been developed (**Chapter 8**).

I designed and synthesized the developed compounds in the Medicinal Chemistry laboratory of Prof. M. L. Bolognesi (University of Bologna) whereas the biological experiments were performed by Dr. Hoang Ngoc Ai Tran in the Prion Biology Laboratory of Prof. G. Legname (Neurobiology Sector, International School for Advanced Studies, SISSA).

5.1. Introduction

Prion diseases are lethal for both humans and animals. Although researchers have attempted for decades to develop effective therapeutics for the therapy of human and animal prion disorders, until now no drug has been available on the market for TSE treatment or cure.[1-4]

The effectiveness of a potential antiprion drug is, in principle, tested by three systems: in vitro systems representing mainly scrapie propagating cells, in vivo systems representing scrapie-infected rodents or macaques, and finally clinical studies. Although a series of drug candidates demonstrated convincing effects in vitro and in vivo, all tested compounds failed to show significant effects in patients with prion diseases.[5] As for other neurodegenerative disorders, the development of an effective antiprion compound is particularly challenging because the drug has to penetrate the blood–brain barrier.[2-4] Thus, although several compounds were effective in cell culture systems, in many cases they lacked any effect in vivo because of their low penetration into the CNS.[5]

Nowadays the protein-only theory has become widely accepted, and therefore current therapeutic strategies are primarily aimed at the development of molecules able to preventing conversion of PrP^{C} to PrP^{Sc} at different levels of this multistage process.[2-4] Targeting PrP^{Sc} may appear the most logical approach, but such targeting might have no effect on disease progression if PrP^{Sc} is a non-pathological end-point. To note, there is increasing evidence that PrP^{Sc} in vivo is not directly neurotoxic, and there is a lack of correlation between PrP^{Sc} deposition and disease severity,[6] suggesting that the conversion of PrP^{C} to PrP^{Sc} is the key event in prion pathogenesis, rather than the accumulation of PrP^{Sc}. Thus, targeting PrP^{C} has the potential to eliminate the substrate (PrP^{Sc}) for the pathogenic conversion, and is applicable regardless of the disease etiology. While the protein-only hypothesis stands for in vitro conversion of PrP^{C} to PrP^{Sc}, the mechanism underlying in vivo conversion, although not fully elucidated yet, seems to be more complex, possibly involving some molecular chaperones.[2-4] Recently, it has been gradually accepted that prion disease pathogenesis involves a complex array of processes (protein aggregation; oxidative stress; unbalance of metal ions; brain inflammation) operating simultaneously and synergistically.[7] Thus, the failures of drug candidates developed according to the traditional drug discovery paradigm "one-molecule-one target" and the current challenge of discovering an efficacious therapy are likely related to the multifactorial nature of these diseases. This is in line with what has been found in other neurodegenerative diseases, such as Alzheimer's disease (AD).[8] Against this backdrop, a polypharmacological approach consists in the concerted pharmacological intervention against multiple targets, and might show superior efficacy and safety towards complex neurological disorders. In this thesis this strategy has been applied for the first time to rationally design new ligands against prion diseases.

5.2. Multi-target directed ligand (MTDL) approach

Drugs that modulate multiple targets simultaneously (polypharmacology) might have the potential to enhance efficacy or improve safety relative to drugs that address only a single target.[9] Since lack of efficacy and poor safety are currently the main causes of failure of clinical candidates, it is not surprising that the multi-target drug discovery (MTDD) area is attracting increasing attention among drug discoverers.[10] Several drugs currently on the market have been found to have activity at more than one target, but in most cases the multiple activities were not deliberately designed, but only discovered in retrospect. A recent trend in medicinal chemistry has been to rationally design ligands that act selectively on multiple targets (selectively nonselective drugs). These compounds have been named MTDLs to distinguish them from the historical multiple agents or so called "promiscuous drugs" that often have poor selectivity and off-target effects as result of a non-rational design.[11] Currently, there are three complementary polypharmacological approaches. The first involves combining two or more different drugs that have different therapeutic mechanisms. In fact, when a single drug is not sufficient to effectively treat a disease, a multiple-medication therapy (MMT) (also referred to as a "cocktail" or "combination of drugs") may be used. However this approach might be disadvantageous for patients with compliance problems. A second approach might be the use of a multiple-compound medication (MCM) (also referred to as a "single-pill drug combination"), which implies the incorporation of different drugs into the same formulation in order to simplify dosing regimens and improve patient compliance. Finally, a third approach involves discovering single agents that are simultaneously capable of addressing two or more targets, i.e. MTDLs (**Figure 23**).[9-12] Increasing numbers of MTDLs are being reported in the literature and have been successfully exploited in the fields of AD and similarly complex diseases.[9-22]

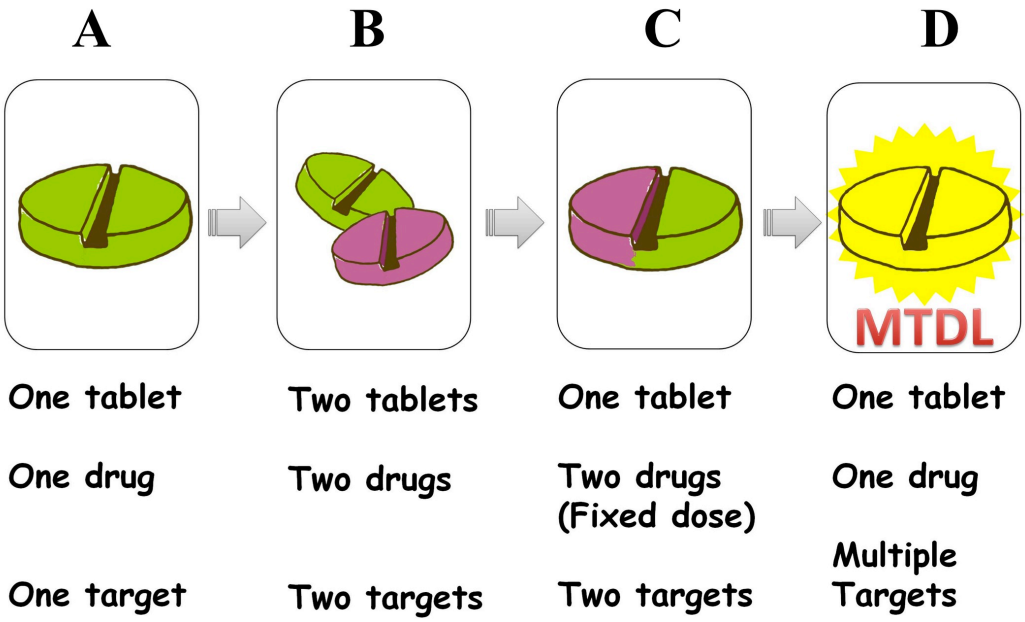

Figure 23. Therapeutic strategies: evolution of monotherapy (A) to therapy with different drugs forming a multiple-medication therapy (MMT) (B) or a multiple-compound medication (MCM) (C) or with a single drug molecule able to modulate multiple targets (D). Strategies depicted in (B), (C), and (D) should, in principle, produce the same therapeutic effect in treating a given disease. However, only (D) avoids the risk of drug-drug interactions that are possible with (B) and (C).

Clearly, therapy with a MTDL (see **Figure 23**) would have intrinsic advantages over MMT or MCM.[23] It would obviate the challenge of administering multiple single-drug entities, which could have altered bioavailability, pharmacokinetics, and metabolism. Indeed, if a single molecular species can show a complex ADMET profile, an MMT/MCM approach might be untenable. Furthermore, in terms of pharmacokinetic and ADMET optimization, the clinical development of a drug able to hit multiple targets should not, in principle, be different from the development of any other single lead molecule. It thus offers a much easier approach than MMT/MCM. More importantly, the risk of possible drug-drug interactions would be avoided and the therapeutic regimen greatly simplified in relation to MMT/MCM. All these considerations are of particular relevance, as one of the major contributions to the attrition rate in drug development continues to be the drug candidate's pharmacokinetic profiling.[24] There is, therefore, a strong indication that the development of drugs able to act at different levels of the neurotoxic cascade might disclose new opportunities for the treatment of major neurodegenerative diseases, for which an effective cure is an urgent need and an unmet goal (**Figure 24**).[25]

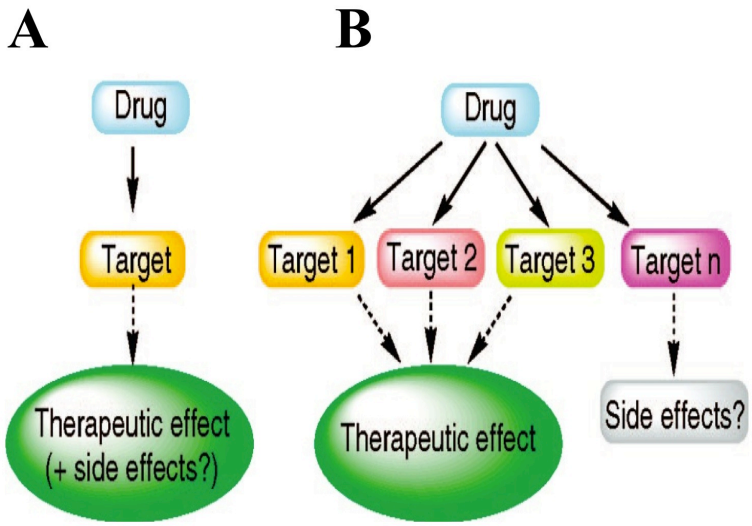

Figure 24. Pathways leading to the discovery of new medications: (A) Target-driven drug discovery approach, that is, the application of the current one-molecule-one-target paradigm. (B) MTDLs approach to drug discovery. A drug could recognize (in principle, with comparable affinities) different targets involved in the cascade of pathological events leading to a given disease. Adapted from Cavalli *et al.* [25]

However, the selection of the therapeutic targets (to seek either a single- or a multi-target-directed ligand) is one of the biggest challenges in designing new molecules for multifactorial neurodegenerative diseases. Clearly, MTDLs should target the most important pathophysiological processes. Obviously, better understanding of which targets are therapeutically relevant should shed light on the underlying causes of this diseases and may also help in the development of more efficacious drugs. However, more clues on the target selection come from the system biology approach which can help to identify targets for intervention.[17,26]

The main criticism to MTDL drug discovery paradigm is that this approach is ambitious, because the rational design of MTDLs has to deal with the critical issues of affinity balancing and pharmacokinetics.[11] However, as proof of principle, and to support the view that MTDLs are destined to become the mainstream of neurodegenerative diseases therapeutics in the next years, it could be useful to mention the successful case of ladostigil (TV-3326), an MTDL developed by Youdim and co-workers, which is currently in phase II clinical trials for AD.[g]

[g] http://clinicaltrials.gov/ct2/show/NCT01354691

5.3. Strategies for Designing MTDLs

Basically, two conceptually different methods[23] have been followed to generate MTDL hit compounds with which to commence a MTDD project. They are:

- **Screening approaches**
- **Knowledge-based approaches**

The first approach involves the random screening of either diverse or focused compound libraries to different targets. The second one is the most common MTDL generation strategy reported in the literature, termed "framework combination". Framework combination starts with two compounds, one of which binds with high selectivity to one of the targets and the other with high selectivity to the other target of interest. The goal is to combine both activities into a single molecule by integrating the frameworks (and the underlying pharmacophores) of the two selective molecules. MTDLs arising from framework combination can be viewed as linked, fused, or merged depending upon the degree to which the frameworks have been integrated (see **Figure 25**).[9-12]

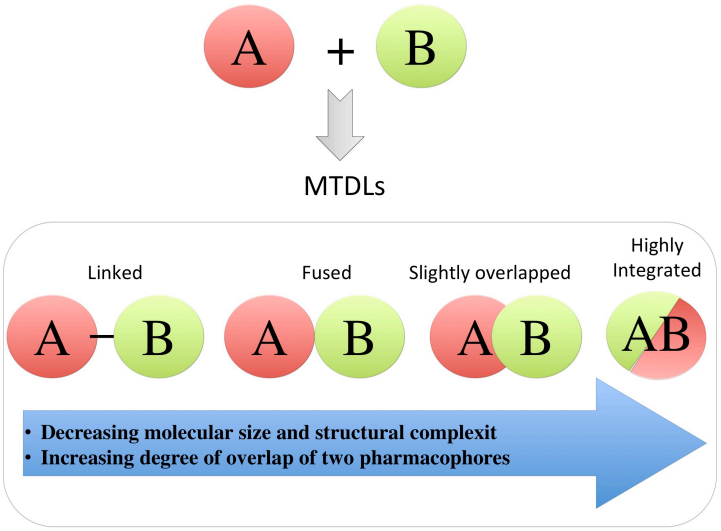

Figure 25. Framework combination is a knowledge-based approach to generate MTDLs.

In linked MTDLs, the molecular frameworks are joined by linker groups that are not found in either of the selective ligands, and the different ends of the molecule are typically responsible for the activity at the different targets. A cleavable or non-cleavable linker might be used. The majority of reported examples of cleavable conjugates (termed "codrug") contain an ester (or amide, disulfide) linker that is cleaved by plasma enzymes to release the two individual drugs that then act independently.[27] The first clinically used codrug for the treatment of rheumatoid arthritis was

sulfasalazine (Salazopyrin), a derivative of mesalazine. It is a combination of sulfapyridine and 5-amino salicylic acid coupled with an azo linkage. The linkage is broken down by the enzyme azoreductase.[28] Currently the drug is used for the treatment of ulcerative colitis.[29] Portoghese *et al.* reported heterodimeric conjugates containing delta-antagonist (naltrindole) and kappa-agonist (ICI-199441) pharmacophores tethered by metabolic stable linkers.[30,31] If the frameworks are in contact but there is neither a discernable linker nor much framework overlap, the MTDL can be viewed as fused. Finally, in merged MTDLs, the frameworks are overlapped by taking advantage of commonalities in the chemical structures of the starting compounds. Normally, medicinal chemists will aspire to maximize the degree of overlap in order to produce smaller and simpler molecules, which have a better chance of oral activity. It might be expected that an MTDL would be larger and more complex than single target ligands. Because larger and more flexible molecules have been associated with poorer PK profiles, optimizing the pharmacokinetics of the lead compound while retaining a balanced target profile is frequently the most challenging aspect of a MTDD project.[9]

5.4. Polypharmacology in prion diseases

Although a polypharmacological approach is still in its infancy in prion diseases, the MMT strategy has been already addressed. Indeed, drug combination (DC) strategy has been applied in numerous in vitro and in vivo approaches with the aim of exploiting synergistic effects. The several examples reported in **Table 3** suggest that inhibition of prion replication can be effectively potentiated by DC treatment.

Table 3. Two-drug or three-drug combinations in prion diseases

Two-drug combination	**Two prion aggregation inhibitors (quinacrine and desipramine)**	**Ref. 35-37**
	Cholesterol ester modulators (everolimus, pioglitazone) + **prion aggregation inhibitors** (chlorpromazine)	**Ref. 32**
	Cholesterol ester modulators (everolimus, pioglitazone) **+ prion aggregation inhibitor** (quinacrine)	**Ref. 32**
	a heparan sulphate mimetic (pentosan polysulfate) **+ ligand targeting PrP^C** (Fe(III)meso-tetra(4-sulfonatophenyl)porphine)	Ref. 34
Three-drug combination	**Two prion aggregation inhibitors** (quinacrine and desipramine) **+ an inhibitor of cholesterol biosynthesis** (simvastatin)	Ref. 39

As for MTDLs, the literature contains cases where the deliberate aim of creating an MTDL has not always been explicitly stated. Instead, the molecular hybridization strategy has been followed, leading, to chimeric molecules capable, in principle, of modulating multiple targets. The first anti-prion chimeric ligand, Quinpramine (**4**, **Figure 26**) was designed on the basis of in vitro synergistic anti-prion effects of drugs Quinacrine (**2**) and Imipramine (**3**). **4**, obtained by linking **2** and **3** moieties through a piperazine ring, showed an improved anti-prion activity as much as 15-fold over **2** and 250-fold over **3**.[39,44]

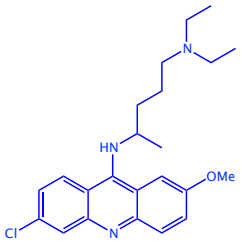

2

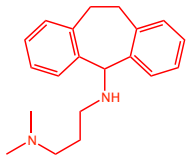

3

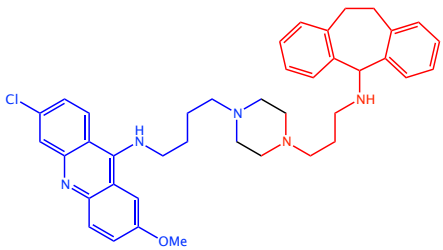

4

Figure 26. Design of **4**

In the following sections, we will describe the fragments used to design MTDLs by exploiting a framework combination approach. Fragments can be divided in three categories:

- Prion recognition motifs (PRMs);
- Antioxidant fragments;
- Metal ion chelator fragments.

5.5. Privileged structures as "Prion-Recognition Motif"

A privileged structure is a molecular scaffold able to provide potent and selective ligands for a range of different biological targets through the modification or insertion of particular functional groups. Privileged structures should possess good drug-like properties, which in turn should lead to more drug-like compounds. The concept of privileged structures was first introduced by Evans et al. in 1988[45] and was later updated by Patchett and Nargund.[46] For nearly 20 years, privileged structures have represented an ideal source of core scaffolds and capping fragments for the design of combinatorial libraries directed at a broad spectrum of targets. Numerous privileged structure-based libraries have proven to be extremely effective for the rapid discovery and optimization of potent and selective ligands for a wide variety of GPCRs,[47] kinases, proteases and even PPIs.[48]

Two heterocyclic motifs, namely quinoline and acridine, are particularly frequent in compounds with multiple and diverse biological activities and also active against prion diseases. For this reason they can be considered truly privileged structures (see **Figure 27**).

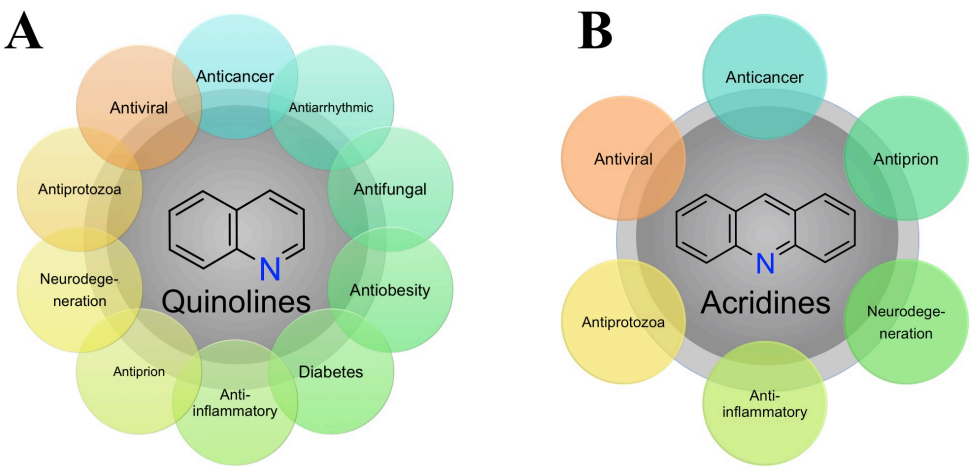

Figure 27. Quinolines (A) and acridines (B) because of their recurrence in a broad variety of biologically active compounds that hit different pharmaceutical targets and pathways are truly privileged scaffolds.

5.5.1. Quinolines and prion diseases

Quinoline derivatives are promising antiprion drug candidates (**Figure 28**). Antimalarial drugs **5** and **6** have been reported in several studies as effective antiprion compounds.[49,50] Stimulated by the findings that the same compounds (i.e., **5** and **6**) cured both prion and protozoan diseases, Korth and co-workers undertook to draw out the structure-activity relationships (SAR) of a series of antiprion and antimalarial quinolines.[39] Interestingly, **7** displayed antiprion activity at nanomolar range in

scrapie-infected cells and inhibited *P. falciparum* growth at the same concentration, suggesting that some molecular targets of antiprion and antimalarial ligands might overlap.[42] As in the antimalarial projects, bis-quinolines were also tested as inhibitors of PrP^{Sc} accumulation in cell cultures. Bis-quinoline **8** inhibited prion fibril accumulation in scrapie-infected cells. Surface plasmon resonance (SPR) studies showed that **8** binds with high affinity to recombinant mouse PrP. In general, bis-quinolines were more effective than quinolines in inhibiting prion fibril formation in vitro, but with marginal effectiveness in vivo.[40] Interestingly, **8** is a highly specific copper chelator and also has a superoxide dismutase-like activity. It was Fukuuchi *et al.* who demonstrated that **8** decreases the total amount of PrP and PrP mRNA expression in prion-infected cells. These results suggest that **8** may inhibit PrP biosynthesis and/or PrP transition to the cell surface and decrease the amount of substrate available for conversion to PrP^{Sc}.[51] Fragment **9** inhibits the aggregation of Syrian hamster PrP ($ShaPrP^{109-149}$, residues 109-149) significantly.[52]

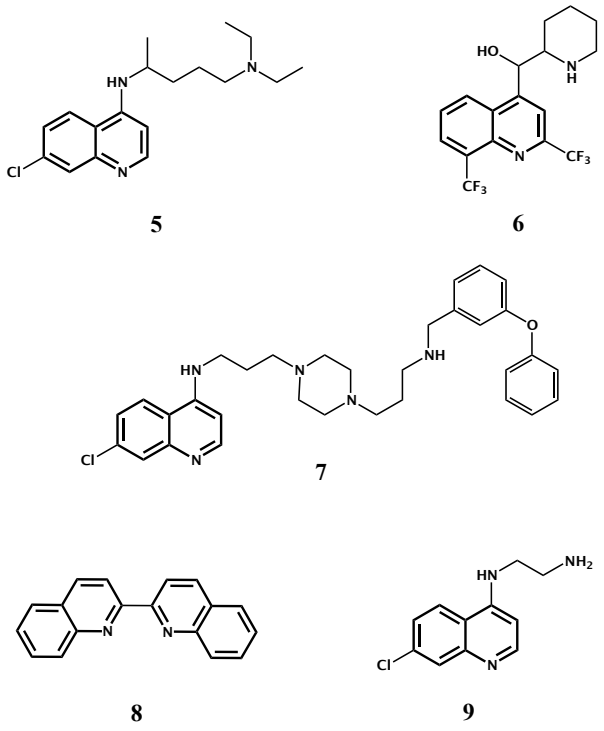

Figure 28. Quinoline derivatives for neurodegenerative diseases.

5.5.2. Acridines and prion diseases

Quinacrine (**2**, **Figure 26**) (EC_{50} = 0.3-0.5 μM) was used to treat malaria until more effective drugs replaced it. A renewed interest arose from its ability to inhibit prion formation, suggesting that it could offer an effective treatment for prion diseases.[53] **2** and several acridine derivatives were shown to block the infectious PrP isoform (PrP^{Sc}) formation in scrapie-infected cells.[54] In a recent clinical trial (PRION-1), **2** was reasonably tolerated but did not significantly affect the clinical course of the disease.[55] One explanation for the lack of benefit from **2** in this study was that adequate drug concentrations were not achieved in the CNS because **2** is known to be a substrate for P-glycoprotein multi-drug resistance (MDR) transporters. Moreover Ghaemmaghani *et al.* demonstrated by using $MDR^{0/0}$ mice that **2** eliminates only a specific subset of PrP^{Sc} conformers, resulting in the survival of drug-resistant prion conformations. The results suggest that the failure of **2** in vivo cannot be attributed solely to its pharmacokinetic properties.[56] The quinacrine analogs (**10-11,** see **Figure 29**), which have dialkylaminoalkyl side chains at 9-amino position, have been qualified by SPR as strong $hPrP^{C}$ binders.[57] To overcome the limitations associated with the use of **2** in prion diseases, several groups began research efforts aimed at identifying more potent analogs with a better pharmacokinetic profile. A focused library of variously substituted 9-aminoacridines was screened for bioactivity against accumulation of PrP^{Sc}.[41] **13** (see **Figure 29**, EC_{50} = 0.4 ± 0.1 μM) showed a reduced cytotoxicity toward liver and kidney cells. SAR studies conducted by Cope *et al.* have shown that an electron-rich aromatic ring attached through an amine linker to the position para to the ring nitrogen is beneficial for both binding to PrP^{C} and suppressing PrP^{Sc} accumulation. **13** demonstrated activity in the micromolar range (EC_{50} = 0.25 μM).[41] A 9-anilinoacridine **14**, structurally related to **13**, displayed a submicromolar EC_{50} value (0.06 μM) on ScN2a cell models, lower than that of **2** (EC_{50} = 0.23 μM).[57]

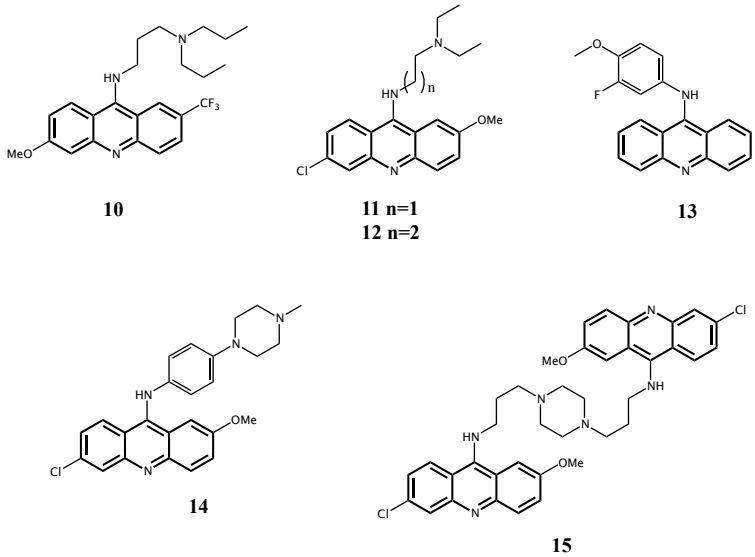

Figure 29. Acridine derivatives for prion diseases.

Due to the propensity of PrP^{Sc} to assemble into multimeric forms, May *et al.* postulated that dimers of **2** could be more potent inhibitors of prion replication. They joined different tricyclic heterocycles through alkyl, polyamine and alkyl ether chains. Interestingly, antimalarial compound **15** (BiCappa) was shown to reduce PrP^{Sc} levels in ScN2a cells with an efficacy 10-fold greater than that of **2** (EC_{50} = 0.30 μM).[43] Another dimeric compound was developed by Korth and co-workers based on the enhanced effect of tricyclic antidepressant imipramine (**3**) in combination with **2**. They thus synthesized the hybrid ligand Quinpramine (**4**, see **Figure 26**).[39,44]

Considering the key role of a planar hydrophobic structure in perturbing PPIs in conformational diseases, and the wide activity of acridine and quinoline derivatives in prion diseases, it is conceivable that these motifs are privileged PRMs.

5.6. Antioxidants used as antiprion compounds

Studies on prion-infected cell and mouse models have provided useful information on the therapeutic potential of antioxidants.[58] Although a clinically viable antioxidant that can alleviate prion disease–associated neurotoxicity is lacking, many observations argue that neutralizing oxidative stress may have therapeutic benefit in prion disease and provide the basis for future investigations in this area.[4] In the following a list of antioxidants studied in prion diseases is reported.

- Flupirtine has the exceptional ability to normalize intracellular glutathione levels and restore oxidative balance within the cell thereby combating accumulation of ROS and other free radicals A study published in 2004 reported some beneficial effects on cognitive function in patients with CJD.[59]
- Curcumine is was shown to also be an efficient inhibitor of PrP^{Sc} propagation by interacting with PrP. Unfortunately, efforts to show in vivo efficacy of curcumin have so far failed.[60,61]
- The nonpsychoactive *Cannabis* constituent cannabidiol, thanks to its multiple property (antioxidant, NMDA antagonist, regulator of microglial migration and activation) inhibited PrP^{Sc} accumulation in both mouse and sheep scrapie-infected cells.[62]
- Vitamin E enhances survival of $Prnp^{0/0}$ cells significantly more than of wild-type cells in a dose-dependent manner.[63]
- Martin *et al.* demonstrated an up-regulation of Coenzyme Q (CoQ) dependent antioxidant systems in response to the increased oxidative stress induced by prion infection

in nervous tissue. Thus, they suggested to use CoQ related agents able to cross the blood–brain barrier.[64]

- Lipoic acid was administered together with other antioxidants to a patient affected by prion disesases, showing moderate therapeutic effects.[65]

5.6.1. Selected Fragments with antioxidant properties

Among the above mentioned antioxidants which showed potential against prion diseases, we focussed on Coenzyme Q (**16**) and lipoic acid (**17**), which may be useful to prevent or treat prion dementias.[65]

5.6.1.1. 1,4-benzoquinones

16 is an important endogenous lipophilic antioxidant found in all organisms. **16** (**Figure 30**) is composed of an isoprenoid tail joined to a BQ nucleus. 10 isoprene units form the tail. It is known to have a role in electron transport and proton transfer in mitochondrial and bacterial respiration (**Figure 31**). **16** is an electron acceptor molecule of the electron transport chain. Ubiquinone is the oxidized form of **16**, while ubiquinol corresponds to a reduced form. When ubiquinone accepts a pair of electrons (along with a pair of hydrogen ions), it becomes ubiquinol, which is the "active" antiozidant form. **16** also a role in the prevention of mitochondrial dysfunction,[66,67] apoptosis,[68,69] and oxidative damage.[66,67] In neurodegenerative disorders, especially in aging and Alzheimer's disease, levels of **16** are altered, suggesting a role in disease progression. In effect, **16** has been used as a therapeutic agent against certain neurodegenerative disorders.[68,69]

The efficacy of **16** in the treatment of TSE neurodegenerative disorders should be improved by studying related agents able to cross the blood–brain barrier better than **16**, because the brain penetration of **16** from a enriched diet or peritoneal inoculation has been described as very poor.[67,70,71] As a further support to the potential of BQ derivatives against neurodegenerative processes, we should mention that **16** and different benzoquinone derivatives have been previously shown to modulate Alzheimer's disease molecular targets, directly inhibiting Aβ aggregation.[14,72]

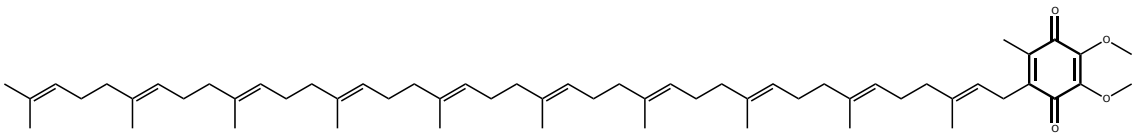

16

Figure 30. Structure of Coenzime Q (**16**)

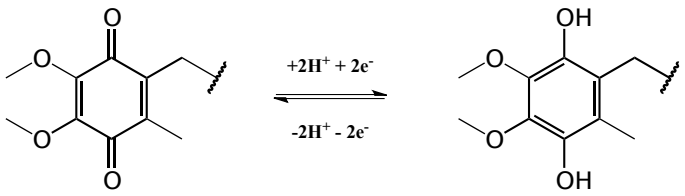

Oxidized **Reduced**

Figure 31. Redox Reactions of **16**.

Based on these findings, we decided to exploit a 2,5-bis-diamino-1,4-benzoquinone nucleus to design new antiprion agents. To note, in this structure, because of the resonance effect of the quinone ring, a hydrophobic and planar π system is generated, which is able in principle to bind amyloid and to perturb protein–protein interactions in the fibrillogenesis process.[73];

5.6.1.2. α–Lipoic acid

Lipoic acid (**17**, see **Figure 32)** is known as a universal antioxidant.

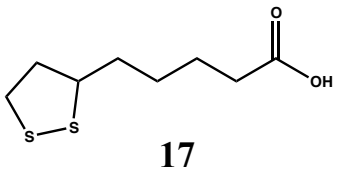

17

Figure 32. Structure of α-lipoic acid

The reduced form of **17** (**Figure 33**) acts as an antioxidant by directly scavenging ROS, by reducing the oxidized form of other endogenous antioxidants, and by chelating transition metals, rendering such metals either redox inactive or facilanting their removal from the cell.[74,75]

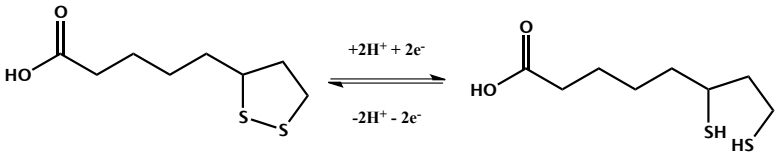

Oxidized **Reduced**

Figure 33. Oxidized and reduced lipoic acid.

17 is readily absorbed by diet, transported, taken up by cells, and reduced to dihydrolipoic acid in various tissues, including brain. It has been demonstrated that dihydrolipoic is an even more potent antioxidant than lipoic acid.

All in all, we selected lipoic acid (**17**) for the following reasons: (i) the molecule is an endogenous antioxidant; (ii) well-tolerated in vivo; (iii) effective against fibril formation; (iv) chemically linkable to the amine group by amide bond formation. On this basis, **17** was proposed by us as a lead structure for designing MTDLs for neurodegeneration.[74,75]

5.7. Metal chelators used as antiprion compounds

As discussed in **Chapter 1**, chelation therapy has been proposed as a valuable therapeutic approach towards prion diseases.[76] As an example, metal chelators shown to be effective are reported.

- Chelation of copper with D-penicillamine, a drug used routinely for treating Wilson disease, decreased brain-copper content of prion-infected mice by 30% and prolonged the incubation period, supporting the idea that increased levels of brain copper promote diseases.[77]
- Clioquinol is an antibiotic that binds to zinc, copper, and iron, and crosses the blood–brain barrier effectively. The use of Clioquinol in scrapie-infected hamsters increases the incubation time, suggesting a future potential for the use of this drug in humans.[79]
- Chrysoidine, a chelating agent, is about 27 times more effective than quinacrine in ScNB cells.[78]

Clioquinol or 5-chloro-7-iodo-8-hydroxyquinoline (**18**, **Figure 34**),[79] was used in the past as an antibiotic for treating diarrhea and skin infection.[80] Moreover, **18** [81] inhibits metal-induced Aβ aggregation[82] and reactive oxygen species generation in vitro and in AD transgenic mice.[80] **18** was thus studied in 2003 in a randomized, placebo-controlled, phase II clinical trial by Ritchie *et al.*[87] Because of toxic effects, clioquinol has been abandoned in favor of a successor compound, PBT2 (**19**), which lacks the iodine atom.[81] **19** targets metal-induced aggregation of Aβ, but is more effective as a Zn/Cu ionophore and has greater BBB permeability than **18**.[83] 8-Hydroxyquinoline compounds have also found application in Parkinson's disease. Youdim and co-workers have discovered a novel multifunctional anti-Parkinsonian drug M-30 (**20**), which possesses iron metal chelating, radical scavenging and neuroprotective properties.[84] Very recently, Dutta and co-workers developed a multifunctional compound with highly potent dopamine D_2/D_3 agonist activity, which

acts as an iron chelator.[88] Hybrid compounds consisting of 6-chlorotacrine and 8-hydroxyquinoline scaffolds connected through an oligomethylene linker have been designed as potential anti-AD drug candidates.[85]

Ghaemmaghami *et al.* have recently proposed a class of 8-hydroxyquinoline derivatives as antiprion compounds (see **21** in **Figure 34**).[86]

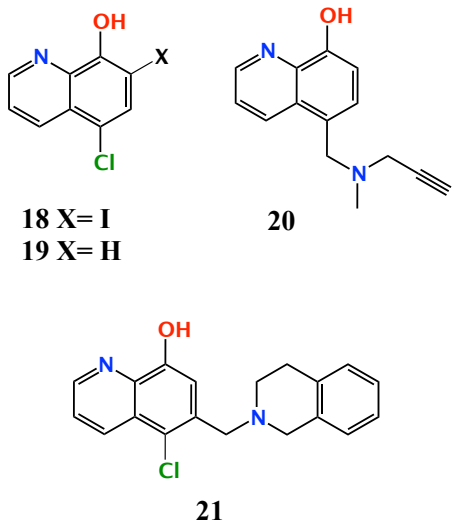

Figure 34. 8-hydroxyquinoline derivatives

References

(1) Ludewigs, H. Zuber, C. Vana, K. Nikles, D. Zerr, I.; Weiss, S. *Expert Rev. Anti. Infect .Ther.* **2007**, *5*, 613-30.

(2) Krammer, C. Vorberg, I. Schätzl, H. M.; Gilch, S. *Infect. Disord. Drug Targets* **2009**, *9*, 3-14.

(3) Nunziante, M. Gilch, S.; Schätzl, H. M. *Chembiochem* **2003**, *4*, 1268-84.

(4) Sim, V. L.; Caughey, B. *Infect. Disord. Drug Targets* **2009**, *9*, 81-91.

(5) Trevitt, C. R.; Collinge, J. *Brain* **2006**, *129*, 2241-65.

(6) Mallucci, G.; Collinge, J. *Nature Rev. Neurosci.* **2005**, *6*, 23-34.

(7) Soto, C.; Satani, N. *Trends Mol. Med.* **2010**, *17*, 14-24.

(8) Perry, V. H. Cunningham, C.; Boche, D. *Curr. Opin. Neurology* **2002**, *15*, 349-54.

(9) Morphy, R. Kay, C.; Rankovic, Z. *Drug Discov. Today* **2004**, *9*, 641-51.

(10) Morphy, R.; Rankovic, Z. *J. Med. Chem.* **2005**, *48*, 6523-43.

(11) Morphy, R.; Rankovic, Z. *J. Med. Chem.* **2006**, *49*, 4961-70.

(12) Morphy, R.; Rankovic, Z. *Curr. Pharm. Des.* **2009**, *15*, 587-600.

(13) Antonello, A. Tarozzi, A. Morroni, F. Cavalli, A. Rosini, M. Hrelia, P. Bolognesi, M. L.; Melchiorre, C. *J. Med. Chem.* **2006**, *49*, 6642-5.

(14) Cavalli, A. Bolognesi, M. L. Capsoni, S. Andrisano, V. Bartolini, M. Margotti, E. Cattaneo, A. Recanatini, M.; Melchiorre, C. *Angew. Chem. Int. Ed.* **2007**, *46*, 3689-92.

(15) Bolognesi, M. L. Banzi, R. Bartolini, M. Cavalli, A. Tarozzi, A. Andrisano, V. Minarini, A. Rosini, M. Tumiatti, V. Bergamini, C. Fato, R. Lenaz, G. Hrelia, P. Cattaneo, A. Recanatini, M.; Melchiorre, C. *J. Med. Chem.* **2007**, *50*, 4882-97.

(16) Bolognesi, M. L. Cavalli, A. Bergamini, C. Fato, R. Lenaz, G. Rosini, M. Bartolini, M. Andrisano, V.; Melchiorre, C. *J. Med. Chem.* **2009**, *52*, 7883-6.

(17) Korcsmáros, T. Szalay, M. S. Böde, C. Kovács, I. A.; Csermely, P. *Expert Opin. Drug Discov.* **2007**, *2*, 799-808.

(18) Petrelli, A.; Giordano, S. *Curr. Med. Chem.* **2008**, *15*, 422-32.

(19) Millan, M. J. *Neurotherapeutics* **2009**, *6*, 53-77.

(20) Pokrovskaya, V.; Baasov, T. *Exp. Opin. Drug Discovery* **2010**, *5*, 883-902.

(21) Zhan, P.; Liu, X. *Curr. Pharm. Des.* **2009**, *15*, 1893-917.

(22) Gal, S. Fridkin, M. Amit, T. Zheng, H.; Youdim, M. B. H. *J. Neural.Transm. Suppl.* **2006**, 447-56.

(23) Rankovic, R.; Morphy, R. *Lead Generation Approaches in Drug Discovery*; Rankovic, Z.; Morphy, R., Eds. John Wiley & Sons, Inc.: Hoboken, NJ, USA, 2010; p. 295.

(24) Kola, I.; Landis, J. *Nat. Rev. Drug Discov.* **2004**, *3*, 711-715.

(25) Cavalli, A. Bolognesi, M. L. Minarini, A. Rosini, M. Tumiatti, V. Recanatini, M.; Melchiorre, C. *J. Med. Chem.* **2008**, *51*, 347-72.

(26) Csermely, P. Agoston, V.; Pongor, S. *Trends Pharm. Sci.* **2005**, *26*, 178-82.

(27) Das, N. Dhanawat, M. Dash, B. Nagarwal, R. C.; Shrivastava, S. K. *Eur. J. Pharm. Sci.* **2010**, *41*, 571-88.

(28) Svartz, N. *Acta Med. Scand.* **2009**, *110*, 577-598.

(29) Dhaneshwar, S. Bhosle, D. Bharambe, S.; Gairola, N. *Indian J. Pharm. Sci.* **2006**, *68*, 286.

(30) Portoghese, P. S. *J. Med. Chem.* **2001**, *44*, 2259-2269.

(31) Bhushan, R. G. Sharma, S. K. Xie, Z. Daniels, D. J.; Portoghese, P. S. *J. Med. Chem.* **2004**, *47*, 2969-2972.

(32) Orrù, C. D. Cannas, M. D. Vascellari, S. Angius, F. Cocco, P. L. Norfo, C. Mandas, A. Colla, P. La; Diaz, G. Dessì, S.; Pani, A. *J. Biol.* **2010**, *5*, 151-165.

(33) Kocisko, D. A. Caughey, B. Morrey, J. D.; Race, R. E. *Antimicrob. Agents Chemother.* **2006**, *50*, 3447-9.

(34) Roberts, B. E. Duennwald, M. L. Wang, H. Chung, C. Lopreiato, N. P. Sweeny, E. A. Knight, M. N.; Shorter, J. *Nature chemical biology* **2009**, *5*, 936-46.

(35) Benito-León, J. *Clinical neuropharmacology 27*, 201-3.

(36) Barret, A. Tagliavini, F. Forloni, G. Bate, C. Salmona, M. Colombo, L. Luigi, A. De; Limido, L. Suardi, S. Rossi, G.; others *J. Virol.* **2003**, *77*, 8462.

(37) Martínez-Lage, J. F. Rábano, A. Bermejo, J. Martínez Pérez, M. Guerrero, M. C. Contreras, M. A.; Lunar, A. *Surg. Neurol.* **2005**, *64*, 542-5, discussion 545.

(38) Bach, S. Talarek, N. Andrieu, T. Vierfond, J.-M. Mettey, Y. Galons, H. Dormont, D. Meijer, L. Cullin, C.; Blondel, M. *Nature Biotechnology* **2003**, *21*, 1075-81.

(39) Klingenstein, R. Löber, S. Kujala, P. Godsave, S. Leliveld, S. R. Gmeiner, P. Peters, P. J.; Korth, C. *J. Neurochemistry* **2006**, *98*, 748-59.

(40) Murakami-Kubo, I. Doh-ura, K. Ishikawa, K. Kawatake, S. Sasaki, K. Kira, J.-ichi; Ohta, S.; Iwaki, T. *J. Virol.* **2004**, *78*, 1281.

(41) Cope, H. Mutter, R. Heal, W. Pascoe, C. Brown, P. Pratt, S.; Chen, B. *Eur. J. Med. Chem.* **2006**, *41*, 1124-43.

(42) Klingenstein, R. Melnyk, P. Leliveld, S. R. Ryckebusch, A.; Korth, C. *J. Med. Chem.* **2006**, *49*, 5300-8.

(43) May, B. C. H. Fafarman, A. T. Hong, S. B. Rogers, M. Deady, L. W. Prusiner, S. B.; Cohen, F. E. *Proc. Natl. Acad. Sci. U S A* **2003**, *100*, 3416-21.

(44) Dollinger, S. Löber, S. Klingenstein, R. Korth, C.; Gmeiner, P. *J. Med. Chem.* **2006**, *49*, 6591-5.

(45) Evans, B. E. Rittle, K. E. Bock, M. G. DiPardo, R. M. Freidinger, R. M. Whitter, W. L. Lundell, G. F. Veber, D. F.; Anderson, P. S. *J. Med. Chem.* **1988**, *31*, 2235-2246.

(46) Patchett, A. A.; Nargund, R. P. *Annu. Rep. Med. Chem.* **2000**, *35*, 289-298.

(47) Bondensgaard, K. Ankersen, M. Thøgersen, H. Hansen, B. S. Wulff, B. S.; Bywater, R. P. *J. Med. Chem.* **2004**, *47*, 888-99.

(48) Che, Y.; Marshall, G. R. *Expert Opin. Therap. Target* **2008**, *12*, 101-14.

(49) Korth, C. May, B. C. Cohen, F. E.; Prusiner, S. B. *Proc. Natl. Acad. Sci. U S A* **2001**, *98*, 9836-41.

(50) Doh-ura, K. Iwaki, T.; Caughey, B. *J. Virol.* **2000**, *74*, 4894.

(51) Fukuuchi, T. Okuda, K. Yoshihara, S.; Ohta, S. *J. Health Sci.* **2009**, *55*, 586-592.

(52) Macedo, B. Kaschula, C. H. Hunter, R. Chaves, J. a P. Merwe, J. D. van der; Silva, J. L. Egan, T. J.; Cordeiro, Y. *Eur. J. Med. Chem.* **2010**, *45*, 5468-73.

(53) Love, R. *Lancet* **2001**, *358*, 563.

(54) May, B. C. H. Witkop, J. Sherrill, J. Anderson, M. O. Madrid, P. B. Zorn, J. A. Prusiner, S. B. Cohen, F. E.; Guy, R. K. *Biochem Biophys Res Commun* **2006**, *16*, 4913-6.

(55) Collinge, J. Gorham, M. Hudson, F. Kennedy, A. Keogh, G. Pal, S. Rossor, M. Rudge, P. Siddique, D. Spyer, M. Thomas, D. Walker, S. Webb, T. Wroe, S.; Darbyshire, J. *Lancet neurology* **2009**, *8*, 334-44.

(56) Ghaemmaghami, S. Ahn, M. Lessard, P. Giles, K. Legname, G. DeArmond, S. J.; Prusiner, S. B. *PLoS Pathog.* **2009**, *5*, e1000673.

(57) Nguyen, T. Sakasegawa, Y. Doh-Ura, K.; Go, M.-L. *Eur. J. Med. Chem.* **2011**, 46, 2917-29

(58) Singh, N. Singh, A. Das, D.; Mohan, M. L. *Antioxid. Redox Signal.* **2010**, *12*, 1271-94.

(59) Otto, M. Cepek, L. Ratzka, P. Doehlinger, S. Boekhoff, I. Wiltfang, J. Irle, E. Pergande, G. Ellers-Lenz, B. Windl, O. Kretzschmar, H. A. Poser, S.; Prange, H. *Neurology* **2004**, *62*, 714-8.

(60) Caughey, B. Raymond, L. D. Raymond, G. J. Maxson, L. Silveira, J.; Baron, G. S. *J. Virol.* **2003**, *77*, 5499.

(61) Hafner-Bratkovic, I. Gaspersic, J. Smid, L. M. Bresjanac, M.; Jerala, R. *Journal of neurochemistry* **2008**, *104*, 1553-64.

(62) Dirikoc, S. Priola, S. a; Marella, M. Zsürger, N.; Chabry, J. *J. Neurosci.* **2007**, *27*, 9537-44.

(63) Brown, D. R. Schulz-Schaeffer, W. J. Schmidt, B.; Kretzschmar, H. a *Exper. Neurology* **1997**, *146*, 104-12.

(64) Martin, S. F. Burón, I. Espinosa, J. C. Castilla, J. Villalba, J. M.; Torres, J. M. *Free Radic. Biol. Med.* **2007**, *42*, 1723-9.

(65) Drisko, J. *J. Am. Coll. Nutr.* **2002**, *21*, 22-5.

(66) Naderi, J. Somayajulu-Nitu, M. Mukerji, A. Sharda, P. Sikorska, M. Borowy-Borowski, H. Antonsson, B.; Pandey, S. *Apoptosis* **2006**, *11*, 1359-69.

(67) Littarru, G. P.; Tiano, L. *Nutrition* **2010**, *26*, 250-4.

(68) Fernández-Ayala, D. J. M. Martín, S. F. Barroso, M. P. Gómez-Díaz, C. Villalba, J. M. Rodríguez-Aguilera, J. C. López-Lluch, G.; Navas, P. *Antioxid. Redox Signal.* **2000**, *2*, 263-275.

(69) Martín, S. F. Gómez-Díaz, C. Navas, P.; Villalba, J. M. *Biochem. Biophys. Res. Commun.* **2002**, *297*, 581-6.

(70) Ferrante, R. J. Andreassen, O. A. Dedeoglu, A. Ferrante, K. L. Jenkins, B. G. Hersch, S. M.; Beal, M. F. *J. Neurosci.* **2002**, *22*, 1592.

(71) Shults, C. W. *et al*. *Arch. Neurol.* **2002**, *59*, 1541-50.

(72) Bragin, V. *Am. J. Alzheimers Dis. Other Demen.* **2005**, *20*, 21-26.

(73) Xu, Y. Shi, J. Yamamoto, N. Moss, J. a; Vogt, P. K.; Janda, K. D. *Biorg. Med. Chem.* **2006**, *14*, 2660-73.

(74) Smith, A. R. Shenvi, S. V. Widlansky, M. Suh, J. H.; Hagen, T. M. *Curr. Med. Chem.* **2004**, *11*, 1135-46.

(75) Bolognesi, M. L. Minarini, A. Tumiatti, V.; Melchiorre, C. *Mini Reviews Med. Chemi.* **2006**, *6*, 1269-1274.

(76) Singh, N. Das, D. Singh, A.; Mohan, M. L. *Curr. Iss. Mol. Biol.* **2010**, *12*, 99-107.

(77) Sigurdsson, E. M. Brown, D. R. Alim, M. A. Scholtzova, H. Carp, R. Meeker, H. C. Prelli, F. Frangione, B.; Wisniewski, T. *J. Biol. Chem.* **2003**, *278*, 46199-46202.

(78) Doh-ura, K. Tamura, K. Karube, Y. Naito, M. Tsuruo, T.; Kataoka, Y. *Cell. Mol. Neurobiol.* **2007**, *27*, 303-16.

(79) a) Pollera, C. Lucchini, B. Formentin, E. Bareggi, S. Poli, G.; Ponti, W. *Veterinary Res. Comm.* **2005**, *29 Suppl 2*, 253-5. b) Ponti, W. Sala, M. Pollera, C. Braida, D. Poli. G. Bareggi, S. *Veterinary Res. Comm.* **2004**, *28*, 307-310.

(80) Yassin, M. S. Ekblom, J. Xilinas, M. Gottfries, C. G.; Oreland, L. *J. Neurol. Sci.* **2000**, *173*, 40-4.

(81) Vaira, M. Di; Bazzicalupi, C. Orioli, P. Messori, L. Bruni, B.; Zatta, P. *Inorganic Chem.* **2004**, *43*, 3795-7.

(82) LeVine, H. Ding, Q. Walker, J. a; Voss, R. S.; Augelli-Szafran, C. E. *Neuroscience Lett.* **2009**, *465*, 99-103.

(83) Adlard, P. *et al. Neuron* **2008**, *59*, 43-55.

(84) Gal, S. Zheng, H. Fridkin, M.; Youdim, M. B. H. *J. Neurochemistry* **2005**, *95*, 79-88.

(85) Fernández-Bachiller, M. I. Pérez, C. González-Muñoz, G. C. Conde, S. López, M. G. Villarroya, M. García, A. G.; Rodríguez-Franco, M. I. *J. Med. Chem.* **2010**, *53*, 4927-37.

(86) Ghaemmaghami, S. May, B. C. H. Renslo, A. R.; Prusiner, S. B. *J. Virol.* **2010**, *84*, 3408-12.

(87) Ritchie, C.W. Bush, A.I. Mackinnon. A. et al. *Arch. Neurol.* **2003**, *60*, 1685–91.

(88) Ghosh, B. Antonio, T. Reith, M.E. Dutta, A.K. *J. Med. Chem.* **2010,** *53*, 2114-25.

6. Parallel synthesis, evaluation, and preliminary structure activity relationship of 2,5-diamino-1,4-benzoquinones as a novel class of bivalent anti-prion compounds

Most of the anti-prion molecules that have been identified so far derive from screening approaches. Structurally, diverse chemical antiprion compounds covering a broad range of the chemical space have been identified. Intriguingly, most of them share a common bivalent structure (**Figure 35**). This is the case of the diphenyl-methane derivatives GN8 (**1**), the bis-acridine analogues (BiCappa, **15**),[1] the natural products curcumin (**22**),[2] bebeerine (**23**),[1,3] and bisepigallocatechin digallate (**24**),[4,5] 2,2'-bisquinolines (**8**),[6] 4,5-dianilinophthalimide (**25**),[6] analogues of Congo red (**26**),[7] and diketopiperazines (DKP) derivatives (**27**).[8]

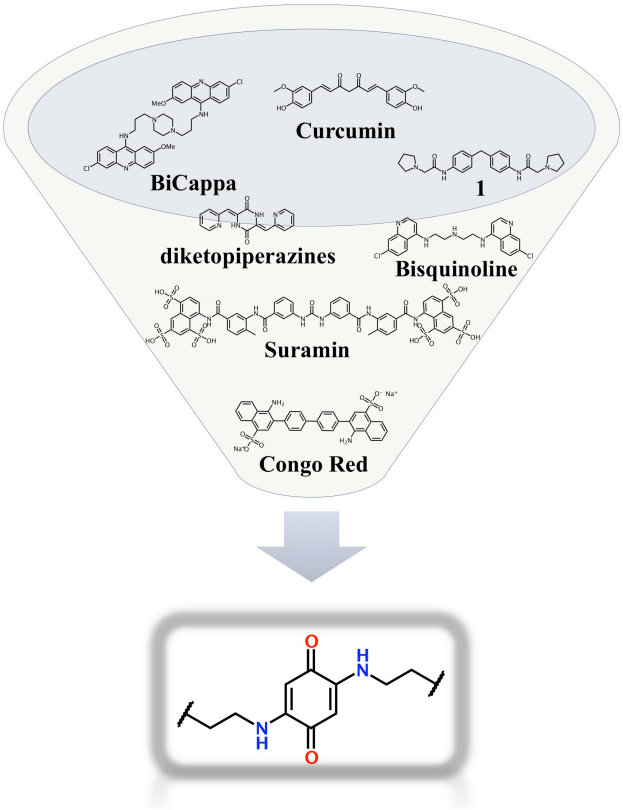

Figure 35. Design strategy leading to novel BQ derivatives

Bivalency, and multivalency in general, is a well-known and efficient strategy widely used by medicinal chemists to enhance binding efficacy in molecular recognition processes.[9] Multivalent chemical probes, featuring multiple copies of an amyloid binding motif connected by a spacer, have been developed with the aim to simultaneously bind to several binding sites or several amyloid peptides, thus achieving higher potency.[9]

Assembling multiple acridine or curcumin moieties to a cyclopeptide scaffold has emerged as a promising strategy for the development of inhibitors against fibril formation.[10,11] and bivalent "molecular tweezers" have been envisaged as the next generation of amyloid ligands.[12]

In prion research, by joining two quinacrine moieties through a piperazine spacer, May *et al.* afforded the first bivalent anti-prion ligand BiCappa (**15**), which was 100 times more potent than monomeric **2**.[1] Building on the bivalent approach, we have designed a library of 14 ligands obtained by combining two different BQ cores with seven amino acid methyl esters. The library was prepared and tested for prion replication inhibition in ScGT1 cells. Despite the small number of synthesized compounds, some of them were active against prion replication.

Based on these results, we envisaged that bivalent ligands bearing two PRMs connected by a central BQ core might possess promising anti-prion activity. Furthermore, thanks to the antioxidant properties of the BQ nucleus, bivalent BQ derivatives might act as MTDLs against prion diseases. Thus, we decided to design a further combinatorial library of twelve entries, featuring an antioxidant BQ nucleus as spacer connecting acridines and quinolines as PRMs.

In the following, the design, synthesis and biological evaluation of the two compound libraries will be reported.

6.1. Development of a library of BQ-amino acids bivalent ligands

As already discussed, the conformational transition process of PrP^{C} to PrP^{Sc} remains enigmatic. However, regardless of the initiating event, PrP^{Sc} appears to act as a conformational template by which PrP^{C} is converted to a new molecule of PrP^{Sc}, through PPIs. PPIs are crucial elements in mediating diverse cellular physiological and pathological events. They play a pivotal role in the pathogenesis of conformational neurodegenerative diseases, as PPIs are involved in fibrillation processes.[13] Systematic analyses of PPI interfaces reveal a highly heterogeneity in size of the contact area, polarity of the interface, protrusion and flatness.[14,15] However, the majority of PPIs deals with cavity-less proteins, where a complex network of weak interactions takes place. Peptides have been proposed to be good PPIs blockers.[16] So far, several peptides have been developed with the specific aim of blocking PPIs and of reversing the aberrant conformational changes. A short synthetic peptide (iPrP13, DAPAAPAGPAVPV)[17] designed by Soto on the basis of sequence homology with PrP^{C}, acted as a β-sheet breaker, inducing unfolding of β-pleated sheet structure. More recently, Gilbert and co-workers[18] have reported on a series of small peptides active in the high micromolar range in two prion disease models and in an in vitro anti-aggregation polymerization assay. However, they are not optimal drug candidates, due to problems with bioavailability and enzymatic degradation. To overcome this limitation, one could use libraries based on small molecules. However, the widely spaced interactions required for PPI's blockers are difficult to mimic with small molecules. In spite of this challenge, Janda and co-workers have recently demonstrated the ability of what they have named "credit card" libraries to disrupt PPIs of biological relevance.[19] The chemical structures of these libraries are built upon flat, rigid scaffolds, decorated with appended groups that span a wide range of size, aromaticity, polarity, and hydrogen-bonding capability.[16,20,21] Their rationale was based on the concept that the "hot spot" regions in protein−protein interfaces are rich in aromatic residues. Prompted by the advantages of using small molecules as PPI inhibitors as opposed to peptides, here we propose the planar BQ scaffold as a privileged motif in modulating PPIs. This is based on (i) Janda's criteria for credit card libraries;[19] (ii) the finding that a 2,5-bisdiamino-benzoquinone derivative binds to β-amyloid (Aβ), and interferes with the native ability of Aβ to self-assemble, by disrupting PPIs.[22] As highlighted above, due to a resonance effect, a hydrophobic and planar system is generated in 2,5-bisdiamino-benzoquinones. This should, in principle, perturb PPIs in the fibrillogenesis processes.[23]

Therefore, in our search for novel anti-prion compounds, we decided to attach seven amino acids methyl esters to two different benzoquinone cores, generating a small combinatorial library of fourteen 2,5-bisdiamino-benzoquinones peptidomimetics (**28a-g** and **29a-g**), reported in **Figure 36**. The selected amino acid esters (AlaOMe (**a**), Nω-Nitro-ArgOMe (**b**), Nε-BOC-LysOMe (**c**), IleOMe (**d**), MetOMe (**e**), PheOMe (**f**), TrpOMe (**g**)) act as capping groups, allowing us to enlarge the library's chemical diversity by exploiting differences in size, aromaticity, polarity, and

hydrogen-bonding capability. Analysis of natural amino acids involved in PPIs revealed that Trp, Phe, Tyr, and Ile are the most important in driving aggregation.[14] Consequently, it is highly conceivable that the novel derivatives bearing these motifs might compete for binding and, therefore, efficiently disrupt the assembly of prion protein.

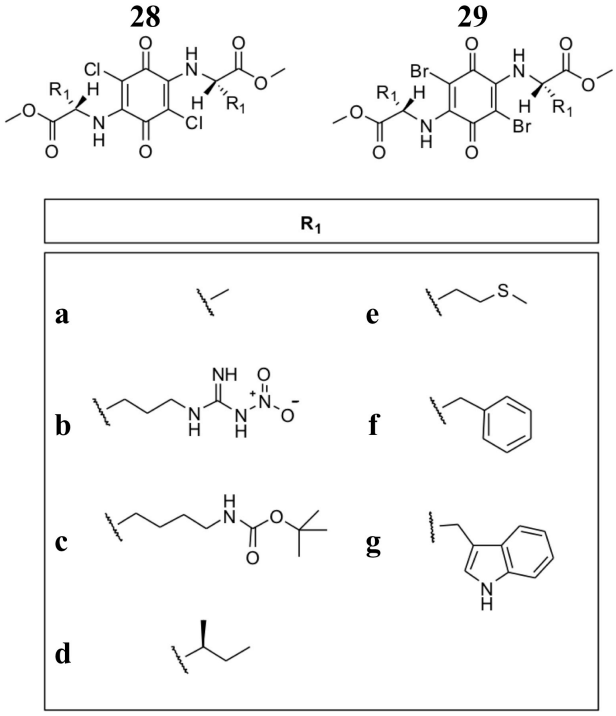

Figure 36. Chemical structures of **28a-g** and **29a-g**.

A cell-based screening assay was used to test anti-prion activity across the synthesized library of compounds (see Experimental Section, **Chapter 10**).

Notably, three hit compounds (**28f-g**, **29f**) of library were active against PrP^{Sc} accumulation. For **28f** a remarkable submicromolar EC_{50} value (0.87 μM) was found, comparable to that of **2** (0.4 μM). The high activity of **28f-g** and **29f** was not unexpected (see Ref. [24]), as it is in line with the well-known central role of pi-stacking interactions in self-assembly processes in the fields of chemistry and biochemistry.[25] To better rationalize the obtained results, a systematic procedure for identifying key fragments responsible for a given activity was applied.[26] In this protocol an algorithm, which breaks down a structure into fragments, was used.[h] Subsequently, all the obtained substructures were related to biological activities to identify hot fragments (**Figure 37,** for method see **Appendix**

[h] Fragmenter was used for molecular decomposition to fragments and R-groups, JChem 5.0.0, 2008, ChemAxon (http://www.chemaxon.com)

A for the methods used). From this preliminary computational study, we have identified that the BQ nucleus connected with two phenyl rings by a linker is a good anti-prion motif. In addition, our analysis suggests the relevance of the atomic size of the substituents in position 3 and 6 at BQ ring (Cl better than Br), with an inverse relation to van der Waals radius (**Figure 37**).

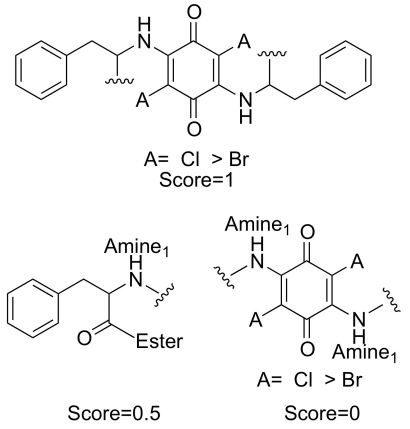

Figure 37. Substructures identified from the synthesized library.

6.2. Development of a library of BQ-PRM bivalent ligands

The data coming from the previous investigation have been exploited for the design of a further series of anti-prion small molecules.

We designed a small combinatorial library of MTDLs, whose general structure is depicted in **Figure 38**. We hypothesized that the presence of a PRM, key element for anti-prion activity,[18] along with a moiety endowed with an alternative mechanism of action against prion diseases might lead to discover more effective compounds.[27] The ligands feature the antioxidant BQ nucleus as central core, with two linkers in position 2 and 5 connecting two PRMs as terminal moieties (see **Figure 38**). As linkers, we selected three polyamine chains (**53-55**, **Scheme 1**) that would allow exploring different lengths and chemical composition for the different molecules. This is of particular importance, since linker length has shown by May *et al.* to be very critical against PrP^{Sc} formation for the bivalent acridines series.[1] As terminal moieties, starting from the consideration that aromatic groups provided the best activity in the previous series of BQ compounds,[24] we selected three aromatic prion recognition motifs, such as 6-chloro-2-methoxyacridine (as in **30-32**, **Scheme 1**), 7-chloroquinoline (**33-35**), and 1,2,3,4-tetrahydroacridine (**36-38**).

The choice of these as PRM was motivated by our [28] and by others' results.[1,29,30] Moreover it was strongly supported by the studies of Cordeiro *et al.* that experimentally demonstrated that **45** reduces the aggregation of the ShaPrP peptide into amyloid-like structures[31], and by the SPR studies

of Go *et al.* demonstrating that **42** and **43** are strong binders of hPrP^{C}.[32,33] As discussed earlier, acridines and quinolines can be classified as a privileged structures, with optimal pharmacokinetic properties and a high degree of drug-likeness, extremely favorable features when starting a drug discovery program.[1,29,30] Given that the derivatives of 1,2,3,4-tetrahydroacridin-9-amine (**58**) are active against yeast prion[34] and antiprion ScN2a cells,[33] **36-38** (see **Scheme 1**), were also designed. As a second step, on the basis of the remarkable profile shown by **34**, three other derivatives (**39-41**) were designed with the aim of further optimizing activity in the existing series of compounds. In the following sections, we present a solution-phase parallel synthesis of the designed library of bivalent BQ derivatives (see **Scheme 1**), which were evaluated for their anti-prion activity in ScGT1 cells, together with their capability of inhibiting PrP^{Sc} aggregation and of reducing OS.

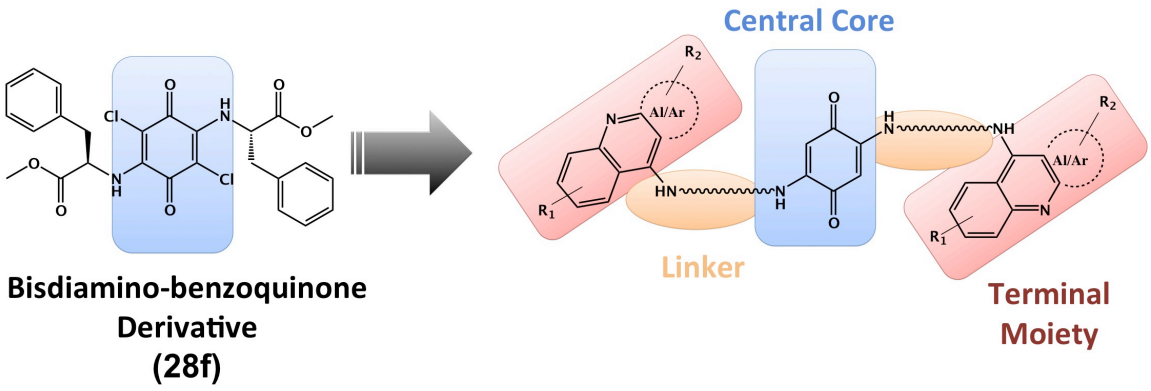

Figure 38. Rational design of library compounds **30-41**.

6.2.1. Chemistry

We synthesized the designed bivalent compounds **30-40** using a solution phase parallel synthesis approach. The group of Prof. Bolognesi has previously reported how a di-substitution reaction of diamines with 2,5-dimethoxy-1,4-benzoquinone provides easy access to a variety of 2,5-diamino-1,4-benzoquinones.[23,35] Encouraged by the good yields and the straightforward work-up associated with this reaction, we followed the following procedure. Eleven N-substituted polyamines (**42-52**, **Scheme 1**) were loaded with 2,5-dimethoxy-1,4-benzoquinone into different vessels of a carousel workstation. After heating at 50 °C for 5 hours, the desired products formed in moderate to good yields (38−88%). Monovalent **41** was obtained by Michael reaction starting from naftoquinone and amine **46** (40%). The preparation of intermediates **42-52** was easily achieved treating in parallel

fashion commercially available polyamines **53-55** with heteroaryl halides **56-60**. Compounds **42-52** were obtained in 25-67% yield by reacting a large excess of the polyamine with the corresponding heteroaryl halide (27:1) in phenol and using NaI as a catalyst (**Scheme 1**). In these conditions we were able to obtain selective mono-substitution at the terminal primary amino group of the polyamine, obviating the need for protection/deprotection of the other amino functionalities.[36] Furthermore, we overcame the low-yield of common S_NAr reactions, and the use of costly reagents of Pd-catalyzed amination methodologies.[37]

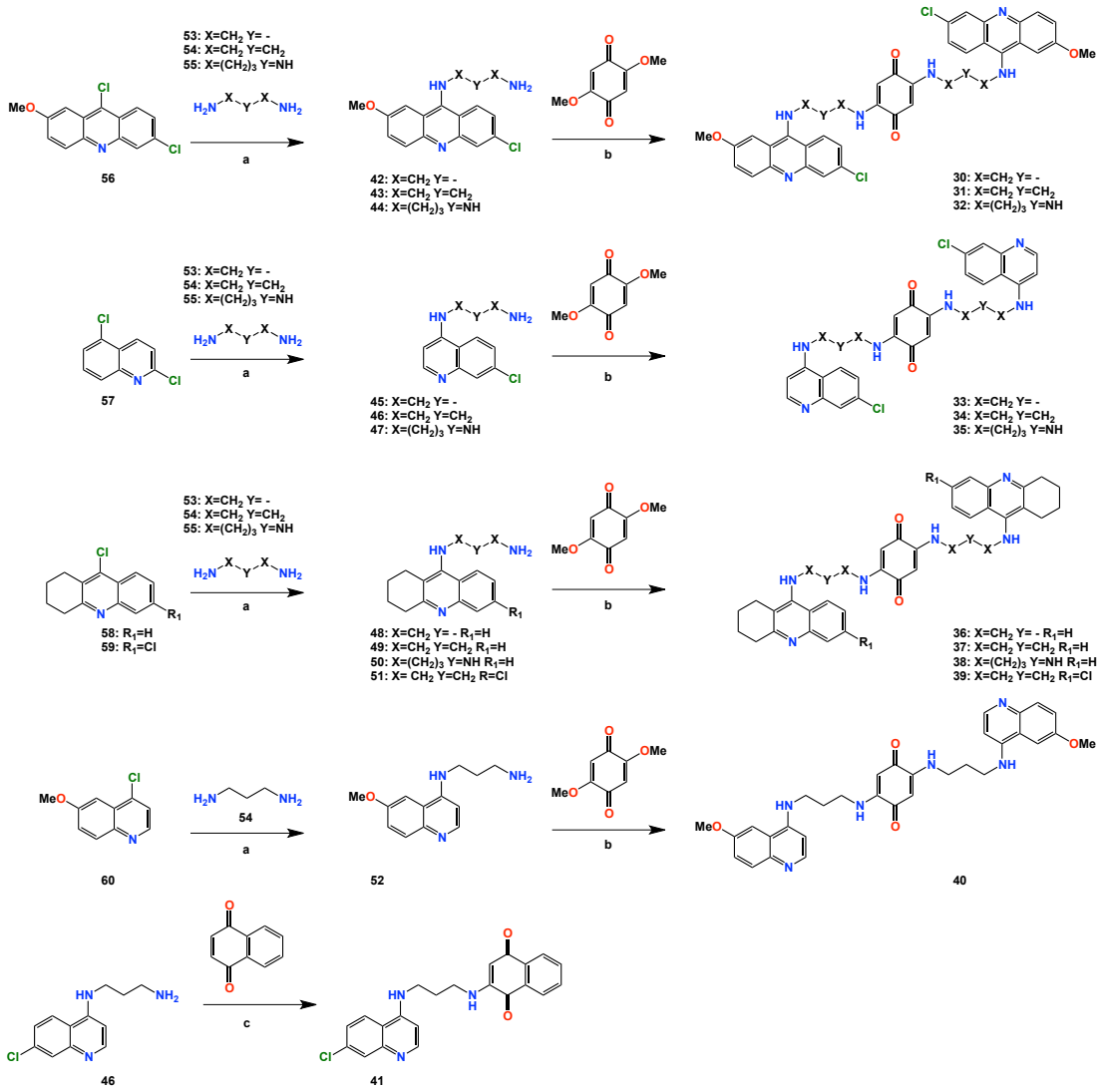

Scheme 1. Reagents and conditions: (a) phenol, NaI, 120 °C (1 h), followed by addition of amine, 5 h, 120 °C; (b) EtOH, 5 h, 60 °C (38-88% yield); (c) EtOH, 80 °C (1 h), followed by addition of amine, 5 h, 50 °C (40%).

6.2.2. Results and Discussion

A cell-screening assay was used to test toxicity and anti-prion activity across the library of synthesized compounds (see Experimental Section, **Chapter 10**). In addition, for compounds **15**, **31**, **34**, **35** and **39**, the capability to inhibit prion fibril formation was studied *in vitro* by using a previously reported amyloid seeding assay[38] Prion fibril formation inhibitory activity was evaluated by measuring the increase of the lag phase of PrP amyloid formation kinetics. Antioxidant potential of the most active BQ derivatives (**16**, **31**, **34**, **35** and **39**) in ScGT1 cell lines was evaluated by using the thiobarbituric acid reactive substances (TBARS) assay and sulforaphan (4-methylsulfinylbutyl isothiocyanate, SFP) assay (see Experimental Section, **Chapter 10**).

Preliminarily, the possible toxicity of the compounds **30-38** was assessed in ScGT1 cells. At 1 μM concentration, the toxicity profiles among the library members varied from 1.5% to 114.8% (see **Table 4**).

Table 4. Cell viability and anti-prion activity on ScGT1 cells of library compounds.

Compound	% of viable cells at 1 μM[b]	% of PrP^{Sc} inhibition at 1 μM[c]	% of viable cells at EC_{50}[b]	EC_{50} (μM)[c]	Lag Phase (hours)[d]
2	98.5 ± 3.9[a]	103.8 ±6.1[a]	100.0 ± 4.3	0.4 ± 0.1[a]	
15	75.6 ± 7.1	102.1 ± 2.7	92.4 ± 6.2[a]	0.32 ± 0.03	55 ± 7[*]
30	18.2 ± 1.2 80.1 ± 6.3 (at 0.2 μM)	ND 3.1 ± 0.3 (at 0.2 μM)			
31	65.5 ± 5.6	89.7 ± 5.1	75.2 ± 8.4	0.68 ± 0.05	45 ± 10[#]
32	1.5 ± 0.2 65.8 ± 4.6(at 0.2 μM)	ND 5.4 ± 0.4 (at 0.2 μM)			
33	114.8 ± 7.9	6.2 ± 0.6			
34	100.4 ± 3.6	85.5 ± 3.9	99.6 ± 2.7	0.73 ± 0.03	53 ± 5[#]
35	105.0 ± 7.4	49.1 ± 2.2	91.3 ± 4.2	1.2 ± 0.1	40 ± 10[*]
36	108.0 ± 8.4	7.1 ± 0.9			
37	104.4 ± 5.6	3.6 ± 0.4			
38	95.4 ± 7.4	3.4 ± 0.2			
39	78.6 ± 5.2	105.3 ± 5.5	101.5 ± 3.6	0.17 ± 0.01	57 ± 6[#]
40	87.2 ± 5.8	4.7 ± 0.3			
41	94.3 ± 3.8	2.9 ± 0.1			

[a] Values are the mean of three experiments, standard deviations are given. [b] ScGT1 cells were cultured in DMEM with 10% FBS, plated 25000 cells in each well of 96-well plates. The compounds were dissolved in DMSO (100%) and diluted in PBS 1X before adding various concentrations (10 nM - 10 µM) and incubated for 5 days at 37°C, 5% CO_2. The results were developed by calcein-AM fluorescence dye and read by microplate reader. [c] The effect of library compounds on inhibition of scrapie prion replication. ScGT1 cells were cultured in DMEM with 10% FBS, split 1:10 into Petri dishes and incubated for 2 days at 37°C and 5% CO_2. Then, various compound concentrations (10 nM - 2 µM), being non-toxic for the cells, were added to the plates. After a 5-day incubation, proteins of cells were extracted, quantified, digested with proteinase K (PK), and western-blotted. [d] Prion fibril formation inhibitory activity in vitro (Control 45 ± 4 h). Statistical analysis was done by analysis of Student's t-test (n=4); (*) p e 0.05, (#) p e 0.01.

Treatment with **30** and **32** decreased cell viability to percentages of 18.2% and 1.5%, respectively. Because of the toxicity shown, **30** and **32** were studied for their anti-prion activity at a lower concentration (0.2 µM), whereas the other library members were assayed at a concentration of 1 µM. The synthesized compounds **31**, **33-35** were found to cover a broad range of activity against PrP^{Sc} formation, with percentages of inhibition spanning from 3.4% to 89.7% (**Table 4**). Compounds **30-32**, bearing an acridine moiety, displayed a general higher toxicity in the cell viability assay. **31** turned out to be the most active anti-prion compound, with a submicromolar EC_{50} value (0.68 ± 0.05 µM) and a percentage of viable cells at EC_{50} of 75.2%. A different toxicity profile was observed for quinoline derivatives **33-35**, which were not toxic to ScGT1 cells (cell viability > 100% at 1 µM concentration). Intriguingly, **34** and **35** showed also remarkable submicromolar EC_{50} values (0.73 ± 0.03 µM, and 1.2 ± 0.1 µM, respectively; **Figure 39**) comparable to that of **15** (0.32 ± 0.03 µM).

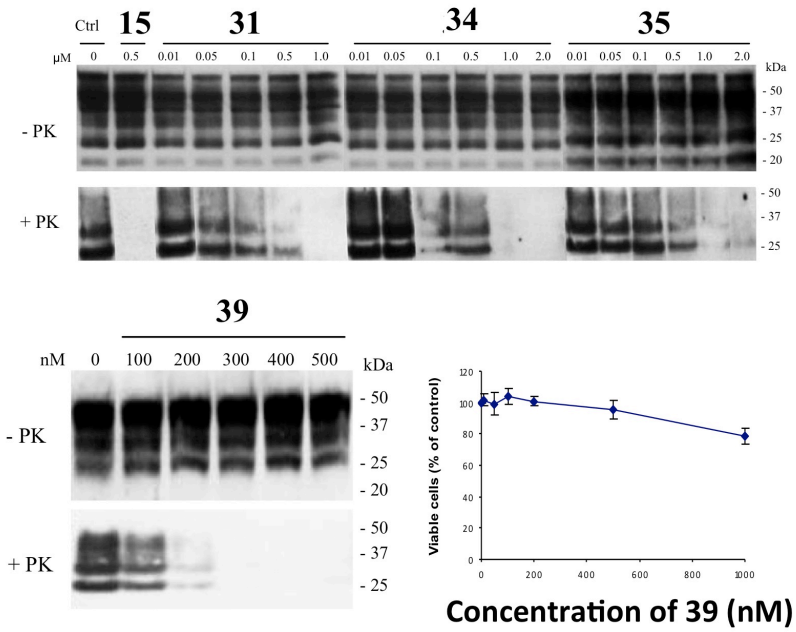

Figure 39. Western blot of protease-digested ScGT1 cell lysates depicting the presence or absence of PrP^{Sc} after treatment with **15**, **31**, **34**, **35**, **39** before (up) or after (bottom) PK: Ctrl = control. Survival of ScGT1 cells treated with **39.**

To note, a series of bisquinolines with a polyamine linker have been already designed and tested in ScN2a cell line, but showed a lower activity against prion infection (in the one-digit micromolar range).[39] This might confirm the design rationale, indicating that the presence of a BQ core is critical for activity. The replacement of the 2,6-disubstited acridine ring of **30-32** with the unsubstituted 1,2,3,4-tetrahydroacridine, as in **36-38**, resulted in a complete loss of activity, pointing out to the role for the aromatic substituents in the recognition process. Interestingly, these latter compounds did not show toxicity in ScGT1 cells. For all the three series (**30-32**, **33-35**, and **36-38**), data from the cell-screening assay suggest that a linker length of three methylenes is important for optimal anti-prion activity. Intriguingly, a similar trend was observed by May et al. in their series of analogous bivalent ligands.[1] Altogether, these preliminary results suggest that a specific length of the linker and the presence of a chlorine substituent on the prion recognition motifs might contribute to activity against PrP^{Sc} formation. Regarding toxicity, the presence of the acridine ring seems to be a major determinant, in line with the reported DNA intercalation properties of this heterocycle.[1] Conversely, quinoline and 1,2,3,4-tetrahydroacridine moieties do not confer cytotoxicity.

As a second step, based on the remarkable profile shown by **34** (**Scheme 1**), three other derivatives (**39-41**) were designed with the aim of further optimizing activity in the existing series of compounds. Indeed, we decided to synthesize a second set of compounds in which the effect of the substituents on the heteroaromatic ring was investigated by synthesizing the 6-chloro-1,2,3,4-tetrahydroacridine (**39**) and the 6-methoxyquinoline (**40**) derivatives. Furthermore, to probe the bivalent mechanism of action of **34**, its corresponding monomeric derivative **41** was designed.

From the biological studies (see Experimental Section, **Chapter 10**), as expected, quinoline **40**, lacking the chlorine atom, resulted not toxic against ScGT1 cells, while displaying negligible activity against prion replication (inhibition of 4.7%, **Table 4**). These results again point out the critical role played by the chlorine substituent of the aromatic ring. This speculation was further confirmed by the outstanding activity shown by the 6-chloro-1,2,3,4-tetrahydroacridine **39**. In contrast to **37**, which does not carry the chlorine atom and is devoid of anti-prion activity, **39** showed a remarkable EC_{50} value of 0.17 μM, which is the lowest among the present series of BQ derivatives, even better than that of BiCappa. Remarkably, **39** showed a concomitant low toxicity (101.5% of viable cells at EC_{50} value, see **Table 4**).

In order to study the mechanism of action of the most active compounds (**31**, **34**, **35** and **39**) at a molecular level, a PrP amyloid fibrillation assay was used. Only **34**, **39** and BiCappa (**15**), at 2 μM, exhibited significant PrP amyloid fibril forming inhibitory activity. In fact, they extended the lag

phase to a time ≥ to 53 hours, showing a significantly slower kinetics than the control (45 hours, **Table 4**). These results, although preliminary, are in agreement with the starting hypothesis that bivalent ligands might interact directly with the recPrP to prevent its conversion to misfolded PrP^{Sc} isoform. Furthermore, the idea that hydrophobic and planar molecular features are crucial to perturb PPIs in the prion fibrillogenesis processes seems confirmed. In addition, a key molecular determinant seems to be the presence of a chlorine substituent on the heteroaromatic terminal moieties.

The PrP^{Sc} infected cells are under OS, mainly caused by mitochondrial dysfunction.[40,41] In light of this, antioxidants able to scavenge or neutralize ROS might be beneficial against prion diseases.[42] Indeed, derivatives of **16** has been proposed for prion and other neurodegenerative diseases.[43-47] Thus, we tested the antioxidant potential of the most active BQ derivatives (2, 5, 6 and 10) in ScGT1 cell lines, by using the thiobarbituric acid reactive substances (TBARS) assay and the antioxidant Trolox as a positive control.[43-46] The assay measures lipid hydroperoxides and aldehydes expressed as an average percent of thiobarbituric acid reactive substances (TBARS) of treated cells versus control untreated cells. As shown in **Figure 40**, derivatives **31**, **34** and **35** displayed low antioxidant activity (83-87%) at 1 μM, while **39** behaves similarly to Trolox (69% Vs 71%, respectively). As expected, BiCappa (**15**), which does not carry a BQ scaffold, did not show any antioxidant capacity (93%).

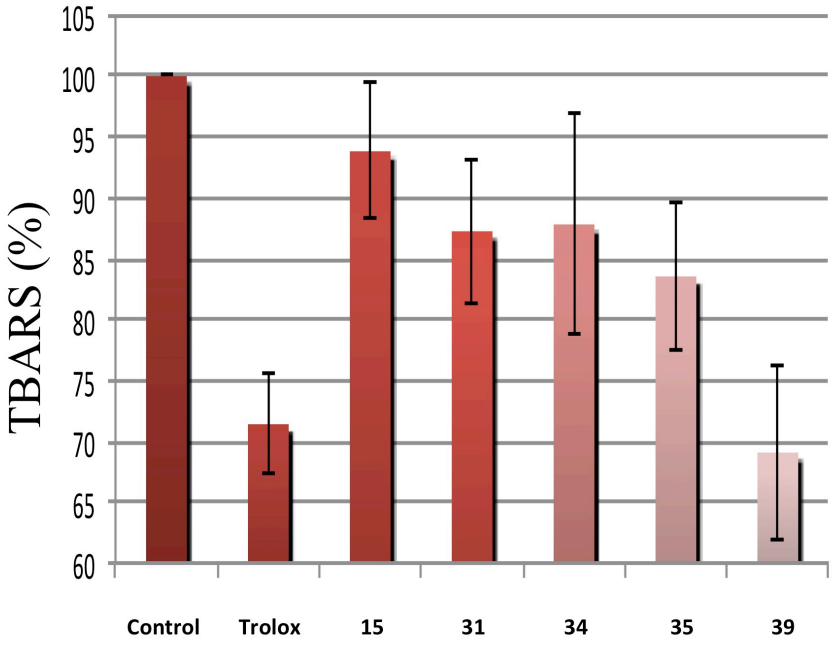

Figure 40. Effect of Trolox, **15**, **31**, **34**, **35** and **39** (1 μM) on ScGT1, evaluated by TBARS formation. Values are the mean ± SD (n = 3).

We have previously demonstrated that the antioxidant property of related BQ derivatives,[23,35] and CoQ (**16**) itself, concerns mainly their reduced hydroquinone forms. NQO1, an inducible enzyme that catalyzes the reduction of quinones to hydroquinones, was shown to be responsible for the production of the **16**-reduced antioxidant forms, as well as that of BQ derivatives.[23,35] Therefore, since **31**, **34**, **35** and **39** share the same BQ nucleus, their antioxidant activity was also evaluated in ScGT1, following exposure to t-BuOOH, and in the absence or presence of pre-treatment with sulforaphane, an inducer of NQO1. **Figure 41** clearly shows that **31**, **34**, **35** and **39** (at 1 μM) in their oxidized form show a basal antioxidant activity, but this activity was increased in cells pre-treated with sulforaphane, confirming that NQO1 is involved in the activation of BQ derivatives. As expected, the antioxidant activity of **15** is not influenced by the overexpression of NQO1.

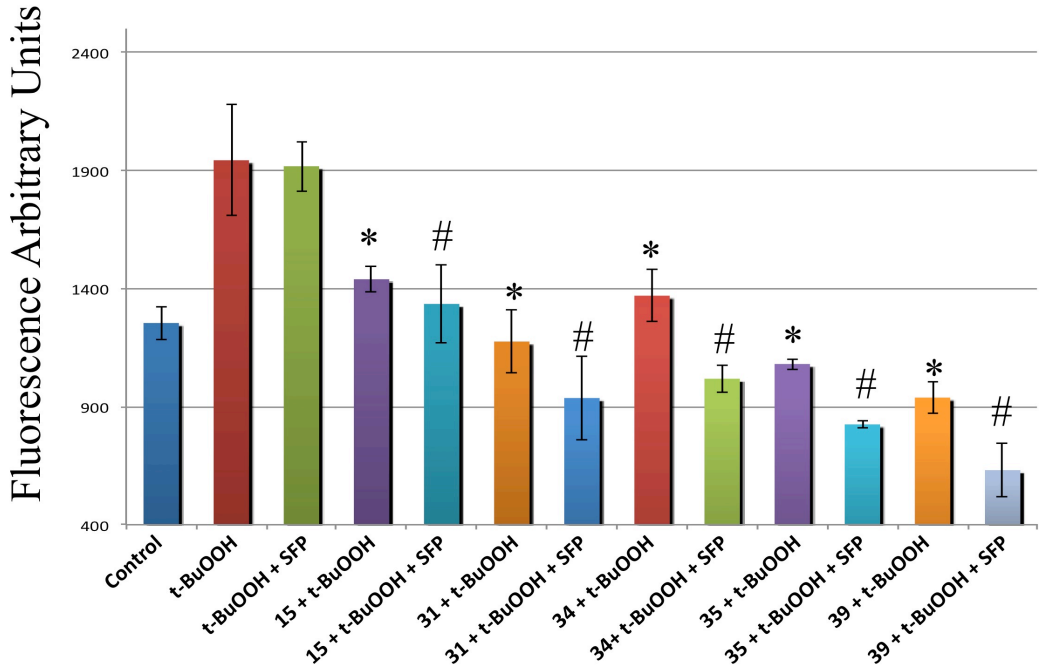

Figure 41. Antioxidant activity of **15**, **31**, **34**, **35** and **39** in ScGT1 cells against ROS formation induced by t-BuOOH. Experiments were performed with ScGT1 cells treated or not with 2.5 μM SFP: (*) $p \leq 0.05$ with respect to t-BuOOH treated samples; (#) $p \leq 0.05$ with respect to t-BuOOH + SFP treated samples.

These results confirmed the rationale for the design of bivalent anti-prion ligands. 7-chloroquinolines (**34** and **35**) and 6-chloro-1,2,3,4-tetrahydroacridine (**39**) derivatives showed a concomitant encouraging low toxicity (**Table 4**). Notably, the EC_{50} value of **39** was even lower than that displayed by **15**, which is a reference compound for prion diseases. Furthermore, **39** showed the largest correlation between the cellular anti-prion activity and the capability to inhibit PrP fibril and ROS formation. Although its mechanism of action is not fully disclosed, we assume that the

bivalent structure of **39** favours the interaction with prion recognition domains, whereas the spacer acts simultaneously as a disrupting element against PPIs and an effective antioxidant moiety. Remarkably, the 6-chloro-1,2,3,4-tetrahydroacridine scaffold emerges as an effective and completely novel prion recognition motif. In conclusion, the present series of molecules are chemical probes that may facilitate the exploration of the molecular mechanism underlying prion disease. We envisage that a better understanding of the molecular framework of bivalent ligands capable of inhibiting prion aggregation and OS would facilitate the creation of new effective anti-prion agents.

References

(1) May, B. C. H. Fafarman, A. T. Hong, S. B. Rogers, M. Deady, L. W. Prusiner, S. B.; Cohen, F. E. *Proc. Natl. Acad. Sci. U S A* **2003**, *100*, 3416-21.

(2) Caughey, B. Raymond, L. D. Raymond, G. J. Maxson, L. Silveira, J.; Baron, G. S. *J. Virol.* **2003**, *77*, 5499.

(3) Csuk, R. Barthel, A. Raschke, C. Kluge, R. Ströhl, D. Trieschmann, L.; Böhm, G. *Archiv der Pharmazie* **2009**, *342*, 699-709.

(4) Kimura, T. Hosokawa-Muto, J. Kamatari, Y. O.; Kuwata, K. *Bioorg. Med. Chem. Letters* **2011**, *21*, 1502-7.

(5) Kuwata, K. Nishida, N. Matsumoto, T. Kamatari, Y. O. Hosokawa-Muto, J. Kodama, K. Nakamura, H. K. Kimura, K. Kawasaki, M. Takakura, Y. Shirabe, S. Takata, J. Kataoka, Y.; Katamine, S. *Proc. Natl. Acad. Sci. U S A* **2007**, *104*, 11921-6.

(6) Kocisko, D. A. Baron, G. S. Rubenstein, R. Chen, J. Kuizon, S.; Caughey, B. *J. Virol.* **2003**, *77*, 10288.

(7) Murakami-Kubo, I. *et al. J. Virol.* **2004**, *78*, 1281.

(8) Bolognesi, M. L. Ai Tran, H. N. Staderini, M. Monaco, A. López-Cobeñas, A. Bongarzone, S. Biarnés, X. López-Alvarado, P. Cabezas, N. Caramelli, M. Carloni, P. Menéndez, J. C.; Legname, G. *ChemMedChem* **2010**, *5*, 1324-34.

(9) Kim, Y. Lee, J. H. Ryu, J.; Kim, D. J. *Current pharmaceutical design* **2009**, *15*, 637-58.

(10) Dolphin, G. T. Chierici, S. Ouberai, M. Dumy, P.; Garcia, J. *Chembiochem* **2008**, *9*, 952-63.

(11) Ouberai, M. Dumy, P. Chierici, S.; Garcia, J. *Bioconjugate Chem.* **2009**, *20*, 2123-32.

(12) Reinke, A. A.; Gestwicki, J. E. *Chemical biology & drug design* **2011**, *77*, 399-411.

(13) Trojanowski, J. Q.; Lee, V. M. *Ann. N. Y. Acad. Sci* **2000**, *924*, 62-7.

(14) Pawar, A. P. Dubay, K. F. Zurdo, J. Chiti, F. Vendruscolo, M.; Dobson, C. M. *J. Mol. Biol.* **2005**, *350*, 379-92.

(15) Nooren, I. M. A.; Thornton, J. M. *EMBO J.* **2003**, *22*, 3486-92.

(16) Arkin, M. R.; Wells, J. a *Nat. Rev. Drug Discov.* **2004**, *3*, 301-17.

(17) Soto, C. Kascsak, R. J. Saborío, G. P. Aucouturier, P. Wisniewski, T. Prelli, F. Kascsak, R. Mendez, E. Harris, D. A. Ironside, J. Tagliavini, F. Carp, R. I.; Frangione, B. *Lancet* **2000**, *355*, 192-197.

(18) Sellarajah, S. Boussard, C. Lekishvili, T. Brown, D. R.; Gilbert, I. H. *Eur. J. Med. Chem.* **2008**, *43*, 2418-27.

(19) Xu, Y. Shi, J. Yamamoto, N. Moss, J. a; Vogt, P. K.; Janda, K. D. *Biorg. Med. Chem.* **2006**, *14*, 2660-73.

(20) Blazer, L. L.; Neubig, R. R. *Neuropsychopharmacology* **2009**, *34*, 126-41.

(21) Gestwicki, J. E.; Marinec, P. S. *Combinatorial chemistry & high throughput screening* **2007**, *10*, 667-75.

(22) Bartolini, M. Bertucci, C. Bolognesi, M. L. Cavalli, A. Melchiorre, C.; Andrisano, V. *ChemBioChem* **2007**, *8*, 2152-61.

(23) Bolognesi, M. L. Banzi, R. Bartolini, M. Cavalli, A. Tarozzi, A. Andrisano, V. Minarini, A. Rosini, M. Tumiatti, V. Bergamini, C. Fato, R. Lenaz, G. Hrelia, P. Cattaneo, A. Recanatini, M.; Melchiorre, C. *J. Med. Chem.* **2007**, *50*, 4882-97.

(24) Tran, H. N. A. Bongarzone, S. Carloni, P. Legname, G.; Bolognesi, M. L. *Bioorg. Med. Chem. Letters* **2010**, *20*, 1866-8.

(25) Gazit, E. *FASEB J.* **2002**, *16*, 77-83.

(26) Lewell, X. Q. Judd, D. B. Watson, S. P.; Hann, M. M. *J. Chem. Inf. Model* **1998**, *38*, 511-522.

(27) Bongarzone, S. Tran, H. N. A. Cavalli, A. Roberti, M. Carloni, P. Legname, G.; Bolognesi, M. L. *J. Med. Chem.* **2010**, 8197-8201.

(28) Bongarzone, S.; Bolognesi, M. L. *Exp. Opin. Drug Discovery* **2011**, 1-18.

(29) Cope, H. Mutter, R. Heal, W. Pascoe, C. Brown, P. Pratt, S.; Chen, B. *Eur. J. Med. Chem.* **2006**, *41*, 1124-43.

(30) Dollinger, S. Löber, S. Klingenstein, R. Korth, C.; Gmeiner, P. *J. Med. Chem.* **2006**, *49*, 6591-5.

(31) Macedo, B. Kaschula, C. H. Hunter, R. Chaves, J. a P. Merwe, J. D. van der; Silva, J. L. Egan, T. J.; Cordeiro, Y. *Eur. J. Med. Chem.* **2010**, *45*, 5468-73.

(32) Nguyen, T. H. T. Lee, C.-Y. Teruya, K. Ong, W.-Y. Doh-ura, K.; Go, M.-L. *Bioorg. Med. Chem.* **2008**, *16*, 6737-46.

(33) Nguyen, T. Sakasegawa, Y. Doh-Ura, K.; Go, M.-L. *Eur. J. Med. Chem.* **2011**, 46, 2917-29

(34) Tribouillard-Tanvier, D. Béringue, V. Desban, N. Gug, F. Bach, S. Voisset, C. Galons, H. Laude, H. Vilette, D.; Blondel, M. *Plos One* **2008**, *3*, e1981.

(35) Bolognesi, M. L. Cavalli, A. Bergamini, C. Fato, R. Lenaz, G. Rosini, M. Bartolini, M. Andrisano, V.; Melchiorre, C. *J. Med. Chem.* **2009**, *52*, 7883-6.

(36) Mamos, P. *Tetrahedron Lett.* **1995**, *36*, 5187-5190.

(37) Margolis, B. J. Long, K. A. Laird, D. L. T. Ruble, J. C.; Pulley, S. R. *ChemInform* **2007**, *38*.

(38) Colby, D. W. Zhang, Q. Wang, S. Groth, D. Legname, G. Riesner, D.; Prusiner, S. B. *Proc. Natl. Acad. Sci. U S A* **2007**, *104*, 20914-9.

(39) Klingenstein, R. Melnyk, P. Leliveld, S. R. Ryckebusch, A.; Korth, C. *J. Med. Chem.* **2006**, *49*, 5300-8.

(40) Choi, S. I. Ju, W. K. Choi, E. K. Kim, J. Lea, H. Z. Carp, R. I. Wisniewski, H. M.; Kim, Y. S. *Acta Neuropathologica* **1998**, *96*, 279-86.

(41) Milhavet, O. McMahon, H. E. Rachidi, W. Nishida, N. Katamine, S. Mangé, A. Arlotto, M. Casanova, D. Riondel, J. Favier, A.; Lehmann, S. *Proc. Natl. Acad. Sci. U S A* **2000**, *97*, 13937-42.

(42) Singh, N. Singh, A. Das, D.; Mohan, M. L. *Antioxid. Redox Signal.* **2010**, *12*, 1271-94.

(43) Pamplona, R. Naudí, A. Gavín, R. Pastrana, M. a; Sajnani, G. Ilieva, E. V. Río, J. A. Del; Portero-Otín, M. Ferrer, I.; Requena, J. R. *Free Radic. Biol. Med.* **2008**, *45*, 1159-66.

(44) Martin, S. F. Burón, I. Espinosa, J. C. Castilla, J. Villalba, J. M.; Torres, J. M. *Free Radic. Biol. Med.* **2007**, *42*, 1723-9.

(45) Cavalli, A. Bolognesi, M. L. Capsoni, S. Andrisano, V. Bartolini, M. Margotti, E. Cattaneo, A. Recanatini, M.; Melchiorre, C. *Angew. Chem. Int. Ed.* **2007**, *46*, 3689-92.

(46) Cavalli, A. Bolognesi, M. L. Minarini, A. Rosini, M. Tumiatti, V. Recanatini, M.; Melchiorre, C. *J. Med. Chem.* **2008**, *51*, 347-72.

(47) Bolognesi, M. L. Cavalli, A.; Melchiorre, C. *Neurotherapeutics* **2009**, *6*, 152-62.

7. Development of hybrid lipoic acid derivatives against prion diseases

In **Chapter 6**, we reported on a new class of anti-prion compounds obtained by linking the antioxidant nucleus of BQ to several heterocyclic scaffolds potentially able to perturb PPIs in prion (9-amino-6-chloro-2-methoxyacridine, or 4-amino-7-chloroquinoline or 9-amino-6-chloro-1,2,3,4-tetrahydroacridine). These compounds displayed a multitarget profile, effectively contrasting both prion fibril formation and OS in a cell culture model of prion replication. We hypothesized that the presence of a PRM along with a moiety endowed with an alternative mechanism of action against prion diseases might lead to discover more effective compounds (**Figure 42**).[1] Building on these consideration, we designed another class of potential MTDLs, where as antioxidant fragment we selected lipoic acid (**17**). This choice was motivated by the following reasons: (i) **17** is an endogenous antioxidant; (ii) well-tolerated in vivo; (iii) effective against fibril formation; (iv) chemically linkable to the amine group of **42-43** and **45-46** by amide bond formation.[2] **17** has also been proposed as a lead structure for designing MTDLs for neurodegeneration.[2] More importantly, **17** was administered together with other antioxidants to a patient affected by prion disesases, showing moderate therapeutic effects.[3]

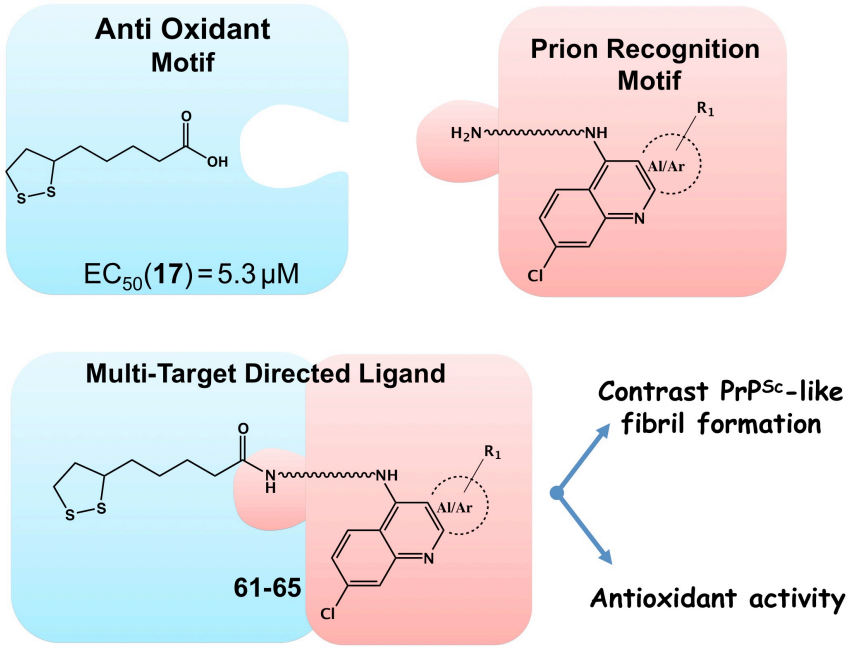

Figure 42. Rational design of **61-65** compounds

Two quinoline- (**61-62**) and two acridine- (**63-64**) lipoic acid hybrids differing in the diamino linker length were hence designed (**Figure 45**) and tested. Based on the structure similarity, also compound **65** (Lipocrine®; PCT Int Appl. 2006, WO2006080043), developed as a promising lead candidate for the treatment of AD, was included in the present investigation.[4]

7.1. Chemistry

We have previously reported how a coupling reaction of diamines with lipoic acid (**17**) provides easy access to a variety of derivatives.[4] We decided to synthesize the designed compounds **61-64** following the reported procedure.[4,5] **17** was loaded with EDCI, HOBT and NEt_3 then the proper N-substituted diamine (**42-43** and **45-46**, **Scheme 2**) was added at 0 °C for 2 hours. After stirring overnight at room temperature, the desired product was obtained in good yields (67-96%). The preparation of intermediate **42-43** and **45-46** was easily achieved by parallel synth esis as described before (see **Scheme 1**).

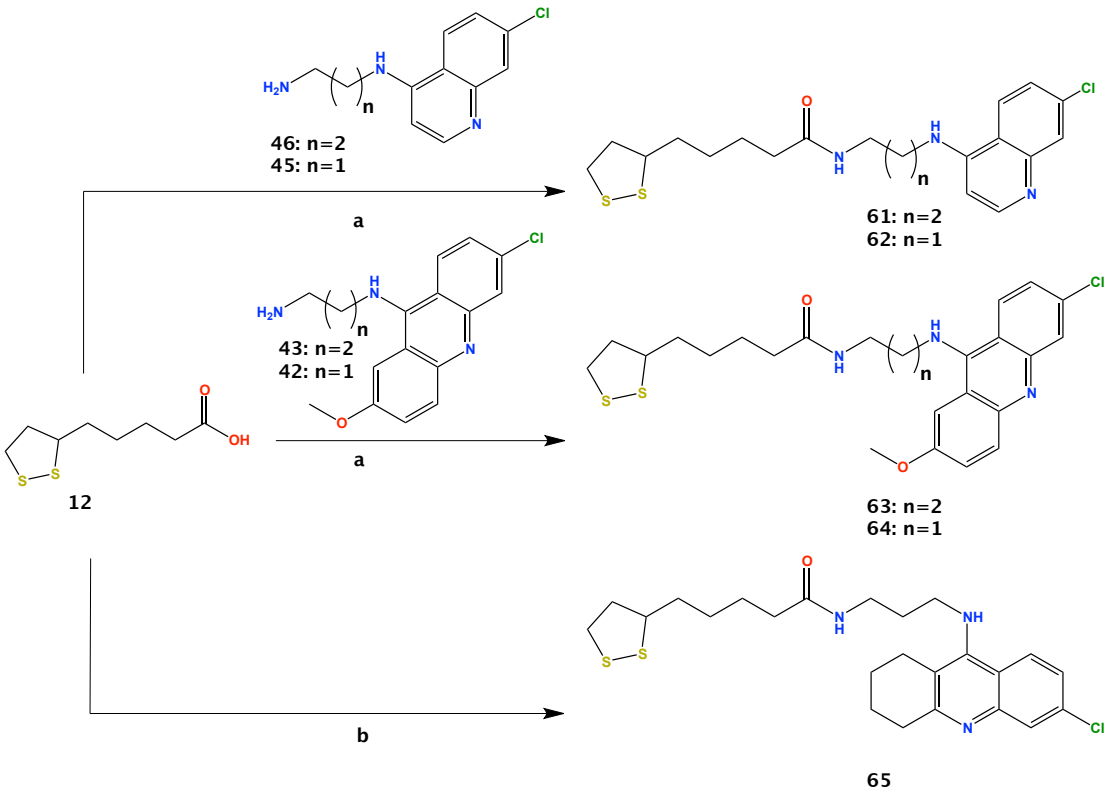

Scheme 2. Reagents and conditions: a) EDCI, HOBt, Et_3N, CH_2Cl_2, 0 °C, 0.5 h; then amine 42-43 and 45-46, RT, overnight, 67– 96% yields; b) see Reference Rosini *et al.* 2005

7.2. Results and Discussion

As for the previous studies, preliminarily, the possible toxicity of the hybrid compounds **61-65** was assessed in ScGT1 cells (see Experimental Section, **Chapter 10**). At 1 μM concentration, the

toxicity profile among **61-65** was low, only acridine **63** caused a decrease in cell viability to 88.0% of control. Therefore they were studied for their anti-prion activity at the same concentration (**47**). Quinoline-based hybrids **61** and **62** turned out to have low anti-prion activity (inhibition of 8.7% and 13.4% at 1 μM, respectively), while acridines **63** and **64** displayed high activity against prion replication (inhibition of 107% and 102%). Tetrahydroacridine **65** showed an intermediate profile (68%). Consistent with the percent inhibition data, **63** and **64** showed remarkable EC_{50} values of 0.18 μM and 0.15 μM, respectively, which are the lowest among the class of the synthesized derivatives and even better than the reference drug **2** (EC_{50} = 0.4 ± 0.1 μM) (**Figure 43** and **Table 5**). From the data of **Table 5**, **64** emerged as the hit compound of the present series. To better investigate its multitarget activity, we thought interesting to test the cellular anti-prion activity of its starting fragments (**17** and **42**; **Scheme 2**). As expected, **42** did inhibit prion replication with a submicromolar activity (0.35 μM), and thus it can be truly considered a PRM. Interestingly, lipoic acid (**17**) possessed a promising activity against PrP^{Sc} formation (EC_{50} = 5.3 ± 0.4 μM), together with an optimal toxicity profile (no toxic effects up to 100 μM). To our knowledge, this is the first time that the proposed anti-prion potential of **17** has been demonstrated in a cellular model. More importantly, **64** showed an improved anti-prion activity as much as 35-fold over **17** and 2.3-fold over **42**.

Table 5. Cell viability and antiprion activity of library compounds on ScGT1 cells.

Compound	% of viable cells at 1 μM[b]	% of PrP^{Sc} inhibition at 1 μM[c]	% of viable cells at EC_{50}[b]	EC_{50} (μM)[c]
2	98.5 ± 3.9[a]	103.8 ± 6.1[a]	100.0 ± 4.3[a]	0.4 ± 0.1[a]
61	100.7 ± 2.2	8.7 ± 0.5	95.8 ± 3.5	5.6 ± 0.1
62	101.6 ± 4.3	13.4 ± 0.6	100.8 ± 2.6	3.2 ± 0.2
63	88.1 ± 2.3	107.1 ± 3.0	101.9 ± 3.3	0.18 ± 0.01
64	94.3 ± 5.6	102.5 ± 5.8	92.1 ± 5.2	0.15 ± 0.01
65	95.9 ± 2.1	68.3 ± 2.2	94.8 ± 5.5	0.85 ± 0.05
17	103.0 ± 1.9	2.6 ± 0.1	95.4 ± 4.2	5.3 ± 0.4
42	88.0 ± 5.7	98.5 ± 5.4	95.4 ± 3.9	0.35 ± 0.02

[a] Values are the mean of three experiments, standard deviations are given. [b] ScGT1 cells were cultured in DMEM with 10% FBS, plated 25000 cells in each well of 96-well plates. The compounds were dissolved in DMSO (100%) and diluted in PBS 1X before adding various concentrations (10 nM - 10 μM) and incubated for 5 days at 37°C, 5% CO_2. The results were developed by calcein-AM fluorescence dye and read by microplate reader. [c] The effect of library compounds on inhibition of scrapie prion replication. ScGT1 cells were cultured in DMEM with 10% FBS, split 1:10 into Petri dishes and incubated for 2 days at 37°C and 5% CO_2. Then, various compound concentrations (10 nM - 2 μM), being non-toxic for the cells, were added to the plates. After a 5-day incubation, proteins of cells were extracted, quantified, digested with proteinase K (PK), and western-blotted.

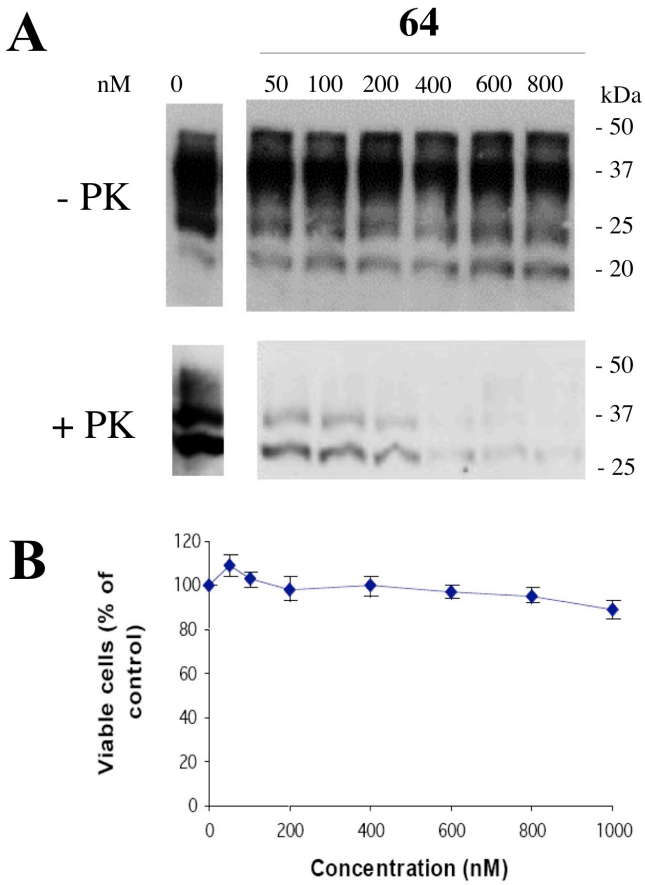

Figure 43. A) Western blot of protease-digested ScGT1 cell lysates depicting the presence or absence of prions (PrP^{Sc}) after treatment with **64**, before (up) or after (bottom) PK. B) Survival of ScGT1 cells treated with **64.**

To study at a molecular level the mechanism of action of the active compounds and fragments (**61-65, 17**, and **42**), a PrP amyloid seeding assay was performed. All molecules were capable of delaying fibril formation, with lag phase spanning from 52 to 70 hours (control 49 hours, **Figure 44**). Intriguingly, their in vitro anti-fibril activity parallels the cellular anti-prion profile. In fact, **63**, **64** and **65**, which were the most active in ScGT1 cell line, resulted the most active also in this assay. **63** and **64** extended the lag phase to a time ≥ 68 hours, showing a significantly slower kinetics than the control (**Figure 44**). The good activity shown by **42**, although preliminary, is in agreement with the starting hypothesis that such a PRM might interact directly with PrP to prevent its conversion to the misfolded PrP^{Sc} isoform. Furthermore, the low anti-amyloid activity of **17** *vs* those of hybrids **61-65** suggests that marked aggregation inhibition may be achieved only when **17** and a suitable PRM are combined into the same structure, as in **63** and **64**.

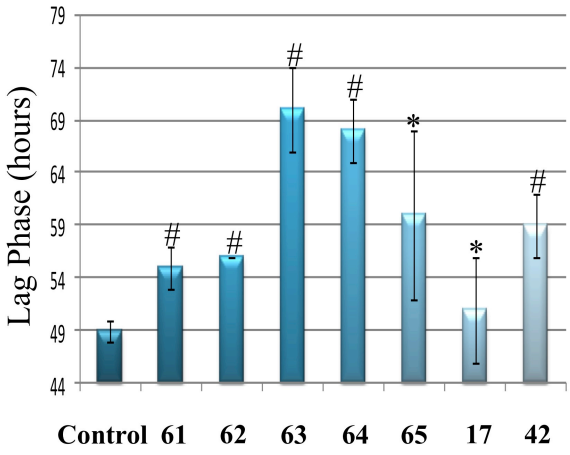

Figure 44. Prion fibril formation inhibitory activity in vitro for **61-65**, **17**, and **42** (10 μM). Statistical analysis was done by analysis of Student's t-test (n=4); (*) $p \leq 0.01$, (#) $p \leq 0.05$; Ctrl = control.

As highlited above, the PrP^{Sc} infected cells are under OS, mainly caused by mitochondrial dysfunction.[6-8] In light of this, antioxidant fragments might be beneficial against prion diseases. Indeed, lipoic acid hybrids, such as **65** [4], scavenge ROS, and they have been proposed for the treatment of other multifactorial neurodegenerative diseases.[2,5] Thus, we tested the antioxidant potential of the most active lipoyl-derivatives (**63-65**) in ScGT1 cell line, by using the TBARS assay. The assay measures lipid hydroperoxides and aldehydes expressed as an average percent of TBARS of treated cells versus control untreated cells. Figure **45** clearly shows that **63** and **64** displayed antioxidant activity (78-82% of control) at 1 μM, while **65** was even better than Trolox (58% *vs* 71%, respectively).

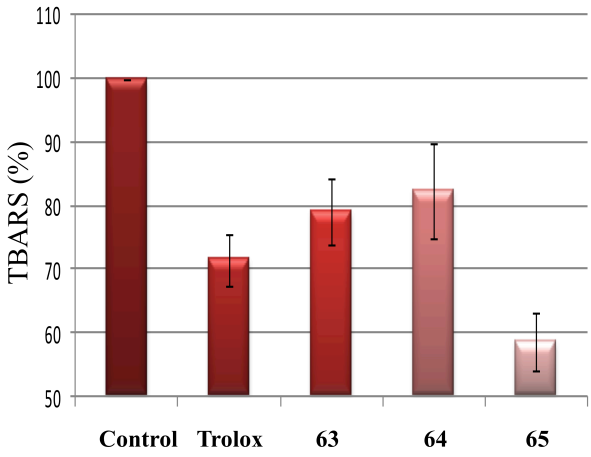

Figure 45. Effect of compounds **63–65** (1 μM) on ScGT1, evaluated by thiobarbituric acid reactive substances (TBARS) formation. Trolox was used as a positive control. Values are means ± SD (n=3).

Although a perfect match with cellular data is not evident, these results confirm the design rationale, indicating that the concomitant presence of a PRM and an antioxidant fragment is suitable to the discovery of anti-prion MTDLs. As an example, **64**, owing to the presence of an antioxidant fragment, the lipoic acid (**17**), and a PRM, the acridine motif (**42**), is able to simultaneously interact with at least two of the multiple targets involved in prion pathology. **64** inhibits PrP^{Sc} accumulation, delays fibril formation and reduces oxidative stress. Altogether, these in vitro results make **64** an effective candidate to be investigated in vivo for its multiple biological properties in prion diseases. Furthermore, given the promising cellular anti-prion profile of fragment **17,** further efforts towards the design of novel lipoyl hybrids are warranted.

References

(1) Bongarzone, S. Tran, H. N. A. Cavalli, A. Roberti, M. Carloni, P. Legname, G.; Bolognesi, M. L. *J. Med. Chem.* **2010**, 8197-8201.

(2) Bolognesi, M. L. Minarini, A. Tumiatti, V.; Melchiorre, C. *Mini Reviews Med. Chemi.* **2006**, *6*, 1269-1274.

(3) Drisko, J. *J. Am. Coll. Nutr.* **2002**, *21*, 22-5.

(4) Rosini, M. Andrisano, V. Bartolini, M. Bolognesi, M. L. Hrelia, P. Minarini, A. Tarozzi, A.; Melchiorre, C. *J. Med. Chem.* **2005**, *48*, 360-3.

(5) Bolognesi, M. L. Cavalli, A. Bergamini, C. Fato, R. Lenaz, G. Rosini, M. Bartolini, M. Andrisano, V.; Melchiorre, C. *J. Med. Chem.* **2009**, *52*, 7883-6.

(6) Milhavet, O.; Lehmann, S. *Brain Res.* **2002**, *38*, 328-39.

(7) Milhavet, O. McMahon, H. E. Rachidi, W. Nishida, N. Katamine, S. Mangé, A. Arlotto, M. Casanova, D. Riondel, J. Favier, A.; Lehmann, S. *Proc. Natl. Acad. Sci. U S A* **2000**, *97*, 13937-42.

(8) Choi, S. I. Ju, W. K. Choi, E. K. Kim, J. Lea, H. Z. Carp, R. I. Wisniewski, H. M.; Kim, Y. S. *Acta Neuropathologica* **1998**, *96*, 279-86.

8. Discovery of novel derivatives as lead antiprion compounds with enhanced cell line activity, good microsomal stability and low toxicity

In this Chapter, we discuss the rational design of an additional series of MTDLs (**66-69***, structure not shown*) potentially able to inhibit prion replication through multiple mechanisms.*

8.1. Results and Discussion

A new MTDL (**69**) showed a remarkable EC_{50} value of 0.04 μM, which is the lowest among all the classes of synthesized derivatives and even better than the reference compound **2** (EC_{50} = 0.4 μM).

* *The data in this chapter are hidden because they have not been published yet.*

9. Conclusions and future perspectives

Prion diseases are transmissible spongiform encephalopathies (TSEs) where the molecular mechanism is based on an aberrant misfolding of the cellular form of the prion protein (PrP^C). Conversion and replication from PrP^C to its pathological form (PrP^{Sc}) is followed by aggregation and ultimately neurodegeneration in the CNS. To date there are no identified therapies against TSEs because the development of antiprion drugs and the understanding of their mechanism of action are very difficult and challenging tasks.

In the first part of my thesis, I presented a computational study on ligand binding to PrP^C. I contributed to the development of a docking procedure able to characterize binding of small ligand **1** (*2-pyrrolidin-1-yl-N-[4-[4-(2-pyrrolidin-1-yl-acetylamino)-benzyl]-phenyl]-acetamide)*) on $hPrP^C$ binding sites. It has been shown that **1** stabilize $hPrP^C$ binding to the globular domain (as shown by NMR experiments published by Kuwata *et al.*[1]). Our computational approach, called EMD (enhanced molecular docking), which combines standard docking methods with molecular dynamics and metadynamics-based free energy simulations (**Figure 16**) has been discussed. EMD protocol was able to account for protein flexibility and it provides detailed information about the binding process, binding affinity and ligand-target interactions. Applying EMD procedure on $hPrP^C$, it has been found a multiple-pose binding pattern for **1** that could not be obtained by applying only standard protocols. Three binding poses are identified, in agreement with NMR data. The predicted dissociation free energy turned out to be in very good agreement with experimental data.[2,3] In our view this result emphasizes the validity of our protocol that it could be now used to predict the potency of **1** analogues interacting on $hPrP^C$.

The second and largest part of my thesis was devoted to design and synthesis of novel ligands against prion diseases. Starting from a deep study of the processes causing prion disease pathogenesis (protein aggregation; oxidative stress; unbalance of metal ions),[4] we rationalized our approach to new ligands acting on multiple targets. A design strategy in which two distinct pharmacophores are combined in the same structure to afford hybrid molecules was applied. I synthesized three libraries of compounds obtained by combining PRMs (acridine and quinoline fragments)[5] with several antioxidants and chelating fragments.

First library: Compounds **30-40** (**Scheme 1**), featuring a BQ nucleus as antioxidant spacer connecting two PRMs, were designed and evaluated against prion infection. A promising hit proved to be **39**, with very good antiprion activity, which is the lowest among the class and even better than the reference drug **2** (**Figure 26**). Although its mechanism of action is not fully disclosed, **39** should favour the interaction with prion recognition domains, whereas the BQ nucleus should act simultaneously as a disrupting element against PPIs[6,7] and an effective antioxidant moiety.[8-10]

Second library: Here, as antioxidant fragment the lipoic acid (**17**, **Scheme 2**) has been selected because it was reported to be moderately effective in a prion infected patient.[13] Five lipoic acid hybrids have been developed and all showed good antiprion activity. PrP amyloid seeding assay demonstrated that **63** and **64** extended the lag phase. Interestingly, **63** and **64**, owing to the presence of an antioxidant fragment, the lipoic acid (**17**), and a PRM, the acridine motif (**43** and **42**, respectively), were able to simultaneously interact with at least two (PPIs and OS) of the multiple targets involved in prion pathology. This finding reinforces the usefulness of MTDL strategy to design new antiprion compounds.[11]

Third library: Here, five ligands able to inhibit prion replication through multiple mechanisms have been designed. A new hybrid compound has shown a potent antiprion profile (*data not shown*).

In summary, I addressed two key issues in antiprion drug discovery:

i) To study ligand interacting with cavity-less proteins, such PrP^C, a computational protocol (EMD) able to predict PrP^C-**1** interactions was presented. EMD protocol combines standard docking calculations with free energy simulations.

ii) To rational design ligands for multifactorial prion disease pathogenesis. For the first time, a design strategy in which two distinct pharmacophores are combined in the same structure to afford potent MTDL antiprion compounds has been applied.

These results represent an excellent initial step toward the development of new ligands for the treatment of prion diseases.

Perspectives

Future work will investigate the pharmacological profile of **34**, **64, 69** (see **Figure 1**) to assess their stability and toxicity *in vivo*. Over recent years, zebrafish assays have emerged as an important tool to predict mammalian adverse drug effects.[12] In order to further evaluate the pharmacological profile of **34**, **64, 69**, the survival rate of zebrafish upon exposure to each compound will be determined in the laboratory of Prof. Edward Málaga-Trillo (Developmental Neurobiology, Department of Biology - University of Konstanz, Germany). Then, it would be very important to confirm the antiprion activity in an *in vivo* mouse model.

The structure of protein-ligand complex provides a detailed insight into the interactions made between the protein and ligand. The determination of the structure of the PrP^C in complex with an antiprion compound is clearly central to structure-based discovery. Further work needs to be performed to estimate the binding of lead compounds presented here to $mPrP^C$. We are planning to

use NMR spectroscopy, in collaboration with Prof. Janez Plavec (NMR center, National Institute of Chemistry, University of Ljubljana, Slovenia), to evaluate the effect of binding of compound **69** to $mPrP^{C}$.

Computational studies will be combined with the NMR data to study PrP^{C}–**69** interactions. This work will investigate the binding of **69** to the globular domain of PrP^{C} by using the EMD protocol that was established in this thesis. It would be highly interesting to use molecular dynamic calculations to design new analogs of **69** with a higher affinity to PrP^{C}, which may eventually show an improved activity against PrP^{Sc} conversion and replication.

References

(1) Kuwata, K. Nishida, N. Matsumoto, T. Kamatari, Y. O. Hosokawa-Muto, J. Kodama, K. Nakamura, H. K. Kimura, K. Kawasaki, M. Takakura, Y. Shirabe, S. Takata, J. Kataoka, Y.; Katamine, S. *Proc. Natl. Acad. Sci. U S A* **2007**, *104*, 11921-6.

(2) Kranjc, A. Bongarzone, S. Rossetti, G. Biarnés, X. Cavalli, A. Bolognesi, M. L. Roberti, M. Legname, G.; Carloni, P. *J. Chem. Theory Comput.* **2009**, *5*, 2565-2573.

(3) Biarnés, X. Bongarzone, S. Vargiu, A. V. Carloni, P.; Ruggerone, P. *J. Comput. Aided Mol. Des.* **2011**, *25*, 395-402.

(4) Soto, C.; Satani, N. *Trends Mol. Med.* **2010**, *17*, 14-24.

(5) Bongarzone, S.; Bolognesi, M. L. *Exp. Opin. Drug Discovery* **2011**, 1-18.

(6) Scherzer-Attali, R. Pellarin, R. Convertino, M. Frydman-Marom, A. Egoz-Matia, N. Peled, S. Levy-Sakin, M. Shalev, D. E. Caflisch, A. Gazit, E.; Segal, D. *PloS one* **2010**, *5*, e11101.

(7) Convertino, M. Pellarin, R. Catto, M. Carotti, A.; Caflisch, A. *Protein science : a publication of the Protein Society* **2009**, *18*, 792-800.

(8) Bongarzone, S. Tran, H. N. A. Cavalli, A. Roberti, M. Carloni, P. Legname, G.; Bolognesi, M. L. *J. Med. Chem.* **2010**, 8197-8201.

(9) Bolognesi, M. L. Banzi, R. Bartolini, M. Cavalli, A. Tarozzi, A. Andrisano, V. Minarini, A. Rosini, M. Tumiatti, V. Bergamini, C. Fato, R. Lenaz, G. Hrelia, P. Cattaneo, A. Recanatini, M.; Melchiorre, C. *J. Med. Chem.* **2007**, *50*, 4882-97.

(10) Bolognesi, M. L. Cavalli, A.; Melchiorre, C. *Neurotherapeutics* **2009**, *6*, 152-62.

(11) Bongarzone, S. Tran, H. N. A. Cavalli, A. Roberti, M. Rosini, M. Carloni, P. Legname, G.; Bolognesi, M. L. *ChemMedChem* **2011**, *6*, 601-5.

(12) Eimon, P. M.; Rubinstein, A. L. *Expert Opin. Drug Met.* **2009**, *5*, 393-401.

(13) Drisko, J. *J. Am. Coll. Nutr.* **2002**, *21*, 22-5.

10. Experimental section

10.1. Chemistry

All starting reagents (**12, 19, 53-60, 70-73**) and **2** and **15** were of the best grade available from Aldrich. 9-chloro-1,2,3,4-thydroacridine (**29**) and 6,9-dichloro-1,2,3,4-tetrahydroacridine (**30)** were synthesized according to the procedure reported by Hu *et al.*.[1] Direct infusion ESI-MS spectra were recorded on Waters ZQ 4000 apparatus. ^{1}H NMR and ^{13}C NMR spectra were recorded either at 200 MHz (^{1}H) and 50.3 MHz (^{13}C) or at 400 MHz (^{1}H) and 100 MHz (^{13}C). Chemical shifts are reported in parts per million (ppm) relative to tetramethylsilane (TMS), and spin multiplicities are given as s (singlet), br s (broad singlet), d (doublet), t (triplet), or m (multiplet). Elemental analysis was used to confirm ≥ 95% sample purity and the elemental compositions of the compounds agreed to within ±0.4% of the calculated value. When the elemental analysis is not included, crude compounds were used in the next step without further purification. Chromatographic separations were performed on silica gel columns by flash (Kieselgel 40, 0.040-0.063 mm; Merck) chromatography. Reactions were followed by thin-layer chromatography (TLC) on Merck (0.25 mm) glass-packed precoated silica gel plates (60 F254), then visualized in an iodine chamber or with an UV lamp. The term "dried" refers to the use of anhydrous sodium sulphate. Compounds were named following IUPAC rules as applied by Beilstein-Institute AutoNom (version 2.1), a PC integrated software package for systematic names in organic chemistry.

General Procedure a for the Synthesis of Library Members 42-52

In distinct reactors, a mixture of the appropriate hetheroaryl halides **56-60** (1 eq) and phenol (10 eq) were prepared and the catalyst NaI (0.3 eq) was added to each reactor. The resulting mixtures were carefully heated at 120 °C for 1 hour under N2 atmosphere. Then the appropriate amine **53-55** (27 eq) were added to each reactor and the resulting solutions were heated for further 5 hours, cooled to room temperature and treated as follows. Each mixture was diluted with EtOAc and shaken with 10% KOH solution. The aqueous layer was extracted with EtOAc, dried over anhydrous Na_2SO_4, evaporated. Purification of each crude product by flash column chromatography using (Dichloromethane/Methanol/ Ammonia solution) yielded the corresponding final amines **42-52**.

General Procedure b for the Synthesis of 2,5-diamino-1,4-benzoquinone Library Members 30-40

In distinct reactors, 2,5-dimethoxybenzoquinone (1 eq) was suspended in EtOH (15 mL) and heated to 80 °C until the solid was completely dissolved. After cooling to 50 °C, the appropriate amines **42-42** (2 eq) were added each reaction mixture that became progressively clear and red. Each mixture was heated at 50 °C for 5 h and, after cooling, precipitates formed, which were collected by filtration. The solid was dissolved in diethylether (7-10 mL) and trifluoroacetic acid (0.2 mL) was added to the solutions to obtain the corresponding trifluoroacetate salts.

2,5-bis[2-(6-chloro-2-methoxyacridin-9-ylamino)ethylamino]cyclohexa-2,5-diene-1,4-dione bis(trifluoroacetate) (30)

Following general procedure (b), it was synthesized in 45% yield from 2,5-dimethoxybenzoquinone (25.22 mg; 150 μmol) and **42** (90.54 mg, 300 μmol). ^{1}H-NMR (DMSO, 200 MHz): δ 3.59-3.61 (m, 4H), 3.91 (s, 6H), 4.27 (m, 4H), 5.38 (s, 2H), 6.98 (s, 2H), 7.11 (s, 2H), 7.23 (s, 2H), 7.47 (d, *J* = 9.2 Hz , 2H), 7.67 (d, *J* = 9.2 Hz , 2H), 8.48 (d, *J* = 9.6 Hz , 2H). ^{13}C-NMR (DMSO, 50.3 MHz) δ 25.63, 43.46, 48.62, 52.77, 56.75, 77.71, 124.43, 151.30, 162.64, 171.50, 183.31, 189.23 Anal. ($C_{38}H_{32}Cl_2N_6O_4$ $2CF_3COOH$ $4H_2O$) C, H, N: calcd, 50.06; 4.20, 8.34; found, 49.98, 3.80, 8.46. ESI-MS *m/z*: 707 [M + $H^{+\,35}$Cl], 709 [M + $H^{+\,37}$Cl].

2,5-bis[3-(6-chloro-2-methoxyacridin-9-ylamino)propylamino]cyclohexa-2,5-diene-1,4-dione bis(trifluoroacetate) (31)

Following general procedure (b), it was synthesized in 81% yield from 2,5-dimethoxybenzoquinone (25.22 mg; 150 μmol) and **43** (94.45 mg, 300 μmol). ^{1}H-NMR (CD_3OD, 200 MHz): δ 2.13 (m, 4H), 3.22 (br s, 4H), 3.93 (s, 6H), 4.13 (br s, 4H), 5.15 (s, 2H), 7.42-7.82 (m, 10H), 8.42 (d, 2H). ^{13}C NMR (DMSO, 50.3 MHz) δ 27.47, 46.76, 56.10, 67.11, 92.22, 110.00, 114.15, 117.36, 120.64, 123.03, 127.04, 138.85, 140.18, 150.86, 155.88, 156.17, 177.23. Anal. ($C_{40}H_{36}Cl_2N_6O_4$ $2CF_3COOH$ $2H_2O$) C, H, N: calcd, 52.86; 4.23, 8.41; found, 52.73, 3.94, 8.41. ESI-MS *m/z*: 735 [M + $H^{+\,35}$Cl], 737 [M + $H^{+\,37}$Cl], 757 [M + $Na^{+\,35}$Cl], 759 [M + $Na^{+\,37}$Cl].

2,5-bis{3-[3-(6-chloro-2-methoxyacridin-9-ylamino)propylamino]propylamino}cyclohexa-2,5-diene-1,4-dione tetrakis(trifluoroacetate) (32)

Following general procedure (b), it was synthesized in 38% yield from 2,5-dimethoxybenzoquinone (25.22 mg; 150 μmol) and **44** (111.89 mg, 300 μmol). ^{1}H-NMR (DMSO, 200 MHz): δ 1.81-1.95 (m, 12H), 2.73-2.83 (m, 8H), 3.25-3.28 (m, 4H), 3.92 (s, 6H), 5.30 (s, 2H), 7.22 (m, 2H), 7.33-7.37 (m, 4H), 7.99-8.11 (m, 6H). ^{13}C NMR (DMSO, 50.3 MHz) δ 24.66, 26.24, 39.07, 45.50, 46.07, 55.55, 92.62, 117.48, 120.40, 124.11, 127.83, 140.89, 151.94, 157.21, 171.89. Anal. ($C_{46}H_{50}Cl_2N_8O_2$ $4CF_3COOH$) C, H, N: calcd, 53.88; 5.34, 8.99; found, 53.32, 5.94, 8.41. ESI-MS *m/z*: 849 [M + $H^{+\,35}$Cl], 852 [M + $H^{+\,37}$Cl].

2,5-bis[2-(7-chloroquinolin-4-ylamino)ethylamino]cyclohexa-2,5-diene-1,4-dione bis(trifluoroacetate) (33)

Following general procedure (b), it was synthesized in 60% yield from 2,5-dimethoxybenzoquinone (25.22 mg; 150 μmol) and **45** (66.51 mg, 300 μmol). ^{1}H-NMR (CD_3OD, 200 MHz): δ 3.62 (t, *J* = 5.4 Hz, 4H), 3.83 (t, *J* = 5.4 Hz, 4H), 5.36 (s, 2H), 6.96 (d, *J* = 7 Hz, 2H), 7.67-7.73 (m, 2H), 7.88 (s, 2H), 8.28 (d, *J* = 9.2 Hz, 2H), 8.43 (d, *J* = 7 Hz, 2H). ^{13}C NMR (CD_3OD, 50.3 MHz) δ 39.74, 41.17, 67.88, 91.95, 97.95, 117.17, 118.54, 123.91, 126.94, 139.20, 142.17, 151.34, 156.09, 177.78. Anal. ($C_{28}H_{24}Cl_2N_6O_2$ $2CF_3COOH$ H_2O) C, H, N: calcd, 48.64, 3.76, 10.59; found, 48.44, 3.56, 10.59. ESI-MS *m/z*: 547 [M + $H^{+\,35}$Cl], 549 [M + $H^{+\,37}$Cl], 569 [M + $Na^{+\,35}$Cl], 571 [M + $Na^{+\,37}$Cl].

2,5-bis[3-(7-chloroquinolin-4-ylamino)propylamino]cyclohexa-2,5-diene-1,4-dione bis(trifluoroacetate) (34)

Following general procedure (b), it was synthesized in 60% yield from 2,5-dimethoxybenzoquinone (25.22 mg; 150 μmol) and **46** (70.72 mg, 300 μmol). ^{1}H-NMR (CD_3OD, 400 MHz): δ 2.12 (q, *J* = 6.8 Hz, 4H), 3.40 (t, *J* = 6.8Hz, 4H), 3.70 (t, *J* = 6.8Hz, 4H), 5.28 (s, 2H), 6.91 (d, *J* = 6.8Hz, 2H), 7.69 (d, *J* = 9.2Hz, 2H), 7.87 (s, 2H), 8.35 (d, *J* = 9.2Hz, 2H), 8.41 (d, *J* = 7.2Hz, 2H). ^{13}C NMR (CD_3OD, 100.5 MHz) δ 21.25, 27.42, 41.01, 42.55, 99.79, 117.03, 118.11, 120.33, 125.95, 128.77, 140.07, 141.05, 143.88, 153.23, 157.68, 179.41. Anal. ($C_{30}H_{28}Cl_2N_6O_2$ $2CF_3COOH$ $2H_2O$) C, H, N: calcd, 48.64; 4.08, 10.01; found, 48.89, 3.69, 10.01. ESI-MS *m/z*: 575 [M + $H^{+\,35}$Cl], 577 [M + $H^{+\,37}$Cl], 597 [M + $Na^{+\,35}$Cl] , 599 [M + $Na^{+\,37}$Cl].

2,5-bis{3-[3-(7-chloroquinolin-4-ylamino)propylamino]propylamino}cyclohexa-2,5-diene-1,4-dione tetrakis(trifluoroacetate) (35)

Following general procedure (b), it was synthesized in 51% yield from 2,5-dimethoxybenzoquinone (25.22 mg; 150 μmol) and **47** (87.84 mg, 300 μmol). ^{1}H-NMR (CD_3OD, 400 MHz): δ 2.03 (t, *J* = 7.2 Hz,4H), 2.20 (t, *J* = 7.6 Hz, 4H), 3.10 (t, *J* = 7.6 Hz, 4H), 3.21 (t, *J* = 7.6 Hz, 4H), 3.30 (m, 4H), 3.71 (t, *J* = 6.8 Hz, 4H), 5.12 (br s, 2H), 6.90 (d, *J* = 7.6 Hz, 2H), 7.65 (d, *J* = 7.6 Hz, 2H), 7.87 (s, 2H), 8.35 (d, 2H), 8.41 (d, *J* = 8 Hz, 2H). ^{13}C NMR (CD_3OD, 100.5 MHz) δ 17.18, 24.68, 39.13, 40.56, 45.32, 45.51, 57.15, 98.67, 115.86, 119.24, 124.90, 127.58, 138.92, 139.87, 142.88, 151.92, 156.51, 178.44. Anal. ($C_{36}H_{42}Cl_2N_8O_2$ $4CF_3COOH$ H_2O) C, H, N: calcd, 45.41; 4.16, 9.63; found, 45.40, 3.66, 9.94. ESI-MS *m/z*: 689 [M + $H^{+\,35}$Cl], 691 [M + $H^{+\,37}$Cl].

2,5-bis[3-(1,2,3,4-tetrahydroacridin-9-ylamino)ethylamino]cyclohexa-2,5-diene-1,4-dione bis(trifluoroacetate) (36)

Following general procedure (b), it was synthesized in 45% yield from 2,5-dimethoxybenzoquinone (25.22 mg; 150 μmol) and **48** (72.40 mg, 300 μmol). ^{1}H-NMR (CD_3OD, 400 MHz): δ 1.91-1.95 (br s, 8H), 2.69 (s, 4H), 2.99 (s, 4H), 3.57 (m, 4H), 4.20 (m, 4H), 5.12 (s, 2H), 7.58 (t, *J* = 8.2 Hz, 2H), 7.70-7.83 (m, 4H), 8.21 (d, *J* = 8.2 Hz, 2H).). ^{13}C NMR (CD_3OD, 50.3 MHz) δ 19.31, 20.98, 22.71, 23.47, 27.41, 29.42, 65.50, 93.87, 115.54, 118.26, 123.96, 124.93, 132.25, 144.83, 150.90, 164.33, 182.95. Anal. ($C_{36}H_{38}N_6O_2$ $2CF_3COOH$ H_2O) C, H, N: calcd, 57.69; 5.08, 10.09; found, 57.03, 4.93, 9.75. ESI-MS *m/z*: 587 [M + H^+].

2,5-bis[3-(1,2,3,4-tetrahydroacridin-9-ylamino)propylamino]cyclohexa-2,5-diene-1,4-dione bis(trifluoroacetate) (37)

Following general procedure (b), it was synthesized in 55% yield from 2,5-dimethoxybenzoquinone (25.22 mg; 150 μmol) and **49** (76.61 mg, 300 μmol). ^{1}H-NMR (CD_3OD, 400 MHz): δ 1.96 (br s, 8H), 2.16 (m, 4H), 2.69 (br s, 4H), 2.99 (br s, 4H), 3.36 (m, 4H), 4.06 (m, 4H), 5.09 (s, 2H), 7.55 (m, 2H), 7.72 (m, 2H), 7.82 (m, 2H), 8.33 (d, 2H). ^{13}C NMR (CD_3OD, 100.5 MHz) δ 21.74, 22.92, 24.95, 29.30, 29.76, 40.71, 46.70, 93.25, 111.33, 113.14, 117.85, 120.06, 126.38, 134.07, 139.74, 151.87, 153.01, 158.10, 178.97. Anal. ($C_{38}H_{42}N_6O_2$ $2CF_3COOH$ H_2O) C, H, N: calcd, 58.60; 5.39, 9.76; found, 57.92, 4.89, 8.95. ESI-MS *m/z*: 615 [M + H^+].

2,5-bis{3-[3-(1,2,3,4-tetrahydroacridin-9-ylamino)propylamino]propylamino}cyclohexa-2,5-diene-1,4-dione tetrakis(trifluoroacetate) (38)

Following general procedure (b), it was synthesized in 88% yield from 2,5-dimethoxybenzoquinone (25.22 mg; 150 μmol) and **50** (93.74 mg, 300 μmol). ^{1}H-NMR (CD_3OD, 200 MHz): δ 1.15-1.25 (m, 4H), 1.97 (br s, 12H), 2.17-2.28 (m, 4H), 2.73 (s, 4H), 3.05-3.33 (m, 12H), 4.08 (m, 4H), 5.27 (s, 2H), 7.55-7.58 (m, 2H), 7.75-7.91 (m, 4H), 8.38 (d, 2H). ^{13}C NMR (CD_3OD, 50.3 MHz) δ 13.52, 19.83, 21.04, 23.13, 24.02, 26.37, 27.46, 38.47, 64.97, 77.56, 91.90, 111.54, 115.40, 118.37, 124.26, 124.75, 132.19, 137.82, 150.34, 151.24, 156.02, 177.69. Anal. ($C_{44}H_{56}N_8O_2$ $4CF_3COOH$ H_2O) C, H, N: calcd, 51.71, 5.09, 9.11 found, 51.91, 5.19, 9.31. ESI-MS *m/z*: 730 [M + H^+].

2,5-bis[3-(6-chloro-1,2,3,4-tetrahydroacridin-9-ylamino)propylamino]cyclohexa-2,5-diene-1,4-dione tetrakis(trifluoroacetate) (39)

Following general procedure (b), it was synthesized in 87% yield from 2,5-dimethoxybenzoquinone (25.22 mg; 150 μmol) and **22** (86.94 mg, 300 μmol). ^{1}H-NMR (CD_3OD, 400 MHz): δ 1.90-1.92 (m, 8H), 2.15 (m, 4H), 2.62 (m, 4H), 2.93 (s, 4H), 3.30 (m, 4H), 3.98 (m, 4H), 5.03 (s, 2H), 7.55 (d, *J* = 9.6 Hz, 2H), 7.63 (s, 2H), 8.23 (d, *J* = 9.6 Hz, 2H). ^{13}C NMR (CD_3OD, 100 MHz) δ 20.72, 21.73, 24.21, 28.48, 38.97, 45.49, 57.09, 57.12, 105.98, 105.99, 112.53, 125.37, 127.90, 151.47, 159.65, 177.65, 181.88. Anal. ($C_{38}H_{40}Cl_2N_6O_2$ $4CF_3COOH$ H_2O) C, H, N: calcd, 54.26, 4.77, 9.04 found, 54.30, 4.81, 9.08. ESI-MS *m/z*: 683 [M + H^+ $^{35}Cl^{35}Cl$], 685 [M + H^+ $^{37}Cl^{35}Cl$] 687 [M + H^+ ^{37}Cl ^{37}Cl].

2,5-bis[3-(6-methoxyquinolin-4-ylamino)propylamino]cyclohexa-2,5-diene-1,4-dione bis(trifluoroacetate) (40)

Following general procedure (b), it was synthesized in 88% yield from 2,5-dimethoxybenzoquinone (25.22 mg; 150 μmol) and **52** (69.39 mg, 300 μmol). ^{1}H-NMR (CD_3OD, 400 MHz): δ 2.12 (q, *J* = 6.8 Hz, 4H), 3.37 (t, *J* = 6.8Hz, 4H), 3.65 (t, *J* = 6.8Hz, 4H), 3.96 (s, 6H), 5.23 (s, 2H), 7.13 (d, *J* = 7.2Hz, 2H), 7.53 (d, *J* = 9.2Hz, 2H), 7.66 (s, 2H), 7.74 (d, *J* = 9.2Hz, 2H), 8.27 (d, *J* = 7.2Hz, 2H). ^{13}C NMR (CD_3OD, 100.5 MHz) δ 23.44, 26.00, 39.66, 40.96, 55.24, 92.02, 97.42, 101.35, 121.30, 124.97, 130.27, 132.86, 139.78, 151.83, 155.27, 158.72, 177.91. Anal. ($C_{32}H_{34}N_6O_4$ $2CF_3COOH$ H_2O) C, H, N: calcd, 53.20; 4.71, 10.34; found, 53.23; 4.74, 10.39. ESI-MS *m/z*: 567 [M + H].

2-[3-(7-chloroquinolin-4-ylamino)propylamino]naphthalene-1,4-dione (41)

A suspension of naphthalene-1,4-dione (100.6 mg; 0.636 mmol) in EtOH (15 mL) was stirred and heated to 80 °C until the solid was completely dissolved (1h). After cooling to 50 °C, amine **46** (150 mg, 0.636 mmol) was added and the resulting mixture was stirred for 5 hours. Removal of the solvent gave a residue that was purified by gravity chromatography (CH_2Cl_2:MeOH:NH_4OH, 9:1:0.05) to afford **41** as orange solid (100 mg, 0.256 mmol, 40%). ^{1}H-NMR ($CDCl_3$, 400 MHz): δ 2.17 (q, 2H), 3.50 (q, 4H), 5.14 (bs, 1H),5.74 (s, 1H), 6.00

(brs, 1H), 6.45 (d, *J* = 5.2Hz, 1H), 7.37 (dd, *J* = 9.2Hz, *J* = 2.0Hz, 1H), 7.63 (t, *J* = 7.6Hz, 1H), 7.68 (d, *J* = 8.8 Hz, 1H), 7.75 (t, *J* = 7.6Hz, *J* = 1.6Hz, 1H), 7.97 (d, *J* = 2Hz, 1H), 8.04 (d, *J* = 6.8 Hz, 1H), 8.10 (d, *J* = 7.6 Hz, 1H), 8.56 (d, *J* = 5.2 Hz, 1H),. ^{13}C NMR (CD_3OD, 100.5 MHz) δ 27.40, 40.30, 40.91, 99.22, 101.25, 117.15, 120.76, 125.64, 126.22, 126.34, 132.15, 133.42, 134.89, 151.98, 182.96. MS *m/z*: 392 [M + $H^{+\,35}$Cl], 394 [M + $H^{+\,37}$Cl], 414 [M + $Na^{+\,35}$Cl], 416 [M + $Na^{+\,37}$Cl].

N^1-(6-chloro-2-methoxyacridin-9-yl)ethane-1,2-diamine (42)

Following general procedure (a), it was synthesized from **56** (300 mg, 1.08 mmol) and **53** (1.9 mL, 29 mmol). The crude residue was purified by flash column chromatography (CH_2Cl_2/CH_3OH/NH_4OH, 9:1:0.1) to yield **42** (110 mg, 38%). ^{1}H-NMR ($CDCl_3$, 200 MHz): δ 3.71 (m, 2H), 3.97 (m, 2H), 4.03 (s, 3H), 7.15 (d, *J* = 9.4 Hz , 1H), 7.36 (s, 1H), 7.41 (s, 1H), 7.92-8.06 (m, 3H) ESI-MS *m/z*: 302 [M + $H^{+\,35}$Cl], 304 [M + $H^{+\,37}$Cl].

N^1-(6-chloro-2-methoxyacridin-9-yl)propane-1,3-diamine (43)

Following general procedure (a), it was synthesized from **56** (300 mg, 1.08 mmol) and **54** (2.4 mL, 29 mmol). The crude residue was purified by flash column chromatography (CH_2Cl_2/CH_3OH/NH_4OH, 9:1:0.1) to yield **43** (110 mg, 33%). ^{1}H-NMR ($CDCl_3$, 200 MHz): δ 1.77 (quintet, 2H), 3.00 (t, *J* = 6 Hz, 2H), 3.83 (s, 3H), 3.86 (t, *J* = 6 Hz, 2H), 7.08-7.14 (m, 2H), 7.19 (s, 1H), 7.87 (d, *J* = 9.2 Hz, 1H), 7.93 (s, 1H), 8.01 (d, *J* = 9.2 Hz, 1H). ESI-MS *m/z*: 316 [M + $H^{+\,35}$Cl]

N^1-(3-aminopropyl)-N3-(6-chloro-2-methoxyacridin-9-yl)propane-1,3-diamine (44)

Following general procedure (a), it was synthesized from **56** (300 mg, 1.08 mmol) and **55** (4,1 mL, 29 mmol). The crude residue was purified by flash column chromatography (CH_2Cl_2/CH_3OH/NH_4OH, 8:2:0.2) to yield **44** (150 mg, 37%). ^{1}H-NMR ($CDCl_3$, 200 MHz): δ 1.61-1.68 (m, 4H), 2.62-2.84 (m, 6H), 3.62-3.80 (m, 2H), 3.83 (s, 3H), 7.04 (m, 1H), 7.24 (m, 2H), 7.79-7.93 (m, 3H). ESI-MS *m/z*: 373 [M + $H^{+\,35}$Cl], 375 [M + $H^{+\,37}$Cl].

N^1-(7-chloroquinolin-4-yl) ethane-1,2-diamine (45)

Following general procedure (a), it was synthesized from **57** (300,0 mg, 1.51 mmol) and **53** (2.7 mL, 41 mmol). The crude residue was purified by flash column chromatography (CH_2Cl_2/CH_3OH/NH_4OH, 9:1:0.1) to yield **45** (223 mg, 67%). ^{1}H-NMR ($CDCl_3$, 200 MHz): δ 3.15 (t, 2H, *J* = 28 Hz), 3.45 (t, 2H *J* = 26 Hz), 6.44 (d, 1H, *J* = 25 Hz), 7.42-7.36 (m, 1H), 7.52 (d, 1H, *J* = 25 Hz), 7.98 (s, 1H), 8.57 (d, 1H, *J* = 27 Hz). ESI-MS *m/z*: 222 [M + $H^{+\,35}$Cl]

N^1-(7-chloroquinolin-4-yl)propane-1,3-diamine (46)

Following general procedure (a), it was synthesized from **57** (300,0 mg, 1.51 mmol) and **54** (3,4 mL, 41 mmol). The crude residue was purified by flash column chromatography (CH_2Cl_2/CH_3OH/NH_4OH, 9:1:0.1) to

yield **46** (223 mg, 67%). ^{1}H-NMR ($CDCl_3$, 200 MHz): δ 2.97 (t, *J* = 6.2 Hz, 2H), 3.41 (t, *J* = 6.2 Hz, 4H), 6.33 (d, *J* = 5.2 Hz, 1H), 7.33 (d, *J* = 9 Hz, 1H), 7.75 (d, *J* = 9 Hz, 1H), 7.90 (s, 1H), 8.42 (d, *J* = 5.2 Hz, 1H). ESI-MS *m/z*: 236 [M + $H^{+\,35}$Cl]

N^1-(3-aminopropyl)-N3-(7-chloroquinolin-4-yl)propane-1,3-diamine (47)

Following general procedure (a), it was synthesized from **57** (300,0 mg, 1.51 mmol) and **55** (5,7 mL, 41 mmol). The crude residue was purified by flash column chromatography (CH_2Cl_2/CH_3OH/NH_4OH, 8:2:0.2) to yield **47** (150 mg, 35%). ^{1}H-NMR ($CDCl_3$, 200 MHz): δ 1.60 (m, 2H), 1.76-1.81 (m, 2H), 2.55-2.75 (m, 6H), 3.20-3.25 (m, 2H), 6.20 (d, *J* = 7.2 Hz, 1H), 7.17 (d, *J* = 8.8 Hz, 1H) , 7.64 (d, *J* = 8.8 Hz, 1H) , 7.81 (s, 1H) , 8.33 (d, *J* = 7.2 Hz, 1H). ESI-MS *m/z*: 293 [M + $H^{+\,35}$Cl], 295 [M + $H^{+\,37}$Cl].

N^1-(1,2,3,4-tetrahydroacridin-9-yl) ethane-1,2-diamine (48)

Following general procedure (a), it was synthesized from **58** (300,0 mg, 1.51 mmol) and **53** (2.7 mL, 41 mmol). The crude residue was purified by flash column chromatography (CH_2Cl_2/CH_3OH/NH_4OH, 9:1:0.1) to yield **48** (30 mg, 25%). ^{1}H-NMR ($CDCl_3$, 200 MHz): δ 1.92-1.95 (br s, 4H), 2.76 (s, 2H), 3.01 (m, *J* = 6 Hz, 4H), 3.16 (t, *J* = 6 Hz, 2H), 7.34 (t, *J* = 8.4 Hz,1H), 7.59 (t, *J* = 8.4 Hz,1H), 8.04 (t, *J* = 8.4 Hz,2H). ESI-MS *m/z*: 242 [M + H^+]

N^1-(1,2,3,4-tetrahydroacridin-9-yl)propane-1,3-diamine (49)

Following general procedure (a), it was synthesized from **58** (300,0 mg, 1.38 mmol) and **54** (3,1 mL, 37 mmol). The crude residue was purified by flash column chromatography (CH_2Cl_2/CH_3OH/NH_4OH, 9:1:0.1) to yield **49** (110 mg, 32%). ^{1}H-NMR ($CDCl_3$, 200 MHz): δ1.77-1.91 (m, 6H), 2.88 (m, 2H), 3.00-3.05 (m, 4H), 3.57-361 (m,2H) 7.32 (t, 1H, *J* = 33 Hz), 7.53 (t, 1H, *J* = 33 Hz), 7.93 (m, 2H). ESI-MS *m/z*: 256 [M + H^+]

N^1-(3-aminopropyl)-N3-(1,2,3,4-tetrahydroacridin-9-yl)propane-1,3-diamine (50)

Following general procedure (a), it was synthesized from **58** (300,0 mg, 1.38 mmol) and **55** (5,2 mL, 37 mmol). The crude residue was purified by flash column chromatography (CH_2Cl_2/CH_3OH/NH_4OH, 8:2:0.2) to yield **50** (150 mg, 44%). ^{1}H-NMR ($CDCl_3$, 200 MHz): δ 1.49-1.78 (m, 8H), 2.52-2.67 (m, 8H), 2.94 (s, 2H), 3.48-3.51 (br s, 2H), 7.19 (t, *J* = 7.2 Hz, 1H), 7.41 (t, *J* = 7.2 Hz, 1H), 7.78 (d, *J* = 8.6 Hz, 1H), 7.90 (d, *J* = 8.6 Hz, 1H). ESI-MS *m/z*: 313 [M + H^+].

N^1-(6-methoxyquinolin-4-yl)propane-1,3-diamine (52)

Following general procedure (a), it was synthesized from **60** (267,2 mg, 1.38 mmol) and **54** (3,1 mL, 37 mmol). The crude residue was purified by flash column chromatography (CH_2Cl_2/CH_3OH/NH_4OH, 8:2:0.2) to yield **52** (223 mg, 70%). ^{1}H-NMR ($CDCl_3$, 200 MHz): δ 1.94 (q, *J* = 12 Hz, 2H), 3.08 (t, *J* = 12 Hz, 2H), 3.46

(brs, *2*H), 6.37 (d, *J* = 10 Hz, 1H), 7.08 (s, 1H), 7.30 (d, *J* = 17 Hz, 1H), 7.92 (d, *J* = 18 Hz, 1H), 8.45 (d, *J* = 10 Hz, 1H). ESI-MS *m/z*: 232 [M + H].

N-[3-(7-chloroquinolin-4-ylamino)propyl]-5-(1,2-dithiolan-3-yl)pentanamide (61).

Following general procedure, it was synthesized in 78% yield from N^1-(7-chloroquinolin-4-yl)propane-1,3-diamine (**46**, 30.0 mg) and **12** (17.5 mg). ^{1}H NMR ($CDCl_3$, 400 MHz) δ 1.35-1.40 (m, 2H), 1.54-1.77 (m, 5H), 2.20-2.32 (m, 5H), 3.01-3.08 (m, 2H), 3.33-3.39 (m, 3H), 3.69-3.73 (m, 2H), 6.25 (d, *J* = 5.6 Hz, 1H), 6.62 (brs, D_2O-exchangeable, 1H), 6.82 (brs, D_2O-exchangeable, 1H), 7.37 (dd, *J* = 9.2, *J* = 2 Hz, 1H), 7.80 (d, *J* = 9.2 Hz, 1H), 7.89 (d, *J* = 2 Hz, 1H), 8.45 (d, *J* = 5.2 Hz, 1H). ^{13}C NMR ($CDCl_3$, 100.5 MHz) δ 25.53, 28.32, 28.91, 34.56, 36.20, 36.54, 38.51, 38.97, 40.30, 56.44, 98.33, 117.50, 122.18, 125.53, 127.86, 135.25, 148.67, 150.24, 151.25, 174.39. Anal. ($C_{20}H_{26}ClN_3OS_2$) C, H, N: calcd, 56.65, 6.18, 9.91 found, 56.75, 6.28, 9.95. MS (ESI+) *m/z* 424 [M + $H^{+\,35}$Cl], *z* 426 [M + $H^{+\,37}$Cl], 446 [M + $H^{+\,23}$Na ^{35}Cl], 448 [M + $H^{+\,23}$Na ^{37}Cl].

N-[2-(7-chloroquinolin-4-ylamino)ethyl]-5-(1,2-dithiolan-3-yl)pentanamide (62)

Following the general procedure, it was synthesized in 96% yield from N^1-(7-chloroquinolin-4-yl)ethane-1,2-diamine (**45**, 53.7 mg) and **12** (33.0 mg). ^{1}H NMR ($CDCl_3$, 400 MHz) δ 1.35-1.42 (m, 2H), 1.54-1.78 (m, 5H), 2.20-2.34 (m, 3H), 2.99-3.11 (m, 2H), 3.33-3.39 (m, 3H), 3.69-3.75 (m, 2H), 6.25 (d, *J* = 5.6 Hz, 1H), 6.62 (brs, D_2O-exchangeable, 1H), 6.82 (brs, D_2O-exchangeable, 1H), 7.37 (dd, *J* = 9.2, *J* = 2, 1H), 7.80 (d, *J* = 8.8 Hz, 1H), 7.89 (s, , *J* = 2 Hz , 1H), 8.45 (d, *J* = 5.2 Hz, 1H). ^{13}C NMR ($CDCl_3$, 100.5 MHz) δ 25.37, 28.68, 34.47, 36.23, 38.41, 38.69, 40.11, 46.06, 56.28, 98.10, 117.19, 122.15, 125.47, 128.03, 134.98, 148.77, 150.25, 151.66, 176.01. Anal. ($C_{19}H_{24}ClN_3OS_2$) C, H, N: calcd, 55.66, 5.90, 10.25 found, 55.49, 5.79, 10.20. MS (ESI+) *m/z* 410 [M + $H^{+\,35}$Cl], *z* 412 [M + $H^{+\,37}$Cl], 432 [M + $H^{+\,23}$Na ^{35}Cl], 434 [M + $H^{+\,23}$Na ^{37}Cl].

N-[3-(6-chloro-2-methoxyacridin-9-ylamino)propyl]-5-(1,2-dithiolan-3-yl)pentanamide (63)

Following the general procedure, it was synthesized in 74% yield from N^1-(6-chloro-2-methoxyacridin-9-yl)propane-1,3-diamine (**43**, 33.9 mg,) and **12** (31.7 mg). ^{1}H NMR ($CDCl_3$, 400 MHz) δ 1.41-1.54 (m, 2H), 1.62-1.77 (m, 4H), 1.83-1.91 (m, 1H), 1.94-2.00 (m, 2H), 2.31-2.35 (m, 2H), 2.38-2.42 (m, 1H), 3.05-3.17 (m, 2H), 3.49-3.57 (m, 3H), 3.86 (t, *J* = 6.0 Hz, 2H), 4.00 (s, 3H), 6.78 (s, D_2O-exchangeable, 1H), 7.20 (dd, *J* = 8.8 Hz, *J* = 2.0 Hz, 1H), 7.35 (dd, *J* = 9.6 Hz, *J* = 2.2 Hz, 1H), 7.63 (d, *J* = 2.8 Hz, 1H), 7.98 (d, *J* = 9.6 Hz, 1H), 8.03 (d, *J* = 2 Hz, 1H), 8.12 (d, *J* = 9.2 Hz, 1H). ^{13}C NMR ($CDCl_3$, 100.5 MHz) δ 25.44, 28.87, 30.98, 34.57, 36.18, 36.31, 38.44, 40.22, 45.49, 55.95, 56.41, 100.58, 113.24, 116.58, 124.00, 125.61, 125.76, 126.90, 128.19, 129.00, 136.86, 144.95, 152.51, 156.28, 174.54 Anal. ($C_{25}H_{30}ClN_3O_2S_2$) C, H, N: calcd, 59.56, 6.00, 8.34 found, 59.57, 6.09, 8.34. MS (ESI+) *m/z* 504 [M + $H^{+\,35}$Cl], *z* 506 [M + $H^{+\,37}$Cl], 526 [M + $H^{+\,23}$Na ^{35}Cl], 528 [M + $H^{+\,23}$Na ^{37}Cl].

N-[2-(6-chloro-2-methoxyacridin-9-ylamino)ethyl]-5-(1,2-dithiolan-3-yl)pentanamide (64)

Following the general procedure, it was synthesized in 67% yield from N^1-(6-chloro-2-methoxyacridin-9-yl)ethane-1,2-diamine (**42**, 33.0 mg,) and **12** (27.9 mg). IR (KBr): 3224, 3060, 2927, 2762, 1629, 1561, 1439, 1398, 1253, 1172, 1029, 871 cm^{-1}. ^1H NMR ($CDCl_3$, 400 MHz) δ 1.37-1.41 (m, 2H), 1.57-1.69 (m, 4H), 1.79-1.84 (m, 1H), 2.29-2.32 (m, 2H), 2.34-2.40 (m, 1H), 3.04-3.12 (m, 2H), 3.41-3.44 (m, 1H), 3.74-3.77 (m, 2H), 4.04 (brs, 5H), 7.16 (m, 1H), 7.38 (dd, *J* = 9.6 Hz, *J* = 2.2 Hz, 1H), 7.42 (d, *J* = 2.4 Hz, 1H), 7.98-8.03 (m, 2H), 8.10 (d, *J* = 9.2 Hz, 1H). ^{13}C NMR ($CDCl_3$, 100.5 MHz) δ 25.19, 28.73, 34.49, 36.22, 38.47, 40.20, 40.23, 52.61, 55.86, 56.29, 99.60, 123.45, 124.99, 125.40, 156.09, 175.55 Anal. ($C_{24}H_{38}ClN_3O_2S_2$) C, H, N: calcd, 58.82, 5.76, 8.57 found, 58.57, 5.49, 8.57. MS (ESI+) *m/z* 490 [M + H^+ ^{35}Cl], 492 [M + H^+ ^{37}Cl], 512 [M + H^+ ^{23}Na ^{35}Cl].

10.2. Biology

Cell culture.

ScGT1 cells were seeded in 10-cm plates containing 10 mL of Dulbecco's modified Eagle's medium (DMEM) culture media supplemented with 10% fetal bovine serum (FBS) and 1% penicillin-streptomycin. The cells were grown at 37°C in 5% CO_2 to 95% confluence for 1 week before splitting at 1:10 for further cultivation.

Drug treatment.

Synthesized compounds were dissolved in 100% dimethyl sulfoxide (DMSO) to a final concentration of 10 mM. This solution was then further diluted into the final stock solution of 1 mM with 10% (v/v) DMSO/PBS. The final concentration of DMSO in the cell medium was never above 0.1%. The media were refreshed and the compounds were added to the cultures 2 days after splitting of the cells and incubated for 5 days. Each experiment was performed using triplicate cultures.

Cell viability.

ScGT1 cells were maintained in DMEM, and supplemented with 10% FBS. After 1 day of incubation, media were aspirated from a confluent 10-cm plate of cells, and cells were detached by addition of 1 mL of 1X trypsin-EDTA solution. Media were added, and cell density determined by cell counting using a haemacytometer. The cell density was adjusted to 2.5×10^5 cells/mL with DMEM for ScGT1cells. A 96-well, tissue culture-treated, clear bottom, black plate (Costar) wetted with 90 µL of DMEM, was incubated at 37°C, prior to use. One hundred µL of the cell suspension were added to each well and the cells were allowed to settle for 2 hours, prior to the addition of the test compound. Compound library stocks were prepared as described above and diluted 1/20 with sterile PBS prior to use at the required concentrations in 96-well plates. Ten µL of the compounds were added to each well, and the plates were incubated at 37°C in 5% CO_2. Final DMSO concentration was never above 0.1% (v/v). Media were aspirated after incubation of 5 days and cells were washed twice with 200 µL of PBS. One hundred µL of 2.5 µM calcein-AM were added, and the plates were incubated at 37°C for 30 min. Fluorescence emission intensity was quantified using a SpectraMax Gemini EM or SpectraMax M5 fluorescence plate reader, excitation/emission ratio equal to 492/525 nm.

PrP^{Sc} detection by western blot.

After 5 days of drug treatment, the accumulation of PrP^{Sc} was detected by immunoblotting of lysed cells. One mL of lysis buffer (10 mM Tris-HCl pH 8.0, 150 mM NaCl, 0.5 % nonidet P-40, 0.5 % deoxycholic acid sodium salt) was added to cell plates and the cell lysates were collected after centrifugation at 2,000 rpm for 5 min in a bench microfuge (Eppendorf). The total protein amount of the samples was measured by the bicinchoninic acid assay (BCA) (Pierce). Five hundred µL of 1 mg/mL ScGT1 cell lysates were digested by 20 µg/mL of PK for 1 hour at 37°C. The reaction was stopped with 2 mM phenylmethylsulphonylfluoride (PMSF) and the PK-digested cell lysates centrifuged at 48,000 rpm for 1 hour at 4°C in an ultracentrifuge (Beckman Coulter). The pellets were resuspended in 1X sample loading buffer. For the non-PK digested sample, 50 µg of cell lysates for ScGT1 were used and 2X loading buffer (125 mM Tris HCl, pH 6.8, 10% 2-mercapethanol, 4 % SDS, 0.2 % bromophenol blue, 20 % glycerol) was added in a 1:1 ratio. The samples

were boiled for 5 min at 100°C, loaded onto a 12% Tris-Glycine SDS- PAGE gel, and transferred overnight onto Immobilon P PVDF membranes (Millipore). Membranes were blocked by 5% nonfat milk, incubated with 1 μg/mL anti-PrP Fab D18 followed by incubation with goat anti-human IgG F(ab)2 fragment conjugated with horseradish peroxidase. Blots were developed with the enhanced chemiluminescent system (ECL, Amersham Biosciences) and visualized on Hyperfilm (Amersham Biosciences).

PrP^{Sc} quantification by ELISA.

PK digestion of cell lysates was as described above. PK-digested PrP^{Sc} was selectively precipitated by the addition of 0.5% aqueous phosphotungstic acid (PTA, Sigma-Aldrich) solution with continuous shaking at 37°C, 350 rpm for 1 hour, and centrifuged at room temperature, 14,000 x *g* for 30 min. Pellets were dissolved and denatured in 50 μL of 8M guanidine hydrochloride (GdnHCl) in coating buffer (0.1 M sodium bicarbonate, pH 8.2) for 1 hour and diluted into 500 μL of coating buffer. Twenty μL of the suspension were transferred to 96-well MaxiSorp ELISA plates (Nunc), with each well containing 180 μL coating buffer and the plates were sealed and incubated overnight at 4°C. To increase the immunoreactivity of PrP^{Sc}, coated proteins were denatured *in situ*. Fifty μL of 8M GdnHCl were added to each well and incubated for 10 min at room temperature. The ELISA plates were washed three times with TBST (20 mM Tris-HCl, 137 mM NaCl, 0.05% Tween-20, pH 7.5) and blocked with 200 μL of 3% BSA, made up in TBS (20 mM Tris-HCl, 137 mM NaCl, pH 7.5) sealed and incubated at 37°C. After 1 hour, the plates were washed three times with TBST, and incubated with 100 μL of anti-PrP antibody D18 (2 μg/mL) in 1% BSA/TBS, at 37°C for 2 hours. They were then washed seven times with TBST. One hundred μL of goat anti-human IgG Fab conjugated to HRP and diluted 1:1000 with 1% BSA/TBS was added to the plates and incubated at 37°C for 1 hour. Again, plates were washed seven times with TBST, and then developed with 100 μL of 1-step TMB (3,3',5,5'-tetramethylbenzidine) Turbo ELISA HRP substrate (Pierce). The reaction was stopped by the addition of 100 μL of 2 M sulfuric acid to the plates. Absorbance at 450 nm was measured using a microplate reader (VersaMax, Molecular Devices). Dose-response curves and EC_{50} values were computed using GraphPad Prism (version 4.0).

Detection of *in vitro* effect of the synthesized compounds on prion fibril formation.

Fibril formation was performed in accordance to the method previously described by Colby *et al.* with a few modifications.[2] Briefly, 20 μL of the diluted compounds at indicated concentrations were added to each well containing 180 μL of reaction solution including 100 μg/mL MoPrP(23-230), 2 M GdnHCl and 10 μM ThT in 1X PBS buffer in a 96-well black plate (BD Falcon). Each sample was performed in four replicates. Each well contained one 3-mm glass bead (Sigma). The plate was covered with sealing tape (Fisher Scientific), incubated at 37°C with continuous shaking and read on SpectraMax M5 fluorescence plate reader (Molecular Devices) for 72 hrs by top fluorescence reading every 15 min at excitation of 444 nm and emission of 485 nm.

Detection of antioxidant activity of the compounds by lipid peroxidation assay.

Lipid peroxidation is an indicator of oxidative stress. The thiobarbituric acid reactive substances (TBARS) assay measures lipid hydroperoxides and aldehydes, such as malondialdehyde (MDA), in the cell media and lysates. The assay was performed in accordance to the method previously described Dubuisson *et al.*.[3] Briefly, 10^6 ScGT1 cells were cultured in 1 mL of DMEM per each well of 6 well-plates for 24 hours. After 24 hrs,

the compounds with various concentrations were added to each well. After 3 hrs, the cell media were collected and the cells were washed twice with PBS and scraped off with 1 mL of 2.5% Trichloroacetic acid (TCA). After centrifugation (13,000 *g*, 2 min), 125 µL the supernatant was added to a mixture of 100 µL 15% TCA and 200 µL 0.67% (w/v) 2-thiobarbituric acid (TBA) and heated at 95^{o}C for 20 min. After cooling, 750 µL of 1-butanol was mixed thoroughly into the solution and centrifuged. Two hundred µL was transferred into 96-well plates. Each sample was performed in three replicates. The fluorescence in the butanol phase was measured at excitation of 521 nm and emission of 552 nm by using M5 fluorescence plate reader (Molecular Devices). A blank was performed for each sample. Standard curves specific for the assay was created using MDA.

Detection of antioxidant activity of Quinone compounds by sulforaphan (4-methylsulfinylbutyl isothiocyanate, SFP) assay.

The assay was performed in accordance to the method previously described by Bolognesi *et al*..[4] Briefly, ScGT1 cells were seeded in 96-well plates at 3 x 10^4 cells/well in DMEM. Experiments were performed after 24 hrs of incubation at 37^{o}C in 5% CO_2 with 4-methylsulfinylbutyl isothiocyanate (2.5 µM), a potent inducer of cytosolic NQO1. After 24 hrs, the cells were washed and treated for 24 hrs with 1 µM of compounds. The antioxidant activity of compounds was evaluated after 30 minutes of incubation with 10 µM fluorescent probe (2',7'-dichlorofluorescein diacetate, DCFH-DA) in PBS. After removal of DCFH-DA, the cells were incubated with 0.1 mM tert- butyl hydroperoxide (t-BuOOH) in PBS for 30 min. The fluorescence of the cells from each well was measured at excitation of 485 nm and emission of 535 nm by using M5 fluorescence plate reader (Molecular Devices). Each sample was performed in three replicates.

References

(1) Hu, M.-K. Wu, L.-J. Hsiao, G.; Yen, M.-H. *J. Med. Chem.* **2002**, *45*, 2277-82.

(2) Colby, D. W. Zhang, Q. Wang, S. Groth, D. Legname, G. Riesner, D.; Prusiner, S. B. *Proc. Natl. Acad. Sci. U S A* **2007**, *104*, 20914-20919.

(3) Dubuisson, M. L. Wergifosse, B. de; Trouet, A. Baguet, F. Marchand-Brynaert, J.; Rees, J. F. *Biochem. Farmacol.* **2000**, *60*, 471-8.

(4) Bolognesi, M. L. Cavalli, A. Bergamini, C. Fato, R. Lenaz, G. Rosini, M. Bartolini, M. Andrisano, V.; Melchiorre, C. *J. Med. Chem.* **2009**, *52*, 7883-6.

Appendix A

Fragmenter is a toolkit of ChemAxon to break down molecules to smaller pieces called fragments by cleaving bonds. The tool is based on two sequential processes:

First, RECAP fragments molecules based on chemical knowledge.[1] The RECAP algorithm raises the following cleavage revision rules:

- Never cut a hydrogen-connecting bond.
- Never cut ring bonds.
- Refuse a cut if the number of open bonds in any of the resulting fragments exceeds the specified limit.
- Refuse a cut if the number of atoms in any of the resulting fragments is less than the predefined minimal atom count.

Then, FragmentStatistics[2] creates statistical results from the output of RECAP. Fragments are sorted by activity, which is calculated in form of a scoring function:

$$ac \times (w1 \times c1 + w2 \times c2 + \ldots wN \times cN)$$

where:

- *ac is the heavy atom count;*
- *w1, w2, ..., wN are the category weights in descending order (Picomolar =1; Micromolar inhibitor=0.2; Less than millimolar= -0.6; Inactive = -1);*
- *c1, c2, ..., cN are the fragment counts in each category, in descending activity order.*

The analysis provides a score [100 – 0] for each fragment, which gives an indication of how often a fragment occurs in the active and inactive structures.

References

(1) Lewell, X. Q. Judd, D. B. Watson, S. P.; Hann, M. M. *J. Chem. Inf. Comput. Sci.* **1998**, *38*, 511-522.

(2) Http://www.chemaxon.com/jchem/doc/user/FragmentStatistics.html FragmentStatistics. *Version 5.5.1.0.*

Acknowledgements

I would like to express my heartfelt gratitude and appreciation to my supervisors, Prof. Maria Laura Bolognesi, Prof. Paolo Carloni and Prof. Giuseppe Legname for their immeasurable guidance and support throughout the course of my PhD research.

I gratefully acknowledge the help provided by Prof. Andrea Cavalli and Prof. Marinella Roberti.

I would like to thank the following people for their support, without whose help this work would never have been possible: Dr. Xevi Biarnes, Dr. Agata Kranjc, Dr. Giulia Rossetti, Dr. Hoang Ngoc Ai Tran and Xiaojing Cong.

I would like to acknowledge Prof. Carlo Melchiorre for fruitfull discussion and allowing me to work in the medicinal chemistry lab in the University of Bologna, Italy.

I owe sincere and earnest thankfulness to Prof. Cristian Micheletti and Prof. Alessandro Laio (Statistical and Biological Physics (SBP) sector, SISSA) for their support. I am also indebted to the students and postdocs of the SBP group for sharing their knowledge, experience and time with me. Particularly, I would like to acknowledge Chuong Nguyen, Dr. Attilio Vargiu, Dr. Fabrizio Marinelli, Dr. Francesco Colizzi, and Gianpaolo Chiriano for advice and valuable discussions.

Thanks to all lab members (Dr. Michela Rosini, Dr. Matera Riccardo, Dr. Simoni Elena, Dr. Andrea Milelli, and Laura Comandini) for welcoming me to the lab.

I would like to conclude by thanking all my friends (from Vietnam, Iran, and Northeast of Italy!) and SISSA JAZZ BAND for making the time spent in Trieste so enjoyable and unforgettable.

Thank you to my parents, my brother and Elisa for believing in me, for all their love and support that helped me to succeed in doing my PhD.